

國立交通大學

材料科學與工程學系

博士論文

運用官能化樹枝狀及高分枝狀結構之非聚集途徑以提
昇高分子發光二極體之性能

**Non-Aggregation Approaches by Functionalized
Dendritic and Hyperbranched Structures to Enhance
Polymer Light-Emitting Diode Properties**



研究生：吳中文

指導教授：林宏洲 博士

中華民國九十五年十月

運用官能化樹枝狀及高分枝狀結構之非聚集途徑以提昇高
分子發光二極體之性能

**Non-Aggregation Approaches by Functionalized Dendritic
and Hyperbranched Structures to Enhance Polymer
Light-Emitting Diode Properties**

研究生：吳中文

Student: Chung-Wen Wu

指導教授：林宏洲

Advisor: Prof. Hong-Cheu Lin



材料科學與工程學系

博士論文

A Thesis
Submitted to Department of Materials Science and Engineering
College of Engineering
National Chiao Tung University
In Partial Fulfillment of the Requirement
For the Degree of Doctor of Philosophy of Science
In Materials Science and Engineering
October 2006
Hsinchu, Taiwan

中華民國九十五年十月

運用官能化樹枝狀及高分枝狀結構之非聚集途徑以提昇高 分子發光二極體之性能

學生：吳中文

指導教授：林宏洲 博士

國立交通大學材料科學與工程研究所

博士班



一系列不同代數包含圻罅雙唑(oxadiazole) (OXD) 雜環之樹枝狀化合物已被合成與鑑定，當不同代數樹枝狀OXD基團懸掛於包含聚萸共軛高分子側鏈上時，這些高分子具有極佳的溶解度與熱性質，並可有效的抑制結晶性與高分子鏈聚集的現象，進而有效提高螢光效率，且避免光色不純的現象產生。此外，當激發側鏈OXD基團時，可發生能量轉移到高分子主鏈上。特別的是，在連接高代數的樹枝狀OXD的高分子時，激發外部OXD基團，其螢光效率更大於直接激發共軛高分子。當作成元件時，連接高代數的樹枝狀OXD的高分子呈現穩定的藍光波長，其光電特性優於傳統聚萸高分子。再者，將一系列不同代數包含圻罅雙唑(OXD)雜環的樹枝狀化合物結構的焦點設計成酸基團時，可與具單吡啶雜環與雙吡啶雜環的發光質子受體形成氫鍵錯合物，這些包含圻罅雙唑(OXD)雜環的氫鍵錯合物可有效防止發光分子聚集，進而提高螢光效率，同時不同代數的氫鍵錯合物可發不同的波長的光色。當激發氫鍵錯合物的OXD基團時，可發生有效能

量轉移到包含單吡啶雜環與雙吡啶雜環的發光質子受體上，同樣地，在高代數的氫鍵錯合物，激發氫鍵錯合物的OXD基團，其螢光效率更大於直接激發單吡啶雜環與雙吡啶雜環的發光質子受體。

另外，在使高分子形成高分枝結構之研究上、利用不同含量與不同官能基數目之carbazole(CAZ)單體與萘 (fluorene) 單體進行聚合，可得一系列高分枝狀高分子，能使聚萘共軛高分子 (Poly(fluorene)) 產生不同之分枝程度結構，這樣方式有效改善分子間聚集之現象並且維持高分子主鏈良好共軛程度，使得產生之高分子具良好的螢光效率。



Non-Aggregation Approaches by Functionalized Dendritic and Hyperbranched Structures to Enhance Polymer Light-Emitting Diode Properties

Student: Chung-Wen Wu

Advisor: Dr. Hong-Cheu Lin

Department of Materials Science and Engineering National Chiao Tung



Functionalized dendritic and hyperbranched structures have been carried out to solve the aggregation-related problems by increasing the structural hindrances of Poly(fluorene)s (PF), and thus to reduce their self-aggregation tendency in the solid state. These dendronized and hyperbranched polymers possessed excellent solubility in common solvents and good thermal stability. Photophysical studies reveal the dendronized and hyperbranched polymers greatly suppress the aggregation of PF backbones and thus to induce pure blue PL emission. It was proven that HOMO and LUMO energy levels of the copolymers can be adjusted by increasing the carbazole and oxadiazole moieties in the electrochemical measurements; hence, the hole injection and electron transport were greatly enhanced. Pure blue electroluminescence

(EL) spectra with narrow fwhm (full width at the half-maximum) values and negligible low-energy excimer emission bands were successfully achieved, indicating that these copolymers could be good candidates for blue light-emitting materials.

Novel asymmetric/symmetric dendritic supramolecules were constructed by two kinds of (single/double) H-bonded acceptor chromophores, i.e. pyridyl/bispyridyl acceptor emitters, encapsulated with (one or two) 1,3,4-oxadiazole (OXD) dendritic donors in proper acceptor/donor molar ratios. Due to shielding effect of bulky OXD dendritic shells in H-bonded donors, the dendritic supramolecules are able to prevent acceptor emitters from spatial aggregation, and thus to induce glass-forming properties and show stronger emission intensities via H-bonds. Besides, the dendritic donors act as efficient light-harvesting antennae capable of transferring light energy from their peripheral OXD arms to their emitting acceptors, where the chromophore luminance induced by energy transfer is more efficient than that by direct excitation of the emitting cores. In compared with acceptor emitters, not only can the emission wavelength be tuned (up to 100 nm of red-shift) by H-bonds, but also much higher emission efficiencies of the H-bonded complexes were induced by reduced aggregation and energy transfer from the OXD donor dendrons.

Table of Contents

Abstract	I
Table of contents	V
Table Lists	VIII
Figure Lists	IX
Chapter 1. Introduction	1
1.1 Introduction to organic light-emitting diodes.....	1
1.2 The organic emitter layer.....	3
1.3 Electron transport and hole blocking materials.	7
1.4 Hole transport materials.	9
1.5 Toward Efficient Single-Layer OLEDs.	10
1.6 Poly(fluorenes)	11
Chapter 2. Synthesis and Characterization of Poly(fluorene-co-alt-phenylene) Containing 1,3,4-Oxadiazole Dendritic Pendants.....	15
2.1 Introduction	15
2.2 Experimental	17
2.2.1 Measurements	17
2.2.2 Materials	18
2.3 Results and Discussion	25
2.3.1 Synthesis and Characterization.	25
2.3.2 Optical Properties	27
2.3.3 Electrochemical Properties.....	34
2.4 Conclusion	36
Chapter 3 Synthesis and Characterization of Poly(fluorene)-Based Copolymers Containing Various 1,3,4-Oxadiazole Dendritic Pendants.....	37

3.1 Introduction	37
3.2 Experimental	39
3.2.1 Measurements	39
3.2.2 EL Device Fabrication.	40
3.2.3 Materials.	40
3.3 Results and Discussion	47
3.3.1 Synthesis and Characterization	47
3.3.2 Optical Properties	49
3.3.3 Electrochemical Properties	56
3.3.4 Electroluminescent Properties	59
3.4 Conclusion	62
Chapter 4. H-Bonded Effects on Novel Supramolecular Dendrimers Containing Electron-Transporting Donor dendron and Single/Double H-Bonded Acceptor Emitters	63
4.1 Introduction	63
4.2 Experimental Section	66
4.2.1 Measurements	66
4.2.2 Materials	66
4.2.3 Preparation of H-bonded complexes	71
4.3. Results and Discussion	76
4.3.1 Synthesis and Characterization	76
4.3.2 Thermal Properties	78
4.3.3 Optical Properties	81
4.4 Conclusions	97
Chapter 5 Synthesis and Characterization of Kinked and Hyperbranched Carbazole/Fluorene-Based Copolymers	98

5.1 Introduction	98
5.2 Experimental	100
5.2.1 Measurements	100
5.2.2 EL Device Fabrication.	100
5.2.3 Materials.	101
5.3 Results and Discussion	107
5.3.1 Synthesis and Characterization	107
5.3.2 Thermal Properties.....	109
5.3.3 Optical Properties	110
5.3.4 Electrochemical Properties	117
5.3.5 Electroluminescence (EL) Properties.	119
5.4 Conclusion	122
Chapter 6 Conclusion	123
References	125



Table Lists

Table 2.1 Molecular Weights and Thermal Properties of Polymers P1-P3.....	27
Table 2.2 Absorption and PL Emission Spectral Data of Polymers P1-P3 in THF and Solid Films.....	33
Table 2.3 HOMO and LUMO Energies, and Electrochemical Properties of Polymers P1-P3	34
Table 3.1 Molecular Weights and Thermal Properties of Polymers.....	49
Table 3.2 Absorption and PL Emission Spectral Data of Polymers in THF Solutions and Solid Films.....	56
Table 3.3 Oxidation Potentials and Calculated HOMO and LUMO Energies of Polymers.....	57
Table 3.4 EL Data of PLED Devices ^a	61
Table 4.1. Transition Temperatures of H-Bonded Donors, Acceptors, and Dendritic Complexes	80
Table 4.2 Photophysical Properties of H-Bonded Acceptors and Dendritic Complexes.....	96
Table 5.1 Molecular Weights and Thermal Properties of Polymers.....	110
Table 5.2. Absorption and PL Emission Spectral Data of Polymers in Solution and Solid States.....	116
Table 5.3 Oxidation Potentials and HOMO and LUMO Energy Values of Polymers.....	119
Table 5.4 EL Data of PLED Devices ^a	121

Figure Lists

Figure 1.1 Schematic configuration of a single-layer OLED.....	2
Figure 1.2 Common OLED architectures with a hole-transport material (HTM) and an electron-transport material (ETM).....	3
Figure 1.3 Structures of PPV, PPP, PF and PT.....	4
Figure 1.4 Examples of conjugated oligomers.....	5
Figure 1.5 Structures of bis(triarylamine) and Alq ₃	6
Figure 1.6 Examples of (a) main chain polymers with isolated chromophores. (b) side chain polymers with linked chromophores.....	7
Figure 1.7 Structures of PBD and triazole derivatives.....	8
Figure 1.8 Structures of TPD and NPD.....	10
Figure 1.9 Examples of oxadiazole-containing electron-transporting polymers.....	11
Figure 1.10 Example of poly(fluorene) containing long side chains.....	12
Figure 1.11 Examples of poly(fluorene)-based copolymers.....	12
Figure 1.12 Examples of poly(fluorene) with dendrons as side chains.....	13
Figure 1.13 Example of end-capping of poly(fluorene) with bulky groups.....	13
Figure 1.14 Examples of poly(fluorene)-based hyperbranched copolymers.....	14
Figure 2.1 TGA traces of polymers P1-P3	26
Figure 2.2 Normalized UV-vis absorption spectra of polymers P1-P3 and the PL emission spectrum of compound 2 in THF, the absorption spectra are normalized at the absorption peaks of polymer backbones ca. 367 nm.....	28
Figure 2.3 Normalized PL spectra of polymers P1-P3 in THF.....	29
Figure 2.4 Normalized PL spectra of polymers P1-P3 in solid film.....	30
Figure 2.5 PL Emission spectra of polymers P1-P3 (a) in solutions (THF) and (b) in solid films, which were excited at the maximum absorption of the polymer backbones	

(for solid symbols) and the polymer periphery OXD dendrons (for open symbols).	32
Figure 2.6. Cyclic voltammetry of polymers P1-P3 during (a) the oxidation processes and (b) the reduction processes.	35
Figure 3.1. Absorption spectra of polymers P4-P9 in THF solutions, normalized at the absorption peak of the polymer backbone.	50
Figure 3.2. Normalized PL spectra of polymers P4-P9 excited at the maximum absorption of backbones in THF solutions.	51
Figure 3.3. Normalized PL spectra of polymers P4-P9 excited at the maximum absorption of backbones in solid films.	51
Figure 3.4. Normalized PL spectra of polymers films excited at the maximum absorption of the polymer backbones after annealing at 150 °C for 1 h in a air atmosphere. ·	53
Figure 3.5. Normalized PL spectra of polymers (a) P4-P6 and (b) P7-P9 in solid films, which were excited at the maximum absorption of the peripheral OXD pendants (open symbols) and at the maximum absorption of the polymer backbone (solid symbols).	55
Figure 3.6. Cyclic voltammograms of the polymers: (a) P4 and P7 , (b) P5 and P8 , (c) P6 and P9	58
Figure 3.7. Normalized EL spectra of the devices with the configuration of ITO/PEDOT/polymer/LiF/Al	60
Figure 3.8. Current density-voltage-brightness (<i>J-V-B</i>) characteristics of the PLED device containing P7 with the configuration of ITO/PEDOT/ P7 /LiF/Al	60
Figure 4.1 Mono-pyridyl (single H-bonded) and bis-pyridyl (double H-bonded) acceptors used in dendritic supramolecules.	67
Figure 4.2 IR spectra of H-bonded moieties PBBCN-OC ₈ , G1COOH, and H-bonded	

complex PBBCN-OC ₈ /G1COOH.....	77
Figure 4.3 UV-vis absorption spectra of uncomplexed H-bond donors and PBBCN-OC₈ in THF solutions.	82
Figure 4.4 UV-vis absorption spectra of PBBCN-OC₈ and its H-bonded dendrimers in solid films, which are normalized at the absorption peak of PBBCN-OC₈ at 423 nm.	82
Figure 4.5 Normalized PL spectra of mono-pyridyl (single H-bonded) acceptor emitter PBBCN-OC₈ and its H-bonded dendrimers.	84
Figure 4.6 Normalized PL spectra of bis-pyridyl (double H-bonded) acceptor emitter PBP-OC₈ and its H-bonded dendrimers	85
Figure 4.7 UV-vis absorption spectra of (single/double H-bonded) acceptor emitters PBBOC₈-OC₈ , PBBCN-OC₈ , PBP-OC₈ , and PBBBP-Me-OC₈ and PL spectrum of compound 2 (containing an OXD unit) in THF. It indicates that an overlap exists between the emission band of the donor and the absorption bands of the acceptor emitters, resulting in energy transfer from OXD units to the emitting core.	86
Figure 4.8 UV-vis absorption and corrected excitation spectra of symmetric H-bonded dendrimers (with different generations of donor dendrimers) PBP-OC₈/G1COOH , PBP-OC₈/G2COOH , and PBP-OC₈/G3COOH monitored at the core of double H-bonded acceptor emitter PBP-OC₈	86
Figure 4.9 PL spectra of symmetric dendritic supramolecules containing double H-bonded acceptor emitter PBP-OC₈ in thin films, which were excited at the dendritic peripheral OXD units (at 305 nm for open symbols) and at the maximum absorption of the emitting core PBP-OC₈ in H-bonded G1-G3 dendrimers (at 418, 415, 408 nm, respectively, for solid symbols).	89

Figure 4.10 PL spectra of asymmetric dendritic supramolecules containing single H-bonded acceptor emitter **PBBCN-OC₈** in thin films, which were excited at the dendritic peripheral OXD units (at 305 nm for open symbols) and at the maximum absorption of the emitting core **PBBCN-OC₈** in H-bonded G1-G3 dendrimers (at 424, 423, 419 nm, respectively, for solid symbols).89

Figure 4.11 Schematic representation of double H-bonded encapsulation of symmetric dendrimers: (a) **PBP-OC₈/G2COOH** and (b) **PBP-OC₈/G1COOH**; and single H-bonded encapsulation of asymmetric dendrimers: (c) **PBBOC₈-OC₈/G2COOH** and (d) **PBBCN-OC₈/G2COOH**.92

Figure 4.12 PL spectra of symmetric dendritic supramolecules containing double H-bonded acceptor emitter **PBBBP-Me-OC₈** in thin films as they were excited at the maximum absorption of the dendritic peripheral OXD units (at 305 nm for open symbols) and at the maximum absorption of the emitting core **PBBBP-Me-OC₈** in H-bonded G1-G3 dendrimers (at 450, 446, 439 nm, respectively, for solid symbols).93

Figure 4.13 PL spectra of the simple mixture (without H-bonds) of **PBP-OC₈/G1COOCH₃**, **PBP-OC₈/G2COOCH₃**, and **PBP-OC₈/G3COOCH₃** in thin films excited at the dendritic peripheral OXD units (at 305 nm for open symbols) and at the maximum absorption of the emitting core **PBP-OC₈** in (at 425 nm for solid symbols).93

Figure 5.1 ¹H-NMR spectra of monomer **21**, **PFDiCAZ**, **P10**, and **P11**.108

Figure 5.2 Normalized UV-vis absorption spectra of polymers in chloroform (10⁻⁶ M). ...111

Figure 5.3. Normalized PL spectra of polymers excited at the maximum absorption of the polymer backbones in chloroform (10⁻⁶ M).113

Figure 5.4. Normalized PL spectra of polymers excited at the maximum absorption of the polymer backbones in solid films.113

Figure 5.5. Normalized PL spectra of polymers excited at the maximum absorption of the polymer backbones in solid films: before annealing (pristine film) and annealing at 200 °C for 0.5 h under air.115

Figure 5.6 Cyclic voltammograms of the polymers: (a) **PFDiCAZ**, **P10**, and **P11**; (b) **P12**, **P13**, **P14**, and **P15**.118

Figure 5.7 (a) Normalized EL spectra of **P10**, **P12**, and **P14** at 10 V. (b) Normalized EL spectra of ITO/PEDOT/**P12**/LiF/Al device at different voltages.120

Figure 5.8 Current -voltage-brightness (*I-V-B*) characteristics of the PLED device containing **P12** with the configuration of ITO/PEDOT/**P12**/LiF/Al.121



Chapter 1

Introduction

1.1 Introduction to organic light-emitting diodes

While current progress in OLED technology is rapid, its history begins more than forty years ago in 1963 when Pope and coworkers discovered electroluminescence in organic semiconductors.¹ The discovery excited little interest at the time, however, because of the high voltage needed and the short lifetime of prototype devices. This changed in 1987 when Tang and VanSlyke of Kodak reported efficient, low voltage electroluminescence in an organic thin-film device with a novel heterojunction structure.²

Another fundamental work concerning the evolution of organic light-emitting diodes (OLEDs) was published by Friend et al. in 1990. They overcame the drawback of expensive and technologically inconvenient vapor deposition of fluorescent dyes and inorganic semiconductors by using a highly fluorescent conjugated polymer, poly(*p*-phenylenevinylene) (PPV), as the active material in a single-layer OLED.³ Although PPV itself is insoluble and difficult to process, Friend et al. found a way to build up PPV-OLEDs via the thermoconversion of a processable precursor polymer. Their greatest merit however was that they indicated for the first time the possibility of producing large area displays by simple coating techniques. The PPV diode embodies the prototype of a single-layer OLED and is typically composed of a thin film of the active organic material (30~500 nm) which is sandwiched between two electrodes (Figure 1.1). Since one of the electrodes needs to be semitransparent in order to observe light emission from the organic layer, usually an indium tin oxide (ITO)-coated glass substrate is used

as the anode. Electropositive metals with low work functions such as Al, Ca, Mg, or In are used as cathodes in order to guarantee efficient electron injection. If an external voltage is applied at the two electrodes, charge carriers, i.e. holes, at the anode and electrons at the cathode are injected into the organic layer beyond a specific threshold voltage depending on the organic material applied. In the presence of an electric field the charge carriers move through the active layer and are non-radiatively discharged when they reach the oppositely charged electrode. However, if a hole and an electron encounter one another while drifting through the organic layer, excited singlet and triplet states, so-called excitons, are formed. The singlet state may relax by emission of radiation (fluorescence).

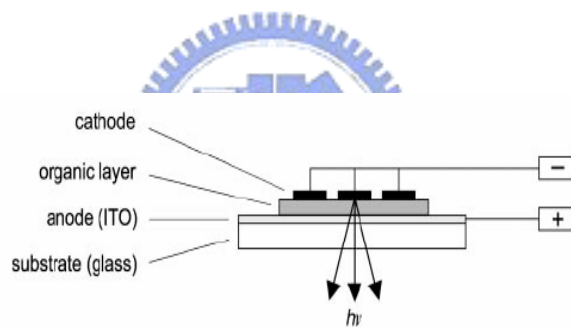


Figure 1.1 Schematic configuration of a single-layer OLED.

OLEDs are double charge injection devices, requiring the simultaneous supply of both electrons and holes to the electroluminescent (EL) material sandwiched between two electrodes. To achieve an efficient OLED with the single-layer configuration shown in Figure 1.2(a), the organic EL material would ideally have a high luminescence quantum yield and be able to facilitate injection and transport of electrons and holes. This demand of multifunctional capabilities from a single organic material is a very difficult one to meet by nearly all current materials. Most highly fluorescent or phosphorescent organic

materials of interest in OLEDs tend to have either p-type (hole-transport) or n-type (electron transport) charge transport characteristics.⁴ A consequence of this is that the simplest OLED configuration shown in Figure 1.2(a), where an organic emitter layer is sandwiched between a transparent anode and a metallic cathode, gives very poor efficiency and brightness. The use of two or more different materials to perform the required functions of efficient light emission and good electron- and hole-injection and transport properties in an OLED has resulted in orders of magnitude improvement in device performance, albeit with the attendant more complex OLED architectures shown in Figure 1.2(b)-(d).

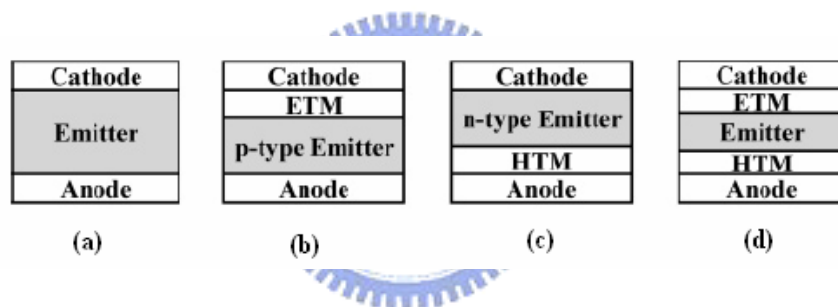


Figure 1.2 Common OLED architectures with a hole-transport material (HTM) and an electron-transport material (ETM).

1.2 The organic emitter layer

The basic requirements for organic electroluminescent materials are the capability to undergo charge transfer to an electrode, the ability to transport charge and to fluoresce efficiently. A variety of organic materials have been investigated as active components in order to optimize device performance.⁵ With respect to their molecular structure they can be distinguished and classified into one of the following four parts:

1. Conjugated polymers in OLEDs. Conjugated polymers are organic semiconductors

with delocalized π -molecular orbitals along the polymeric chain. Different types of conjugated polymers such as polyacetylene (PA), poly(fluorine) (PF), poly(pphenylene) (PPP), poly(p-phenylenevinylene) (PPV), polyaniline (PAni), polypyrrole (PPy) and polythiophene (PT) have been developed and intensively investigated. Their chemistry and physics have been reviewed in some excellent articles and book publications.⁶

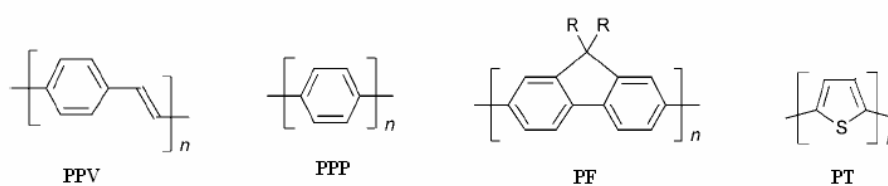


Figure 1.3 Structures of PPV, PPP, PF and PT.

2. Conjugated oligomers in OLEDs. Main chain conjugated polymers inevitably contain random dispersed defects leading to a statistical distribution of lumophore lengths. In contrast, well-defined conjugated oligomers allow strict control of the effective conjugation length. Initially, they have been synthesized as model compounds in order to gain more insight into the structural and electronic peculiarities of the corresponding polymers.⁷ However, on account of their controllable and rigorously defined structure, conjugated oligomers have also been used as novel materials and potential alternative in electrooptical applications.

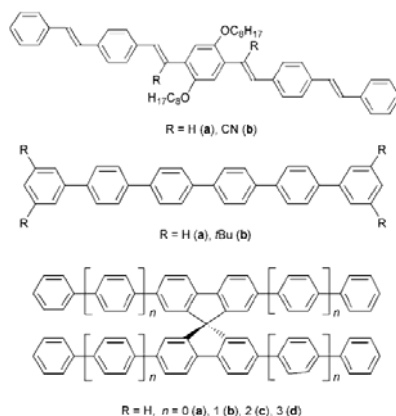


Figure 1.4 Examples of conjugated oligomers.

3. Low molecular weight materials in OLEDs. Since the basic principles of electroluminescence are essentially the same, no matter which type of organic material is used, the choice of materials is usually determined by the method of fabrication preferred. As previously mentioned, conjugated polymers are processed from solution by coating techniques. Due to their low molecular weight, small organic semiconductors can also be vacuum deposited as thin films. This preparation technique to build up electroluminescent devices was first utilized by Tang and VanSlyke at Kodak in their basic work on OLEDs in 1987.² Their device contained two layers of different carrier transport properties (ITO/bis(triarylamine)/Alq₃/Mg:Ag). Alq₃ is used for electron transport and at the same time as an emitting layer, but is unable to carry holes. In contrast, bis(triarylamine) was inserted to provide efficient hole transfer. Therefore, recombination was largely confined to a region near the interface between both organic materials.

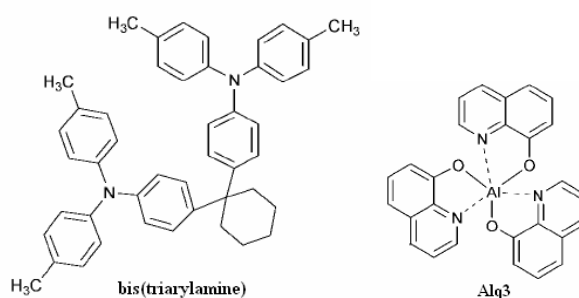


Figure 1.5 Structures of bis(triarylamine) and Alq₃.

4. Main chain polymers with isolated chromophores and side chain polymers with linked chromophores in OLEDs. Taking advantage of the processability of polymers and the defined optical and electrical properties of low molecular weight materials, a new class of materials for EL devices has been developed. In order to overcome several drawbacks of established compounds, defined charge transporting and/or emissive chromophores have been incorporated as conjugated main chain segments into a polymeric backbone or have alternatively been attached as pendant groups to a non-conjugated polymer. This approach ensures control of the conjugation length as well as emissive color while diminishing the probability of non-emissive relaxation due to π -stack formation. With respect to low molecular weight oxadiazoles and triarylamines, recrystallization processes can be suppressed and the covalent attachment to a polymeric network impedes phase separation, which was found to be the main disadvantage of blend systems. Finally, the polymeric nature yields amorphous films and warrants morphological stability.

sublimation¹⁰ or by spin-coating as a dispersion in several standard polymers (PMMA, PS etc.¹¹) or electroluminescent polymers.¹² In particular, blend systems PBD/polymer have been reported to exhibit high performances. External quantum efficiencies larger than 1% have been reported for multilayer OLEDs based on phenyl and alkoxy substituted PPVs even with air-stable aluminium cathodes.¹³

Triazoles are another interesting class of electron deficient thermostable materials similar to oxadiazoles. The use of 1,2,4-triazoles as electron transporting and hole blocking material was first demonstrated by Kido et al. The most representative derivative is 3-(1,1'-biphenyl-4-yl)-5-(4-*tert*-butylphenyl)-4-phenyl-4*H*-1,2,4-triazole, which is not only a good electron transporter but also a better hole blocker than PBD.¹⁴ Since most organic materials are efficient hole transport materials, the employment of hole blocking triazoles as electron transport layers in OLEDs¹⁵ enables exciton confinement at the organic interfaces. This material is therefore advantageous with respect to a high efficient performance of the corresponding devices.

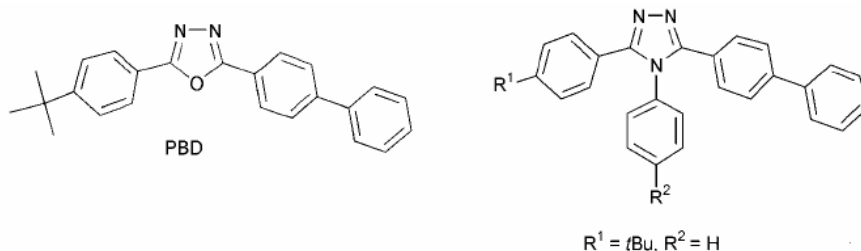


Figure 1.7 Structures of PBD and triazole derivatives.

1.4 Hole transport materials.

Numerous materials have been developed as hole transport layers in organic EL devices.¹⁶ The triarylamine derivatives have gained importance due to their ability to be vacuum deposited and their high hole drift mobilities. *N,N*-Diphenyl-*N,N*-bis(3-methylphenyl)-1,1'-biphenyl-4,4'-diamine (TPD) and *N,N*-bis(1-naphthyl)-*N,N*-diphenyl-1,1'-biphenyl-4,4'-diamine (NPD) are the most prevalent derivatives, which have been widely used as hole transport layers in OLEDs. However, the propensity of simple triarylamines to crystallize on aging is thought to be one of the main reasons of degradation in organic EL devices. Vacuum deposited TPD, for instance, was found to crystallize at ambient temperature after a few hours. Similar to PBD, several approaches have been used to overcome this problem. One successful strategy was the insertion of TPD into polymer matrices like PMMA, PS, polysulfone, polycarbonate, etc.¹⁷ However, blending was found to be occasionally affected by phase separation which limits the durability of the corresponding devices. Morphological stability can forcibly be obtained when TPD moieties are covalently attached as side groups to a polymer backbone or integrated in the backbone itself. Another approach to prevent crystallization induced degradation was the design of amorphous materials with high glass transition temperatures that enable the preparation of high quality and morphologically stable films. Besides simple molecular modifications by virtue of bridging, anellation, and substitution at the TPD scaffold,¹⁸ different structural patterns have been examined to provide the required properties.

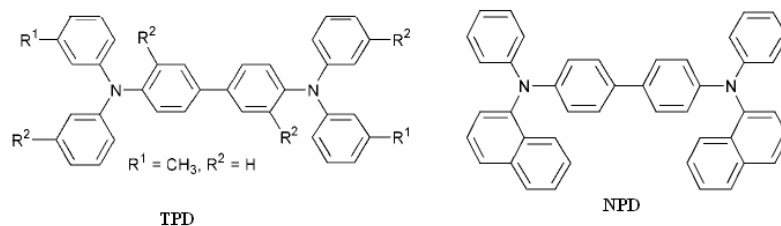


Figure 1.8 Structures of TPD and NPD.

1.5 Toward Efficient Single-Layer OLEDs.

Instead of bilayer or multilayer diodes with a separate ETM layer, an alternative strategy to achieving balanced charge injection and transport in OLEDs is through blending of an ETM with an emissive material. Although this approach has successfully been explored, the control of phase separation and morphology in such blends remains a challenge.¹⁹ Ideally, the functions of hole-transport, light emission, and electron-transport would be designed into one material, thereby facilitating balanced charge injection and transport in single-layer OLEDs. The electron-transport (n-type) moieties have been incorporated into emissive p-type organic materials and thereby creating essentially bipolar emissive materials. Bipolar small molecules based on n-type moieties such as oxadiazoles, dimesitylboryls, or benzothiadiazoles in combination with p-type triaryl amines or fluorenes have been reported.²⁰ The strategy of creating bipolar (or donor/acceptor) materials is more readily implemented by polymerization or copolymerization since the n-type moieties can be incorporated either directly into a p-type polymer backbone²¹ or as pendants to the main chain.²²

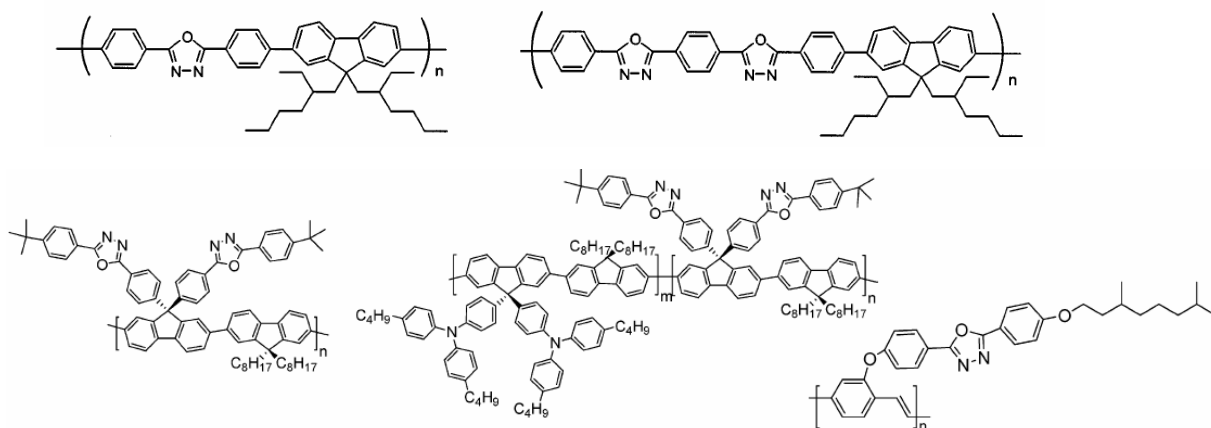


Figure 1.9 Examples of oxadiazole-containing electron-transporting polymers.

These copolymers highlight the potential of combining charge transport and emissive functionalities into one material for OLED applications. Achieving balanced hole and electron injection/transport in one material greatly simplifies device fabrication. However, judicious choice of the hole- and electron-transporting moieties is needed to obtain targeted emission colors from the copolymers, making design and synthesis of such multifunctional copolymers a challenging task for the materials chemist.

1.6 Poly(fluorenes)

In the past decade, fluorene-based conjugated polymers have emerged as a very outstanding class of blue-light emitting materials because of their high photoluminescence (PL) and electroluminescence (EL) quantum efficiencies, thermal stability, good solubility, high hole mobility, and facile functionalization at the C-9 position of fluorene.²³ However, devices are restricted by their tendency to form aggregates,²⁴ excimers,²⁵ or ketone defects²⁶ during either annealing or passage of

current, leading to red-shifted and less efficient emissions. To avoid this detrimental behavior, many studies have been carried out to solve the aggregation-related problems by increasing the structural hindrances of PFs, and thus to reduce their self-aggregation tendency in the solid state. For example, they can be distinguished and classified into one of the following several parts:

1. PFs containing long (or bulky) and branched side chains.²⁷

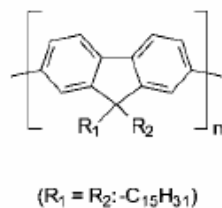


Figure 1.10 Example of poly(fluorene) containing long side chains.

2. Copolymerization techniques. The carbazole or thiophene units can be incorporated to polyfluorene derivatives. The introduction of a “kinked” disorder on the conjugated polymer chain to depress the aggregation phenomena and its effect on the excimer formation.²⁸

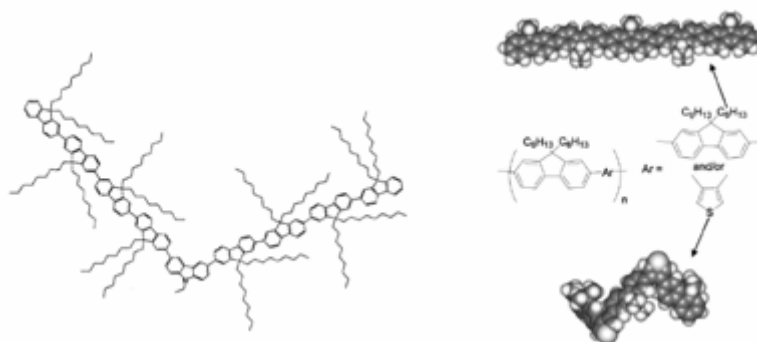


Figure 1.11 Examples of poly(fluorene)-based copolymers

3. The encapsulation of PF backbones into dendritic envelopes. The synthesis of a polyfluorene with dendrons as side chains have shown that the materials possess very

promising properties. It was shown that the chemical stability and the shape persistence of Fréchet or Müllen-type dendrimers allows an effective shielding of the polyfluorene backbone.²⁹

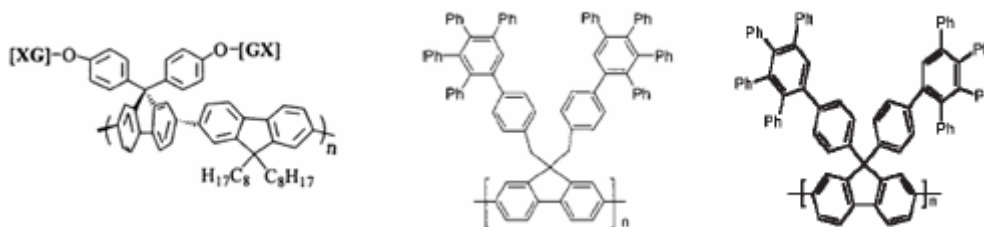


Figure 1.12 Examples of poly(fluorene) with dendrons as side chains

4. The end-capping of PFs with bulky groups. The end-capping of the main chain of a PF homopolymer with hole-transporting moieties (HTM) opens a way to blue LEDs with high efficiency and excellent color stability, without altering the electronic properties of the conjugated polymer backbone. Furthermore, the end-capping with HTM does not disturb the LC properties or the orientational abilities of the PF polymer.³⁰

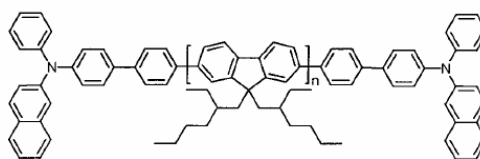


Figure 1.13 Example of end-capping of poly(fluorene) with bulky groups

6. Hyperbranched light-emitting polymers. It was shown that the introduction of branching unit into the PF to make the polymers with hyperbranched structure to avoid the excimer formation and to improve the charge transport-balance properties of PFs. The resulting hyperbranched polyfluorenes show stable blue light emission even in the air at the elevated temperatures.³¹

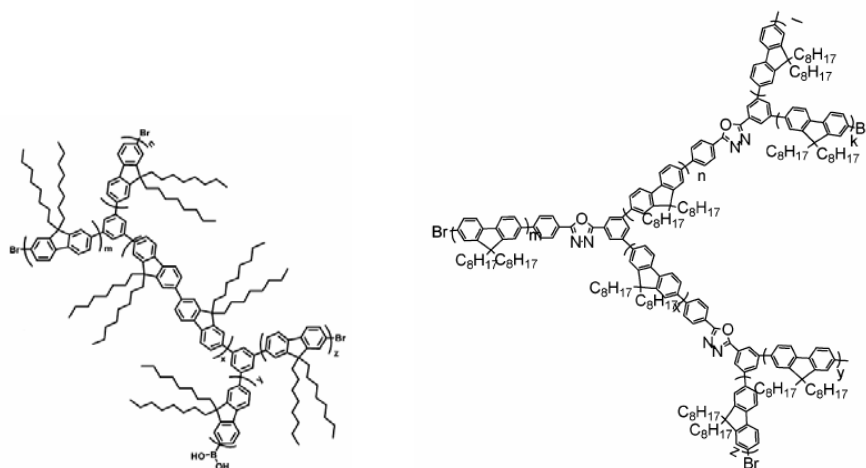


Figure 1.14 Examples of poly(fluorene)-based hyperbranched copolymers

On the other hand, another problem of PFs is their large band gaps between the LUMO and HOMO energy levels.³² The high energy-barrier between the emissive layer and the electrodes as well as the imbalance between the hole and electron transporting properties in the emissive layer are also possible to cause poor performance of a light-emitting diode (LED) device. In this regard, it is well recognized that the charge injection and transport can be facilitated by sandwiching the emissive layer between a hole-injecting/transporting layer (HTL) above the anode and an electron-injecting/transporting layer (ETL) under the cathode. An alternative approach addressing these issues is to vary the chemical structures of PFs. For example, the incorporation of electron-withdrawing or electron-donating groups into the PF main chains or side chains can influence the electron- or hole-injecting/-transporting capabilities of the polymers.^{22, 33}

Chapter 2

Synthesis and Characterization of

Poly(fluorene-*co-alt*-phenylene) Containing 1,3,4-Oxadiazole

Dendritic Pendants

2.1 Introduction

Organic light-emitting diodes (OLEDs) have the potential to achieve low-cost and full-color flat panel displays due to their merits of high brightness, easy fabrication, and wide ranges of emission colors. However, some important and fundamental challenges remain unsolved, including maximization of external quantum efficiencies (EQEs), design and synthesis of new materials with purer colors, and modes of addressing devices for a full-color display with optimized resolution. A major factor responsible for low device EQEs is that the charge (electron and hole) injection and transportation in emissive materials are generally unbalanced. In general, most of the electroluminescent (EL) polymers inject and transport holes more efficiently than electrons due to their inherent richness of π -electrons. One approach for improving electron transporting properties of polymers is to incorporate electron deficient segments into main chains³⁴ or as pendants attached to the backbones.^{22, 35} Oxadiazole (OXD) units are among the most widely investigated electron transporting structures for OLEDs, which are due to the high electron affinity of the OXD segments in OLED molecules. Several OXD-containing light-emitting polymers have also been prepared in recent years.³⁶

Dendronized polymers may exhibit superior properties in future applications as

compared to their non-dendronized analogues for a number of reasons. The dendritic side chains acting as solubilizers can enhance processability without the loss of mechanical or thermal stability provided by the rigid polymer backbones. The dense dendron decorations may provide efficient shields, such as protection against chemical reactants and prevention of molecular aggregation. In addition, the dendrons may serve, depending on their chemical nature, as light harvesting antennae, charge carriers, and so on.³⁷

In hopes of combining both excellent electron affinities and energy transfer (light antenna) properties into polymers, a new family of polyfluorene-*co-alt*-phenylenes carrying peripheral oxadiazole (OXD) functional dendrons attached to the 2- and 5-positions of the phenylene rings will be presented in this report. Thus, the dendritic wedges play both roles of efficient site isolation and excellent electron affinities. Especially, the enhanced PL emission properties of dendronized polymers were observed in contrast to those of analogous conjugated main-chain without dendritic pendants. Therefore, the light harvest of chromophores from the luminescence of the dendritic pendants by the light antenna design is more efficient than the direct excitation at the maximum absorption of light-emitting segments by an external light source.

2.2 Experimental Section

2.2.1 Measurements.

¹H NMR spectra were recorded on a Varian unity 300M Hz spectrometer using CDCl₃ solvent. Elemental analyses were performed on a HERAEUS CHN-OS RAPID elemental analyzer. Monomers **7-9** were characterized by ¹H NMR, elemental analyses, and FAB (or MALDI-TOF) mass spectroscopy. Transition temperatures were determined by differential scanning calorimetry (DSC, Perkin Elmer, Model: Diamond) with a heating and cooling rate of 10 °C/min. Thermogravimetric analysis (TGA) was conducted on a Du Pont Thermal Analyst 2100 system with a TGA 2950 thermogravimetric analyzer under a heating rate of 20 °C/min. Gel permeation chromatography (GPC) analysis was conducted on a Water 1515 separation module using polystyrene as a standard and THF as an eluant. UV-visible absorption spectra were recorded in dilute THF solutions (10⁻⁶ M) on a HP G1103A spectrophotometer, and fluorescence spectra were obtained on a Hitachi F-4500 spectrophotometer. Polymer solid films were spin-coated on quartz substrates from THF solutions with a concentration of 10 mg/ml. The relative photoluminescent quantum yields (Φ_{PL}) of the compounds in THF were determined using a solution of 9,10-diphenylanthracene as a standard (cyclohexane, Φ_{PL} = 0.90). Dilute sample solutions were used for the determinations (absorbance < 0.1). Values are calculated according to the equation, $\Phi_{\text{unk}} = \Phi_{\text{std}}(I_{\text{unk}}/A_{\text{unk}})(A_{\text{std}}/I_{\text{std}})(n_{\text{unk}}/n_{\text{std}})^2$, where Φ_{unk} is the fluorescence quantum yield of the sample, Φ_{std} is the fluorescence quantum yield of the standard, I_{unk} and I_{std} are the integrated emission intensities of the sample and the standard, respectively, A_{unk} and A_{std} are the absorbances of the sample and the standard at the excitation wavelength, respectively, and n_{unk} and n_{std} are the refractive indexes of the corresponding solutions (pure solvents were assumed). Cyclic voltammetry measurements of polymer films were performed on a BAS 100 B/W electrochemical

analyzer in acetonitrile with 0.1 M tetrabutylammonium hexafluorophosphate (TBAPF₆) as the supporting electrolyte at a scan rate of 100 mV/s. A polymer film on a glassy carbon disk electrode was used as the working electrode. A platinum wire was used as the counter electrode and a silver wire was used as the reference electrode. All preparations and measurements were carried out at room temperature under nitrogen. The potentials were measured against an Ag/Ag⁺ (0.01M AgNO₃) reference electrode with ferrocene as the internal standard. The onset potentials were determined by the intersection of two tangents drawn at the rising current and background current of the cyclic voltammogram.

2.2.2 Materials.

2,7-Bis(4,4,5,5-tetramethyl-1,3,2-dioxaborolane-2-yl)-9,9-dihexylfluorene (**10**), was synthesized according to literature procedures.³⁸ Chemicals and solvents were reagent grades and purchased from Aldrich, ARCROS, TCI, and Lancaster Chemical Co. Dichloromethane and tetrahydrofuran (THF) were distilled to keep anhydrous before use. The other chemicals were used without further purification.

4-Chloromethyl-benzoic acid N'-[4-(2-ethyl-hexyloxy)-benzoyl]-hydrazide (1). 0.57 g (3.02 mmol) of 4-chloromethyl-benzoyl chloride was added into a solution containing 0.40 g (1.51 mmol) of 4-(2-ethyl-hexyloxy)-benzoic acid hydrazide and 0.25 mL (3.02 mmol) of pyridine in 10 mL of N-methyl-2-pyrrolidinone (NMP). The reaction mixture was stirred for 12 h and then poured into water. Finally, the product was filtered and crystallized from methanol. Yield: 87%. ¹H NMR (ppm, CDCl₃): δ 0.90-0.97 (m, 6H), 1.33-1.56 (m, 8H), 1.80 (m, 1H), 3.99 (d, *J* = 5.7 Hz, 2H), 4.60 (s, 2H), 6.89 (d, *J* = 9 Hz, 2H), 7.43 (d, *J* = 8.1 Hz, 2H), 7.81 (d, *J* = 9 Hz, 2H), 7.85 (d, *J* = 8.4 Hz, 2H), 9.48 (d, *J* = 5.4 Hz, 1H), 9.81 (d, *J* = 5.4 Hz, 1H).

2-(4-Chloromethyl-phenyl)-5-[4-(2-ethyl-hexyloxy)-phenyl]-[1,3,4]oxadiazole

(2). 0.43 g (1.02 mmol) of **1** was dissolved in 10 mL of POCl₃. The reaction mixture was heated to reflux overnight and then cooled to room temperature. Most POCl₃ in reaction mixture was removed at reduced pressure. Later, water was added, and the aqueous layer was extracted with CH₂Cl₂. After drying of the organic layer and removal of the solvent under reduced pressure, the crude product was purified by column chromatography with CH₂Cl₂ to get a white solid. Yield: 76%. ¹H NMR (ppm, CDCl₃): δ 0.90-0.97 (m, 6H), 1.33-1.56 (m, 8H), 1.76 (m, 1H), 3.92 (d, *J* = 5.7 Hz, 2H), 4.64 (s, 2H), 7.03 (d, *J* = 9 Hz, 2H), 7.55 (d, *J* = 7.8 Hz, 2H), 8.06 (d, *J* = 8.7 Hz, 2H), 8.14 (d, *J* = 7.8 Hz, 2H).

General Synthetic Procedures of Dendritic Benzyl Alcohols (3 and 5). A mixture of **2** or **4** (2.1 equiv), 3,5-dihydroxybenzyl alcohol (1 equiv), K₂CO₃ (2.5 equiv), and 18-crown-6 (0.2 equiv) in dry THF was heated to reflux and stirred under nitrogen for 24 h. The mixture was evaporated to dry under reduced pressure, and the residue was partitioned between water and CH₂Cl₂. Then, the aqueous layer was extracted with CH₂Cl₂, and the organic layer was dried over MgSO₄. Finally, the crude products **3** and **5** were collected without further purification.

General Synthetic Procedures of Dendritic Benzyl Bromides (4 and 6). (OXD)₂-(G-1)-OH (**3**) or (OXD)₂-(G-2)-OH (**5**) was dissolved in THF under nitrogen, PBr₃ (1 equiv) was added dropwise via an addition funnel over 10 min at 0 °C. The mixture was heated to reflux for 30 min and evaporated to dryness under reduced pressure. The residue was partitioned between water and CH₂Cl₂. Then, the aqueous layer was extracted with CH₂Cl₂, and the organic layers dried over MgSO₄. Consequently, the crude products **4** and **6** were purified as outlined in the following text.

The First Generation of Benzyl Bromide (4). The (OXD)₂-(G-1)-Br (**4**) was purified by column chromatography with EA/CH₂Cl₂ (1:10) to get a white solid. Yield:

83%. ¹H NMR (ppm, CDCl₃): δ 0.90-0.98 (m, 12H), 1.24-1.56 (m, 16H), 1.75-1.79 (m, 2H), 3.93 (d, *J* = 5.7 Hz, 4H), 4.43 (s, 2H), 5.13 (s, 4H), 6.57 (s, 1H), 6.68 (s, 2H), 7.03 (d, *J* = 8.7 Hz, 4H), 7.58 (d, *J* = 8.7 Hz, 4H), 8.06 (d, *J* = 8.4 Hz, 4H), 8.15 (d, *J* = 8.4 Hz, 4H).

The Second Generation of Benzyl Bromide (6). The (OXD)₄-(G-2)-Br (**6**) was purified by column chromatography with THF/CH₂Cl₂ (1:10) to get a white solid. Yield: 85%. ¹H NMR (ppm, CDCl₃): δ 0.89-0.97 (m, 24H), 1.26-1.57 (m, 32H), 1.74-1.78 (m, 4H), 3.91 (d, *J* = 5.4 Hz, 8H), 4.40(s, 2H), 4.98 (s, 4H), 5.11 (s, 8H), 6.48 (s, 1H), 6.57(s, 2H), 6.60 (s, 2H), 6.67(s, 4H), 7.01 (d, *J* = 8.7 Hz, 8H), 7.55 (d, *J* = 8.4 Hz, 8H), 8.04 (d, *J* = 8.7 Hz, 8H), 8.11 (d, *J* = 8.1 Hz, 8H).

General Synthetic Procedure of Dendronized Monomers (7-9). A mixture of corresponding compound **2**, **4**, or **6** (2.1 equiv), 2,5-dibromo-benzene-1,4-diol (1 equiv), K₂CO₃ (2.5 equiv), and 18-crown-6 (0.2 equiv) in dry THF was heated to reflux and stirred under nitrogen for 48 h. The mixture was evaporated to dryness under reduced pressure, and the residue was partitioned between water and CH₂Cl₂. The aqueous layer was extracted with CH₂Cl₂, and the organic layers dried over MgSO₄. The crude product was purified as outlined in the following text.

Monomer 7. Monomer **7** was purified by column chromatography with EA/CH₂Cl₂ (1:10) to get a white solid. Yield: 75%. ¹H NMR (ppm, CDCl₃): 0.90-0.97 (m, 12H), 1.34-1.54 (m, 16H), 1.75-1.77 (m, 2H), 3.92 (d, 4H), 5.16 (s, 4H), 7.03 (d, 4H), 7.21 (s, 2H), 7.63 (d, 4H), 8.06 (d, 4H), 8.16 (d, 4H). Anal. Calcd for C₅₂H₅₆Br₂N₄O₆: C, 62.91; H, 5.69; N, 5.64. Found: C, 63.01; H, 5.73; N, 5.64. MS (FAB): *m/z* [M⁺] 993.20, calcd *m/z* 992.83.

Monomer 8. Monomer **8** was purified by column chromatography with EA/CH₂Cl₂ (1:6) to get a white solid. Yield: 78%. ¹H NMR (ppm, CDCl₃): 0.91-0.97 (m, 24H), 1.35-1.55 (m, 32H), 1.72-1.78 (m, 4H), 3.92 (d, 8H), 5.01 (s, 4H), 5.14 (s, 8H), 6.58

(s, 2H), 6.70 (s, 4H), 7.01 (d, 8H), 7.09 (s, 2H), 7.57 (d, 8H), 8.05 (d, 8H), 8.13 (d, 8H). Anal. Calcd for $C_{112}H_{120}Br_2N_8O_{14}$: C, 68.56; H, 6.16; N, 5.71. Found: C, 68.91; H, 6.27; N, 5.80. MS (MALDI-TOF): m/z [M^+] 1962.84, calcd m/z 1962.00.

Monomer 9. Monomer **9** was purified by column chromatography with EA/ CH_2Cl_2 (1:12) gradually increasing to EA/ CH_2Cl_2 (1:8) to get a white solid. Yield: 65%. 1H NMR (ppm, $CDCl_3$): 0.91-0.96 (m, 48H), 1.25-1.54 (m, 64H), 1.70-1.76 (m, 8H), 3.89 (d, 16H), 4.96 (s, 4H), 4.99 (s, 8H), 5.08 (s, 16H), 6.50 (s, 2H), 6.54 (s, 4H), 6.65 (s, 4H), 6.66 (s, 8H), 6.99 (d, 16H), 7.06 (s, 2H), 7.53 (d, 16H), 8.02 (d, 16H), 8.08 (d, 16H). Anal. Calcd for $C_{232}H_{248}Br_2N_{16}O_{30}$: C, 71.44; H, 6.41; N, 5.75. Found: C, 71.34; H, 6.50; N, 5.76. MS (MALDI-TOF): m/z [M^+] 3900.28, calcd m/z 3900.35.

General Synthetic Procedure of Dendronized Polymers P1-P3. A mixture of corresponding dendritic monomer **7**, **8**, or **9**, 2,7-bis(4,4,5,5-tetramethyl-1,3,2-dioxaborolane-2-yl)-9,9-dihexylfluorene (**10**), K_2CO_3 , toluene, and H_2O was degassed, and $Pd\{P(p\text{-tolyl})_3\}_3$ was added under a nitrogen atmosphere. The reaction mixture was heated to reflux and stirred under nitrogen for 48 h. End group capping was performed by heating the solution under reflux for 6 h sequentially with phenylboronic acid and iodobenzene. After cooling, the crude polymers were dissolved in THF and purified by precipitation from methanol, and dendronized polymers **P1-P3** were collected and dried under vacuum.

Dendronized Polymer P1.

2,7-Bis(4,4,5,5-tetramethyl-1,3,2-dioxaborolane-2-yl)-9,9-dihexylfluorene (**10**) (273.5 mg, 0.46 mmol), **7** (463 mg, 0.46 mmol), K_2CO_3 (1.1 g), $Pd\{P(p\text{-tolyl})_3\}_3$ (8.00 mg), toluene (10 mL), and H_2O (4 mL) were used in the reaction mixture. Polymer **P1** was obtained as a slightly yellow solid. Yield: 75%. 1H NMR (ppm, $CDCl_3$): 0.62-0.97 (m, 18H), 1.26-1.75 (m, 34H), 1.97(broad, 4H), 3.90 (d, 4H), 5.16 (s, 4H), 7.00 (d, 4H), 7.20 (s, 2H), 7.49 (d, 4H), 7.63 (broad, 4H), 7.83 (d, 2H), 8.03 (d, 4H), 8.09 (d, 4H).

Anal. Calcd for $[C_{77}H_{88}N_4O_6]_n$: C, 79.35; H, 7.61; N, 4.81. Found: C, 78.12; H, 7.56; N, 4.45.

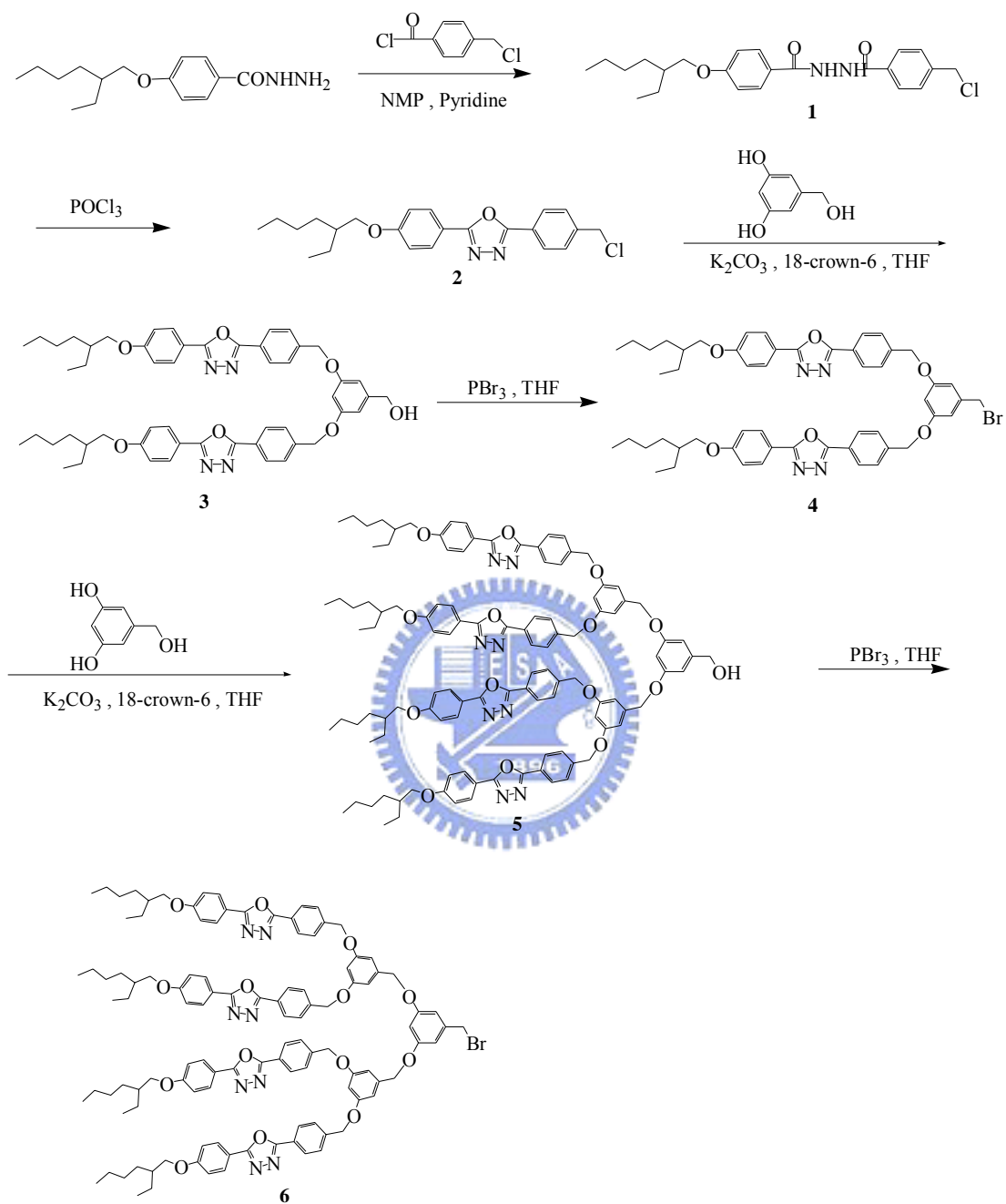
Dendronized Polymer P2.

2,7-Bis(4,4,5,5-tetramethyl-1,3,2-dioxaborolane-2-yl)-9,9-dihexylfluorene (**10**) (120 mg, 0.20 mmol), **8** (400 mg, 0.20 mmol), K_2CO_3 (1.1 g), $Pd\{P(p\text{-tolyl})_3\}_3$ (8.00 mg), toluene (10 mL), and H_2O (4 mL) were used in the reaction mixture. Polymer **P2** was obtained as a slightly yellow solid. Yield: 68%. 1H NMR (ppm, $CDCl_3$): 0.63-0.97 (m, 30H), 1.31-1.73 (m, 52H), 2.05(broad, 4H), 3.84-3.92 (broad, 8H), 4.89 (s, 8H), 5.10 (broad, 4H), 6.46 (s, 2H), 6.61 (s, 4H), 6.93-7.03 (broad, 10H), 7.42 (d, 8H), 7.74 (broad, 6H), 7.97-8.14 (broad, 16H). Anal. Calcd for $[C_{137}H_{152}N_8O_{14}]_n$: C, 77.08; H, 7.18; N, 5.25. Found: C, 75.99; H, 7.17; N, 4.67.

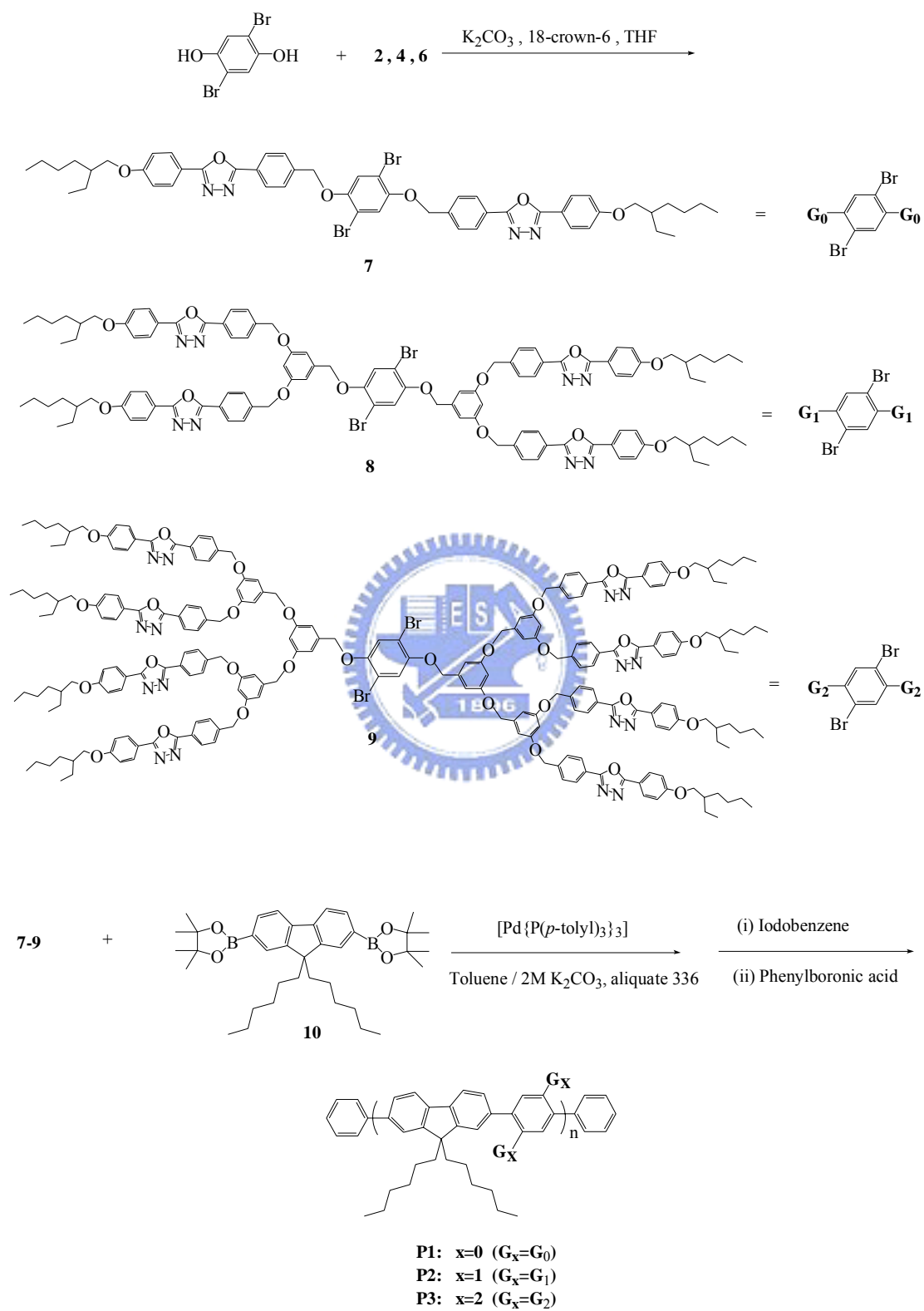
Dendronized Polymer P3.

2,7-Bis(4,4,5,5-tetramethyl-1,3,2-dioxaborolane-2-yl)-9,9-dihexylfluorene (**10**) (60 mg, 0.10 mmol), **9** (400 mg, 0.10 mmol), K_2CO_3 (1.1 g), $Pd\{P(p\text{-tolyl})_3\}_3$ (8.00 mg), toluene (10 mL), and H_2O (4 mL) were used in the reaction mixture. Polymer **P3** was obtained as a slightly yellow solid. Yield: 70%. 1H NMR (ppm, $CDCl_3$): 0.63-0.95 (m, 54H), 1.29-1.66 (m, 88H), 2.05(broad, 4H), 3.80-3.89 (broad, 16H), 4.88 (broad, 28H), 6.44-6.59 (broad, 18H), 6.87-6.98 (broad, 18H), 7.39-7.57 (broad, 22H), 7.88-8.07 (broad, 32H). Anal. Calcd for $[C_{257}H_{280}N_{16}O_{30}]_n$: C, 75.78; H, 6.93; N, 5.50. Found: C, 74.75; H, 6.91; N, 5.05.

Scheme 2.1 The synthetic route of dendritic benzyl bromides 4 and 6



Scheme 2.2 The synthetic route of monomers 7-9 and polymers P1-P3



2.3 Results and Discussion

2.3.1 Synthesis and Characterization.

The synthetic routes of monomers **7-9** and polymer **P1-P3** are shown in Scheme 2.1 and Scheme 2.2. 2-(4-Chloromethyl-phenyl)-5-[4-(2-ethyl-hexyloxy)-phenyl]-[1,3,4]oxadiazole (**2**) was firstly prepared according to the literature procedure.³⁹ In the beginning, acylation of 4-(2-ethyl-hexyloxy)-benzoic acid hydrazide with 4-chloromethyl-benzoyl chloride was followed by cyclodehydration of acylated hydrazide in the presence of POCl₃. Dendritic benzylic alcohol (**3**) of functionalized first-generation (G1) was prepared by the Williamson ether reaction of 3,5-dihydroxybenzyl alcohol with the corresponding functionalized benzyl chloride (**2**) in the presence of K₂CO₃ and 18-crown-6. A subsequent reaction of compound **3** with PBr₃ afforded dendritic benzylic bromide (**4**) of functionalized G1. An iterative Williamson ether reaction of 3,5-dihydroxybenzyl alcohol with dendritic benzylic bromide (**4**) of functionalized G1 produced the corresponding dendritic benzylic alcohol (**5**) of functionalized second-generation (G2), which reacted with PBr₃ to give the corresponding dendritic benzylic bromide (**6**) of functionalized G2. In the presence of K₂CO₃ in THF at reflux, 2,5-Dibromo-benzene-1,4-diol with the corresponding different generation dendrons was achieved to obtain the monomers (**7-9**), which was then copolymerized with 2,7-bis(4,4,5,5-tetramethyl-1,3,2-dioxaborolane-2-yl)-9,9-dihexylfluorene (**10**) using the Suzuki coupling. In the beginning, when Pd(PPh₃)₄ was used as a catalyst precursor, polymer **P3** could not be obtained due to the shielding effect of monomer **9** on the reactive site, so Pd{P(*p*-tolyl)₃}₃ seems to be a superior choice in many SPC cases.⁴⁰ Freshly prepared Pd{P(*p*-tolyl)₃}₃ was used as the catalyst precursor⁴¹ with aliquate 336 as the phase-transfer reagent in a biphasic system (toluene/aqueous K₂CO₃), to give alternating copolymers **P1-P3**. All dendronized polymers could be

fully dissolved in common organic solvents, such as methylene chloride, chloroform, toluene, and THF. The molecular weights of polymers determined by GPC using polystyrene standards are summarized in Table 2.1. GPC analysis showed that the weight-average molecular weights (M_w) and polydispersity indexes (PDI) of the dendronized polymers are in the range of $(3.3-4.4) \times 10^4$ and 1.4-2.4, respectively. The data reveal that the degree of polymerization decreases as the size of the dendritic monomer increases. The same observation was also reported in the synthesis of similar dendronized polymers.²⁹ The thermal properties of the dendronized polymers were investigated using thermogravimetric analysis (TGA) and differential scanning calorimetry (DSC), and the results are presented in Table 2.1. All polymers exhibit good thermal stability, where less than 5% of weight-loss decompositions at ca. 310-353 °C under nitrogen but more than 50% of weight-loss decompositions at 450-460 °C (Figure 2.1) were observed. The glass transition temperatures (T_g) of the dendronized polymers are in the range of 77-122 °C, which are declined by increasing the size of the attached dendrons. Compared with a previous report, T_g s of dendronized polymers **P1-P3** are higher than that of poly[(9,9-dihexylfluorene)-*alt*-co-(2,5-dihexyl-2,5-phenylene)] ($T_g = 50$ °C) or poly[(9,9-dihexylfluorene)-*alt*-co-(2,5-dihexyloxy-1,4-phenylene)] ($T_g = 72$ °C).⁴²

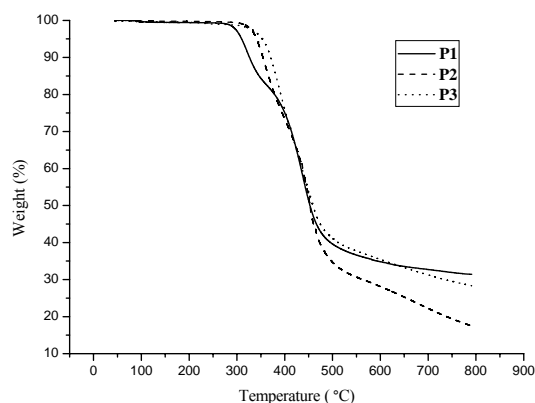


Figure 2.1 TGA traces of polymers **P1-P3**.

Table 2.1 Molecular Weights and Thermal Properties of Polymers P1-P3

Polymer	M_n^a	M_w^a	PDI ^a	T_g^b (°C)	T_d^c (°C)
P1	17500	42000	2.4	122	310
P2	24100	44300	1.8	94	341
P3	24000	33500	1.4	77	353

^a Molecular weights determined by GPC in THF, based on polystyrene standards.
(PDI = M_w/M_n)

^b Glass transition temperature (°C) determined by DSC at a heating rate of 10 °C min⁻¹.

^c Temperature (°C) at 5% weight loss measured by TGA at a heating rate of 20 °C min⁻¹ under nitrogen.

2.3.2 Optical Properties

The spectroscopic properties of polymers **P1-P3** were measured in both solutions (THF) and solid films. The optical properties of polymers **P1-P3** are summarized in Table 2.2. The dendronized polymers show very similar absorption and emission characteristics in THF. As shown in Figure 2.2, polymers in THF solutions exhibit the absorption peak at ca. 300 nm whose intensities increase with the generation number, which are due to the absorption of the peripheral OXD moieties. This result further confirms the accomplishment of various generations of OXD dendrimers. The additional absorption peak at ca. 367 nm is assigned to the π - π^* transition contributed from the conjugated backbones of the polymers, which is not affected by the generation of dendronized polymers.

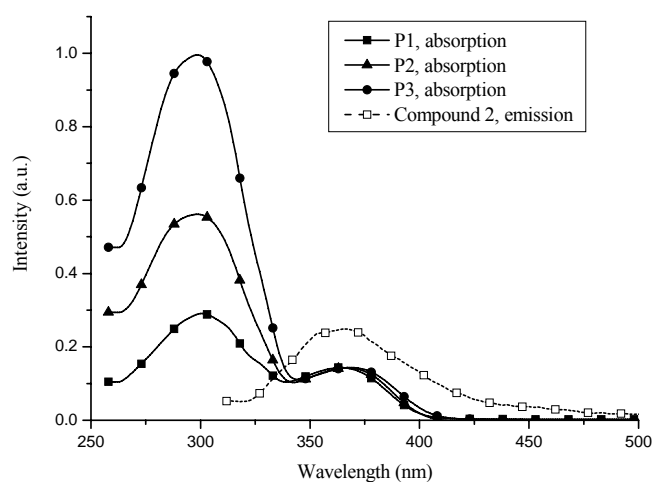


Figure 2.2 Normalized UV-vis absorption spectra of polymers **P1-P3** and the PL emission spectrum of compound **2** in THF, the absorption spectra are normalized at the absorption peaks of polymer backbones ca. 367 nm.

Upon excitation of the backbones of polymers **P1-P3** at 367 nm, the PL emission spectra display the value of λ_{max} at ca. 414 nm. The PL spectra in THF are almost identical for polymers **P1-P3** as shown in Figure 2.3. In contrast to dilute solutions (in THF), the absorption spectra of the polymers in solid films are similar (a little red-shifted) to those in solutions. Optical band gaps (E_g) determined from the absorption edges of the UV-vis spectra of polymers **P1-P3** in solid films are found to be 3.03 eV. The PL emission spectra of polymers **P1-P3** in solid films are only 4-7 nm bathochromically red shifted compared with those in solutions. Especially, due to the stronger aggregation in the solid films of the lowest generation polymer, **P1** containing the smallest dendron size show a more obvious shoulder and followed by a long featureless tail (extending into the red region) than the higher generation polymers **P2** and **P3** (Figure 2.4). It can be concluded that the higher generation polymers have more site-isolation or dilution effects due to the larger size of the dendrons. A previous paper reported that various lengths of alkoxy side chains in

poly[(9,9-dihexylfluorene)-*alt*-co-1,4-phenylene)] (PDHFP) were attached to the phenylene rings of the backbones and the full width at half-maximum (fwhm) values of these polymers strongly depend on the lengths of the attached alkoxy side chains.⁴³ The fwhm value decreases from 62 nm in PDHFP (without any side chain on the phenylene ring) to 46 nm in PDHFDDOP (longer side chains of -OC₁₀ on the phenylene ring). It explained that the smaller fwhm value of the polymers with longer side chains were due to the emission resulting from more isolated main-chain fluorophores. Thus, the fwhm values of the emission curves in solid films of dendronized polymers **P1-P3** are also quite narrow (44-45nm) to yield purer blue light emission due to their outstanding site-isolation effect. In addition, compared with PDHFP, the vibronic structures in PL emissions of **P2** and **P3** are remarkably reduced and no noticeable spectral shoulder above 500 nm is observed.

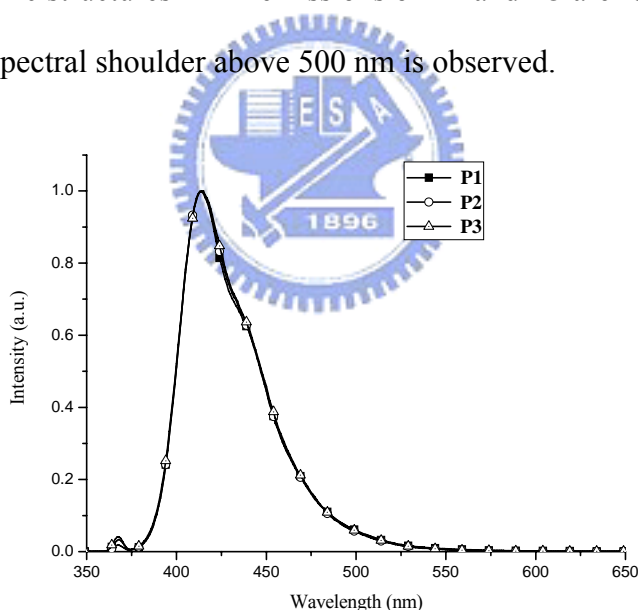


Figure 2.3 Normalized PL spectra of polymers **P1-P3** in THF.

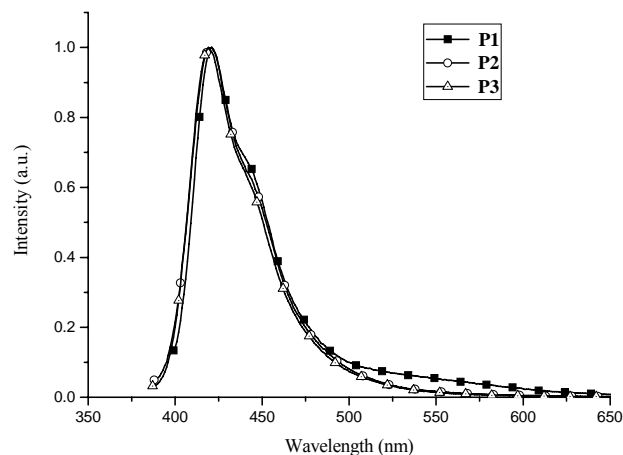
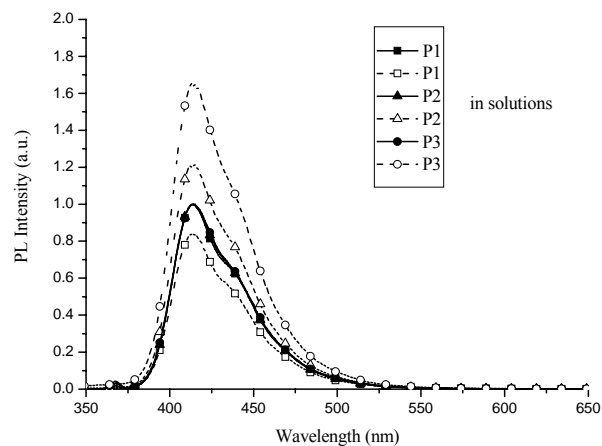


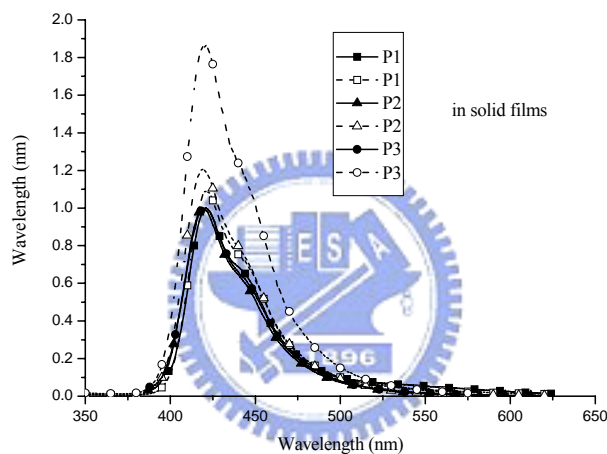
Figure 2.4 Normalized PL spectra of polymers **P1-P3** in solid film.

As comparing the PL emission spectrum of model compound **2** and the absorption spectra of dendronized polymers **P1-P3** in THF (Figure 2.2), the overlap of OXD emission peak (363 nm) and **P1-P3** backbones absorption peaks (ca. 367 nm) is extremely large. The large spectral overlap between the two interacting chromophores indicates that the probability of donor-acceptor energy transfer should be high. The energy transfer efficiency (ETE) of the dendritic wedge is estimated by the intensity ratio between the maximum absorption of OXD dendrons in the absorption spectrum and that in the fluorescence excitation spectrum.⁴⁴ According to this estimation, the energy transfer efficiencies of various generations of OXD dendrons are 59%, 43%, and 49% for **P1**, **P2**, and **P3**, respectively. It was consistently found that the energy transfer efficiency decreased as the generation (i.e. the size) of the surface-functionalized poly(benzyl ether)-type dendritic wedge increased. Upon excitation either at OXD dendrons or polymer backbones of polymers **P1-P3** in THF, the obtained PL emission spectra are identical as shown in Figure 2.5(a). The almost complete disappearance of OXD emission at 363 nm indicates that energy transfer efficiency is extremely high in these molecules. A comparison between the PL

emission intensity from the sensitized excitation (excited at the maximum absorption of OXD dendrons) and that from the direct excitation (excited at the maximum absorption of the polymer backbones) of dendronized polymers, **P2** and **P3** gain more intense PL backbone emissions by the sensitized excitation from the energy transfer of OXD dendrons than those by the direct excitation from the absorption of chromophore backbones. This indicates that the overall fluorescence of these dendronized polymers **P1-P3** result not only from the contribution of the polymer backbones but also from that of the peripherally dendritic OXD units. In addition, the OXD-functionalized dendritic wedges are very efficient light-harvesting moieties for funneling energy to the polymer backbones. As shown in Figure 2.5(b), the excitations of the peripherally OXD moieties of dendronized polymers **P1-P3** in solid films result in similar fluorescence patterns as those excited at the maximum absorption of polymer backbones alone. Especially, the PL emission intensities by the sensitized excitations of OXD dendrons in solid films of polymers **P1-P3** are all stronger than those by the direct excitations of their polymer conjugated backbones. Actually, the PL emission intensity of polymer **P3** in solid film excited at peripheral OXD dendrons is about 86% higher than that excited at the backbones. In general, similar effects were commonly described for dye-labeled dendrimers.⁴⁵ However, the result demonstrates that the dendronized polymers may show stronger emissions through efficient energy transfer from peripheral dendrons to emitting backbones.



(a)



(b)

Figure 2.5 PL Emission spectra of polymers **P1-P3** (a) in solutions (THF) and (b) in solid films, which were excited at the maximum absorption of the polymer backbones (for solid symbols) and the polymer periphery OXD dendrons (for open symbols).

As listed in Table 2.2, the PL quantum yields (Φ_F) of polymers **P1-P3** in THF solutions were measured with 9,10-diphenylanthracene as a reference standard⁴⁶ (cyclohexane, $\Phi_F = 0.9$), and the highest quantum yield reaches 0.87. The PL quantum yields in solid films were measured using the same standard in poly-(methyl methacrylate).⁴⁷ The shielding effect of the dendritic side chains on the polymer

backbones is also reflected on the emission efficiency of the dendronized polymers. Although this relative method can only give an estimation of the fluorescence quantum yields of the polymers, the data still indicate that the fluorescence quantum yields of the polymers depend on the sizes of the attached dendrons, i.e. the larger the dendrons, the higher the PL quantum yields. Therefore, the second generation of dendronized polymer **P3** in the solid film shows the highest quantum yield, which is attributed to the minimization of the self-quenching by attaching bulky pendent dendrons on the polymer backbones.

Table 2.2 Absorption and PL Emission Spectral Data of Polymers P1-P3 in THF and Solid Films

Polymer	$\lambda_{\text{abs,sol}}$ (nm)	$\lambda_{\text{abs,film}}$ (nm)	Band gap ^a (eV)	$\lambda_{\text{PL,sol}}$ (nm)	$\lambda_{\text{PL,film}}$ (nm)	Fwhm _{PL,film} (nm)	$\Phi_{\text{PL,sol}}$ ^b	$\Phi_{\text{PL,film}}$ ^c
P1	301,364	323,388	3.03	414	421	44	0.60	0.08
P2	300,367	322,380	3.03	414	421	45	0.87	0.18
P3	300,367	321,376	3.03	415	419	44	0.82	0.26

^a Band gaps were calculated from the onsets of UV-visible absorption spectra of **P1-P3** in solid films.

^b Solution fluorescence quantum efficiency measured in THF, relative to 9,10-diphenylanthracene ($\Phi_{\text{PL}} = 0.90$).

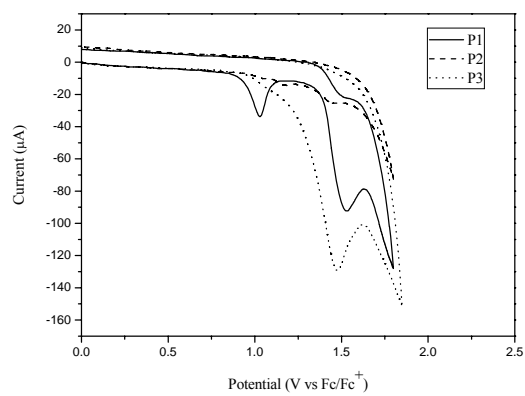
^c PL quantum efficiency estimated relative to 9,10-diphenylanthracene in poly(methyl methacrylate) as a standard ($\Phi_{\text{PL}} = 0.83$).

2.3.3 Electrochemical Properties.

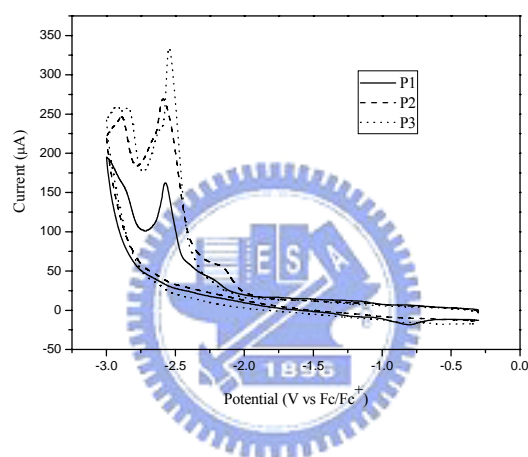
Cyclic voltammetry measurements were carried out to determine the energies of the highest occupied molecular orbital (HOMO) and the lowest unoccupied molecular orbital (LUMO) of polymers **P1-P3**. Their HOMO, LUMO, and electrochemical properties of polymers are summarized in Table 2.3. As shown in Figure 2.6, polymers **P1-P3** almost show identical behavior during anodic and cathodic scans due to the same backbone structure of poly(fluorene-*co-alt*-phenylene) with different generations of OXD dendrons. In the cyclic voltammogram of polymer **P1**, the difference between the anodic and cathodic onset potentials is 3.00 V, which implies that the π - π^* band gap of the polymer is 3.00 eV. The data is similar to that obtained from the absorption edge of the UV-vis spectrum. With regard to the energy level of the ferrocene reference (4.8 eV below the vacuum level),⁴⁸ the HOMO and LUMO energy levels of polymer **P1** were estimated to be -5.73 and -2.73 eV, respectively. Besides, the HOMO and LUMO energy levels of polymer **P1-P3** are similar to that reported for poly(9,9-dihexylfluorene-*co-alt*-2,5-didecyloxy-*para*-phenylene).⁴⁹

Table 2.3 HOMO and LUMO Energies, and Electrochemical Properties of Polymers P1-P3

polymer	$E^{\text{red/onset}}$ (V)	$E^{\text{red/peak}}$ (V)	$E^{\text{ox/onset}}$ (V)	E^{HOMO} (eV)	E^{LUMO} (eV)	E_g (eV)
P1	-2.07	-2.57	0.93	-5.73	-2.73	3.00
P2	-2.01	-2.58	0.94	-5.74	-2.79	2.95
P3	-2.03	-2.54	0.93	-5.73	-2.77	2.96



(a)



(b)

Figure 2.6. Cyclic voltammetry of polymers **P1-P3** during (a) the oxidation processes and (b) the reduction processes.

2.4 Conclusion

A series of novel poly(fluorene-*co-alt*-phenylene)s containing different generations of dendronized side chains, including Fréchet-type poly(aryl ether) dendrons and functional peripheral OXD groups were synthesized. The resulting polymers possess good thermal stability and excellent solubility in common organic solvents. The emission spectral quality (narrow fwhm and reduced tail) can be improved by inserting bulky OXD dendrons as side chains of polymers because of less molecular close stacking. In addition, it also demonstrated that the peripheral OXD dendrons have specific light-antenna and enhanced backbone luminescence properties. The PL emission intensities by the sensitized excitations of OXD dendrons in solid films of polymers **P1-P3** are all stronger than those by the direct excitations of their polymer conjugated backbones.



Chapter 3

Synthesis and Characterization of Poly(fluorene)-Based Copolymers Containing Various 1,3,4-Oxadiazole Dendritic Pendants

3.1 Introduction

To reduce the formation of excimers and the aggregation of emitters, dendronized polymers are a promising approach to be used as multi-functional light-emitting materials. The dendrons not only protect the polymer rods from both aggregation and degradation but also tune unbalanced carrier-transporting properties, where proper charge-transporting functionalities are incorporated to the periphery of the dendrons.⁵⁰ Furthermore, the peripheral donor units can transfer excitation energy to the polymer backbones and enhance fluorescent properties. Here, we report a family of dendronized poly(fluorene)s bearing OXD units on the outer surface of poly(aryl ether) dendritic wedges. To determine the minimal steric requirements for prevention of aggregation, we prepared polymers bearing OXD side chains with three generations of dendrons. We hope the dendronized polymers can take advantage of the bulky OXD pendants to avoid the tendency of spontaneous aggregation and crystallization normally encountered in polyfluorenes, so as to show specific light-antenna capacity and tunable charge-transporting characteristics. On the other hand, the previous research²² reported that the ionization potential of polyfluorene with pendant OXD units is 5.76 eV, which is similar to that of poly(9,9-dioctyl-fluorene) (5.8 eV). This means that there is a

significant energy barrier for hole injection and it needs to be improved in order to further enhance the device performance. It is well-known that the carbazole (CAZ) unit reduces the hole-injection barrier in polyfluorene thus to facilitate hole injection from ITO electrodes. For this reason, we also introduce hole-transporting CAZ groups to the PF backbones as pendants for a comparative investigation. The absorption, PL emission, as well as EL spectra were also studied to gain the insight in the interaction between peripheral units and polyfluorene backbones.



3.2 Experimental Section

3.2.1 Measurements.

¹H NMR spectra were recorded on a Varian unity 300 MHz spectrometer using CDCl₃ solvent. Elemental analyses were performed on a HERAEUS CHN-OS RAPID elemental analyzer. Transition temperatures were determined by differential scanning calorimetry (Perkin-Elmer Diamond) with a heating and cooling rate of 10 °C/min. Thermogravimetric analysis (TGA) was conducted on a Du Pont Thermal Analyst 2100 system with a TGA 2950 thermogravimetric analyzer under nitrogen with a heating rate of 20 °C/min. Gel permeation chromatography (GPC) analysis was conducted on a Water 1515 separation module using polystyrene as a standard and THF as an eluant. UV-visible absorption spectra were recorded in dilute chloroform solutions (10⁻⁶ M) on a HP G1103A spectrophotometer, and fluorescence spectra were obtained on a Hitachi F-4500 spectrophotometer. PL excitation and emission slits in solution were 5 nm and 2.5 nm, respectively. PL excitation and emission slits in thin films were both 5 nm. Electrochemistry measurements were performed using an Autolab PGSTAT30 potentiostat/galvanostat with a standard three-electrode electrochemical cell containing a 0.1 M tetrabutylammonium hexafluorophosphate solution in acetonitrile at room temperature under nitrogen at a scanning rate of 100 mV/s. A platinum working electrode, platinum wire counter electrode, and an Ag/AgCl reference electrode were used. The onset potentials were determined from the intersection of two tangents drawn at the rising current and background current of the cyclic voltammogram. Polymer thin films were spin-coated on quartz substrates from THF solutions with a concentration of 10 mg/ml.

3.2.2 EL Device Fabrication.

The devices were fabricated on ITO substrates that had been ultrasonicated and sequentially washed in detergent, methanol, 2-propanol, and acetone, and further treated with O₂ plasma for 10 min before use. A thin layer of PEDOT (40 nm) and polymers (70-100 nm) (from a 15 mg/mL solution of the polymers in dichloroethane solution) was spin-coated on the ITO surface, after which a thin layer of LiF(1 nm)/Al(100 nm) was deposited on the polymer film by thermal evaporation under a vacuum of 10⁻⁶ Torr. The luminance-current-voltage characteristics were recorded on a power source (Keithley 2400) and photometer (MINOLTA CS-100A).

3.2.3 Materials.

2,7-Bis(4,4,5,5-tetramethyl-1,3,2-dioxaborolan-2-yl)-9,9-dihexylfluorene (**10**)³⁸ and 9,9-bis(4-carbazol-9-ylhexyl)-2,7-dibromofluorene (**14**)^{36(c)} were synthesized according to the literature procedures. Chemicals and solvents were reagent grades and purchased from Aldrich, Acros, TCI, and Lancaster Chemical Co. Dichloromethane and THF were distilled to keep anhydrous before use. The other chemicals were used without further purification.

General Procedure for the Synthesis of Dendronized Macromonomers 11-13. A mixture of 2,7-dibromofluorene and triethylbenzylammonium chloride (TEBAC) in THF was degassed three times; a 50 wt % aqueous KOH solution was added and stirred for 10 min under nitrogen. To this mixture, the solution of **2** (or **4** or **6**) was added in degassed THF under nitrogen; the reaction mixture was stirred under nitrogen for 10 h, water was added, and the aqueous layer was extracted with CH₂Cl₂. The combined organic phases

were dried over MgSO_4 . After removal of the solvent, the crude product was purified as outlined in the following text.

Macromonomer 11. 2,7-Dibromofluorene (0.13 g, 0.39 mmol), TEBAC (3.0 mg, 0.01 mmol), THF (140 mL), aqueous KOH solution (2 mL, 50 wt %), and compound **2** (0.33 g, 0.82 mmol) were used. Chromatography on silica gel eluted with CH_2Cl_2 afforded **11** as a white solid (0.41 g, 62%). ^1H NMR (ppm, CDCl_3): 0.87-0.94 (m, 12H), 1.24-1.53 (m, 16H), 1.69-1.75 (m, 2H), 3.46 (s, 4H), 3.88 (d, $J = 5.7$ Hz, 4H), 6.76 (d, $J = 8.7$ Hz, 4H), 6.97 (d, $J = 9.0$ Hz, 4H), 7.16 (d, $J = 8.1$ Hz, 2H), 7.35 (dd, $J = 1.5, 8.4$ Hz, 2H), 7.66-7.70 (overlap, 6H), 7.97 (d, $J = 9.0$ Hz, 4H). MS (FAB): m/z [M^+] 1049.3, calcd m/z [M^+] 1048.94. Anal. Calcd. for $\text{C}_{59}\text{H}_{60}\text{Br}_2\text{N}_4\text{O}_4$: C 67.56, H 5.77, N 5.34. Found: C 67.42, H 5.69, N 5.26.

Macromonomer 12. 2,7-Dibromofluorene (0.13 g, 0.39 mmol), TEBAC (3.0 mg, 0.01 mmol), THF (140 mL), aqueous KOH solution (2 mL, 50 wt %), and compound **4** (0.76 g, 0.82 mmol) were used. Chromatography on silica gel eluted with EA/ CH_2Cl_2 (2:1) afforded **12** as a white solid (0.51 g, 65%). ^1H NMR (ppm, CDCl_3): 0.91-0.97 (m, 24H), 1.34-1.53 (m, 32H), 1.72-1.78 (m, 4H), 3.19 (s, 4H), 3.92 (d, $J = 5.4$ Hz, 8H), 4.82 (s, 8H), 5.91 (s, 4H), 6.29 (s, 2H), 7.02 (d, $J = 9.0$ Hz, 8H), 7.26 (d, $J = 8.1$ Hz, 2H), 7.41 (d, $J = 8.1$ Hz, 2H), 7.48 (d, $J = 8.4$ Hz, 8H), 7.58 (s, 2H), 8.05 (d, $J = 9.0$ Hz, 8H), 8.11 (d, $J = 8.1$ Hz, 8H). MS (MALDI-TOF): m/z [M^+] 2018.78, calcd m/z [M^+] 2018.11. Anal. Calcd. for $\text{C}_{119}\text{H}_{124}\text{Br}_2\text{N}_8\text{O}_{12}$: C 70.82, H 6.19, N 5.55. Found: C 70.88, H 6.27, N 5.57.

Macromonomer 13. 2,7-Dibromofluorene (0.04 g, 0.1 mmol), TEBAC (0.6 mg), THF (90 mL), aqueous KOH solution (2 mL, 50 wt %), and compound **6** (0.46 g, 0.24 mmol) were used. Chromatography on silica gel eluted with THF/ CH_2Cl_2 (1:5) afforded **13** as a

white solid (0.22 g, 55%). ^1H NMR (ppm, CDCl_3): 0.89-0.96 (m, 48H), 1.29-1.56 (m, 64H), 1.68-1.76 (m, 8H), 3.08 (s, 4H), 3.89 (d, $J = 5.7$ Hz, 16H), 4.70 (s, 8H), 5.03 (s, 16H), 5.87 (s, 4H), 6.32 (s, 2H), 6.48 (s, 4H), 6.60 (s, 8H), 6.99 (d, $J = 8.4$ Hz, 16H), 7.22 (d, $J = 7.8$ Hz, 2H), 7.32 (d, $J = 8.1$ Hz, 2H), 7.43 (s, 2H), 7.51 (d, $J = 7.8$ Hz, 16H), 8.01 (d, $J = 8.4$ Hz, 16H), 8.07 (d, $J = 8.1$ Hz, 16H). MS (MALDI-TOF): m/z [M^+] 3957.87, calcd m/z [M^+] 3956.46. Anal. Calcd. for $\text{C}_{239}\text{H}_{252}\text{Br}_2\text{N}_{16}\text{O}_{28}$: C 72.55, H 6.42, N 5.66. Found: C 72.65, H 6.41, N 5.73.

General Procedure for the Synthesis of Dendronized Polymers P4-P9. The synthetic route of polymers is shown in Scheme 3.2. A general procedure of polymerization is proceeded through the Suzuki coupling reaction. For polymers **P4-P6**, a mixture of 2,7-bis(4,4,5,5-tetramethyl-1,3,2-dioxaborolan-2-yl)-9,9-dihexylfluorene (**10**) (1 equiv), monomer **11** (or **12** or **13**) (1 equiv), and freshly prepared $\text{Pd}\{\text{P}(p\text{-tolyl})_3\}_3$ (1.0 mol %) were added in a degassed mixture of toluene ([monomer] = 0.2 M) and aqueous 2 M potassium carbonate (3:2 in volume). The mixture was vigorously stirred at 80 °C for 72 h. After the mixture was cooled to room temperature, it was poured into 200 mL of methanol. A fibrous solid was obtained by filtration. The solid was washed sequentially with methanol, water, and methanol. A similar procedure is carried out for the synthesis of **P7-P9**, and the feed ratio of 2,7-bis(4,4,5,5-tetramethyl-1,3,2-dioxaborolan-2-yl)-9,9-dioctylfluorene (**10**) / **11** (or **12** or **13**) / 9,9-bis(4-carbazol-9-ylhexyl)-2,7-dibromofluorene (**14**) is 2/1/1. The actual m/n ratio of the resulting polymers **P7-P9** is about 1:1, which is calculated from proton NMR.

P4 (GO-OXD). Yield: 87%. ^1H NMR (ppm, CDCl_3): 0.79–0.95 (m, 22H), 1.16–1.49 (m, 28H), 1.72–1.74 (m, 2H), 2.16 (br, 4H), 3.67 (br, 4H), 3.89 (d, 4H), 6.99-7.02 (m,

8H), 7.61-7.81 (m, 16H), 8.03 (d, $J = 8.4$ Hz, 4H). Anal. Calcd for $C_{84}H_{92}N_4O_4$: C, 82.58; H, 7.59; N, 4.59. Found: C, 81.71; H, 7.56; N, 4.06.

P5 (G1-OXD). Yield: 83%. 1H NMR (ppm, $CDCl_3$): 0.64–0.94 (m, 34H), 1.32–1.49 (m, 44H), 1.70–1.72 (m, 4H), 2.09 (br, 4H), 3.40 (br, 4H), 3.86 (d, $J = 5.4$ Hz, 8H), 4.77 (s, 8H), 6.12 (s, 4H), 6.36 (s, 2H), 6.96 (d, $J = 9.0$ Hz, 8H), 7.32 (d, $J = 7.5$ Hz, 8H), 7.64 (m, 12H), 7.99 (d, $J = 9.0$ Hz, 16H). Anal. Calcd for $C_{144}H_{156}N_8O_{12}$: C, 78.94; H, 7.18; N, 5.11. Found: C, 78.21; H, 7.23; N, 4.61.

P6 (G2-OXD). Yield: 80%. 1H NMR (ppm, $CDCl_3$): 0.64–0.94 (m, 58H), 1.29–1.44 (m, 76H), 1.68 (m, 8H), 2.05 (br, 4H), 3.40 (br, 4H), 3.82 (d, 16H), 4.80 (m, 24H), 6.36-6.48 (m, 18H), 6.92 (d, $J = 8.1$ Hz, 16H), 7.35 (d, $J = 8.7$ Hz, 16H), 7.64 (m, 12H), 7.92 (d, $J = 9.0$ Hz, 32H). Anal. Calcd for $C_{264}H_{284}N_{16}O_{28}$: C, 76.79; H, 6.93; N, 5.43. Found: C, 75.73; H, 7.01; N, 4.74.

P7 (G0-OXDCAZ). Yield: 80%. 1H NMR (ppm, $CDCl_3$): 0.77–1.11 (m, 36H), 1.30–1.59 (m, 48H), 1.71 (m, 6H), 2.08 (br, 12H), 3.63 (br, 4H), 3.88 (d, 4H), 4.16 (t, 4H), 6.99 (d, $J = 9.0$ Hz, 8H), 7.18 (t, 4H), 7.27-7.38 (m, 8H), 7.64-7.81 (m, 28H), 8.00-8.06 (m, 8H). Anal. Calcd for $C_{158}H_{170}N_6O_4$: C, 85.59; H, 7.73; N, 3.79. Found: C, 83.78; H, 7.65; N, 3.41.

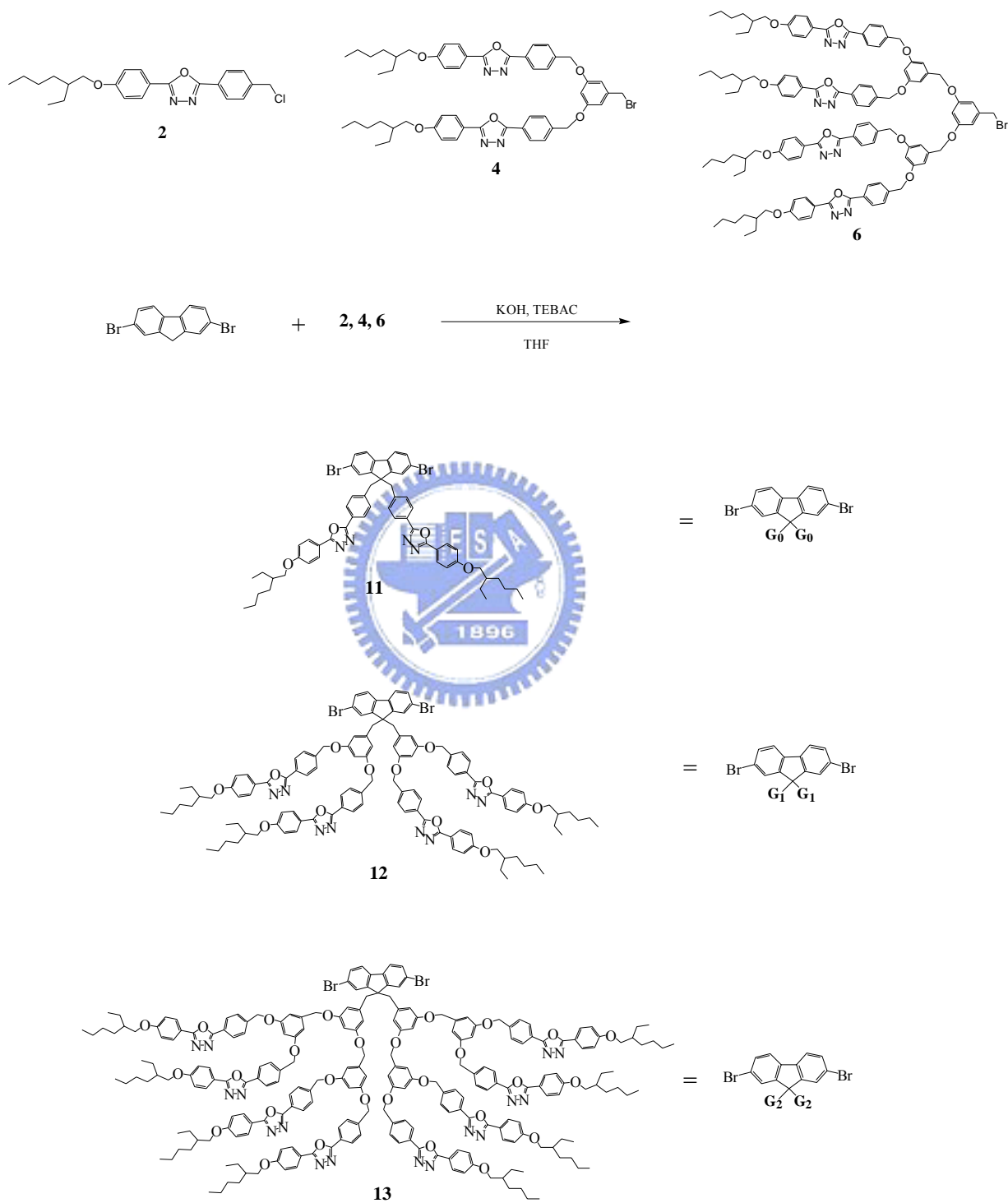
P8 (G1-OXDCAZ). Yield: 77%. 1H NMR (ppm, $CDCl_3$): 0.64–0.95 (m, 48H), 1.01–1.45 (m, 64H), 1.66-1.70 (m, 8H), 2.05 (br, 12H), 3.40 (br, 4H), 3.86 (d, $J = 4.8$ Hz, 8H), 4.15 (t, 4H), 4.78 (s, 8H), 6.12 (s, 4H), 6.35 (s, 2H), 6.96 (d, $J = 8.7$ Hz, 8H), 7.13-7.38 (m, 20H), 7.65-7.80 (m, 24H), 8.01-8.04 (m, 20H). Anal. Calcd for $C_{218}H_{234}N_{10}O_{12}$: C, 82.18; H, 7.40; N, 4.40. Found: C, 81.56; H, 7.26; N, 4.20.

P9 (G2-OXDCAZ). Yield: 73%. 1H NMR (ppm, $CDCl_3$): 0.70–1.08 (m, 76H),

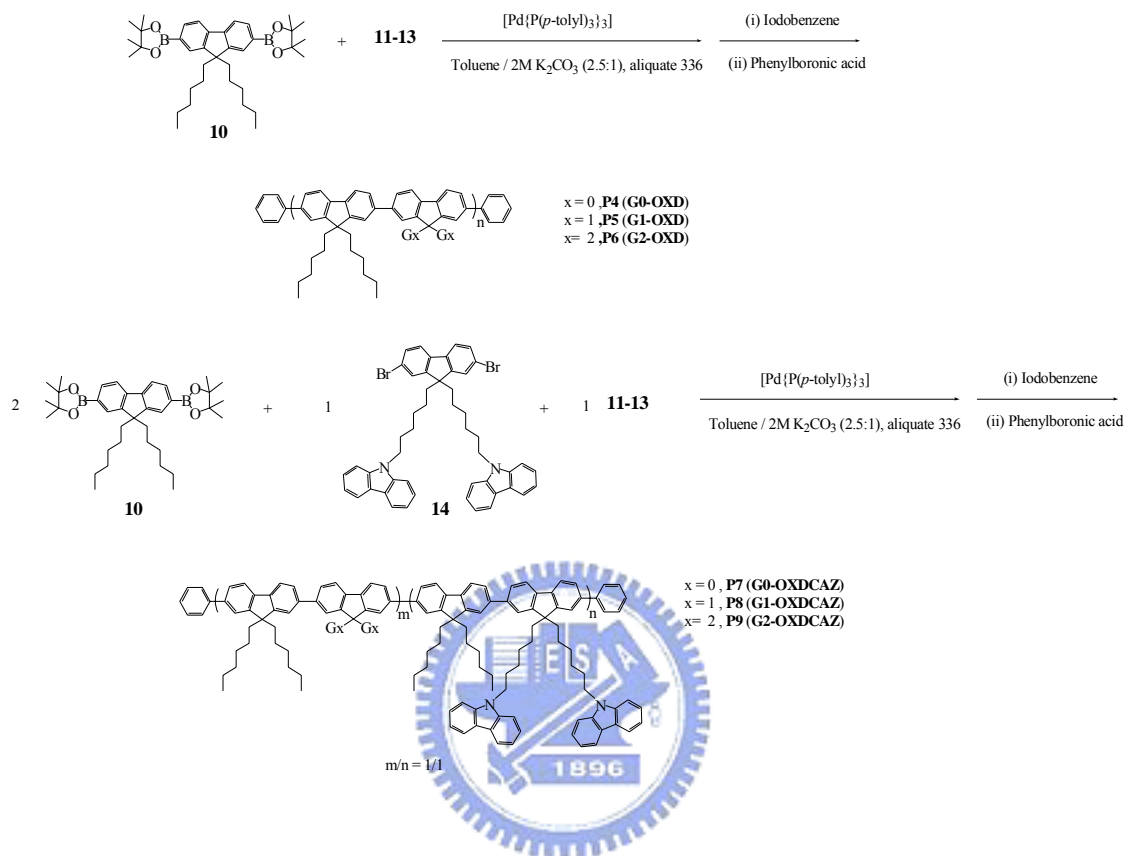
1.31–1.46 (m, 92H), 1.69-1.71 (m, 12H), 2.05 (br, 12H), 3.40 (br, 4H), 3.84 (d, $J = 5.4$ Hz, 16H), 4.13 (t, 4H), 4.70-4.89 (m, 24H), 6.14 (s, 4H), 6.40-6.52 (m, 14H), 6.94 (d, $J = 7.2$ Hz, 16H), 7.14-7.30 (m, 12H), 7.40 (d, $J = 8.7$ Hz, 16H), 7.64 (m, 24H), 7.94-8.05 (m, 36H). Anal. Calcd for $C_{338}H_{362}N_{18}O_{28}$: C, 79.22; H, 7.12; N, 4.92. Found: C, 78.79; H, 7.14; N, 4.74.



Scheme 3.1 The synthetic route of macromonomers 11-13



Scheme 3.2 The synthetic route of dendronized polymers P4-P9



3.3 Results and Discussion

3.3.1 Synthesis and Characterization.

The chemical structures of dendronized macromonomers **11-13** are shown in Scheme 1. The attachment of compounds **2 (4 or 6)** to 2,7-dibromofluorene was done by following a literature procedure⁵¹ with THF as a solvent, aqueous KOH as a base, and triethylbenzylammonium chloride (TEBAC) as a phase transfer catalyst (PTC). Pure monomers **11-13** were confirmed by ¹H NMR, elemental analyses, and FAB (or MALDI-TOF) mass spectroscopy. The dendronized polymers **P4-P9** were synthesized from a Suzuki coupling reaction in a biphasic system (toluene/aqueous K₂CO₃) with freshly prepared Pd{P(*p*-tolyl)₃}₃ as a catalyst precursor.⁴¹ In the beginning, when Pd(PPh₃)₄ is used as a catalyst precursor, the G2-substituted polymer (**P6** and **P9**) can not be obtained due to the bulky side group of **13** to hide the reactive site, where Pd{P(*p*-tolyl)₃}₃ seems to be a superior choice in many SPC cases.⁴⁰ Copolymers **P7-P9** containing hole-transporting CAZ pendent groups were also synthesized to compare with those polymer counterparts without CAZ pendants (**P4**, **P5**, and **P6**). Standard workup afforded the dendronized polymers **P4-P9** as amorphous, slightly yellow materials. All polymers could be fully dissolved in common organic solvents, such as dichloromethane, chloroform, and THF. The molecular weights determined by GPC against polystyrene standards are summarized in Table 3.1. These data show that considerable molecular weights were achieved in these dendronized polymers, which have number-average molecular weights (*M_n*) ranging 20200-34500 with polydispersity indices (*M_w/M_n*) of 1.36-2.97.

The thermal stability of the polymers was determined by thermogravimetric analysis

(TGA) under nitrogen. All polymers exhibited degradation temperatures (T_d) higher than 370 °C (5 % weight loss under nitrogen). The degradation patterns of these polymers are quite similar, which possess a main weight loss step at the onset temperatures of T_d in the range of 430-450 °C. Phase transition temperatures of the polymers were also investigated by differential scanning calorimetry (DSC) under nitrogen. Though polyfluorenes usually reveal a crystallization temperature due to their crystalline nature in the solid state, DSC curves showed no crystallization and melting peaks but only glass transition temperatures (T_g s) in polymers **P4-P9**. This obviously indicates that the presence of OXD and CAZ units in these copolymers suppresses the crystallinity and chain aggregation of the polymers effectively. The T_g s of the polymers are in the range of 85-143 °C and gradually drop by increasing the size of the dendritic OXD wedges, i.e. **P4>P5>P6** and **P7>P8>P9**. However, the copolymers containing CAZ pendent units (**P7**, **P8**, and **P9**) have lower glass transition temperatures (T_g s) than those polymer counterparts without CAZ pendants (**P4**, **P5**, and **P6**), respectively, which might be due to the longer spacer length in CAZ side chains.

Table 3.1 Molecular Weights and Thermal Properties of Polymers

Polymer	M_n^a	M_w^a	PDI	T_g^b (°C)	T_d^c (°C)
P4 (G0-OXD)	34500	102600	2.97	143	372
P5 (G1-OXD)	35600	66700	1.87	102	395
P6 (G2-OXD)	21300	29000	1.36	87	405
P7 (G0-OXDCAZ)	33800	95800	2.83	118	378
P8 (G1-OXDCAZ)	21100	40900	1.93	95	394
P9 (G2-OXDCAZ)	20200	42900	2.12	85	410

^a Molecular weight determined by GPC in THF, based on polystyrene standards.

^b Glass transition temperature (°C) determined by DSC at a heating rate of 10 °C min⁻¹.

^c Temperature (°C) at 5% weight loss measured by TGA at a heating rate of 20 °C min⁻¹ under nitrogen.

3.3.2 Optical Properties

The absorption and PL data of dendritically functionalized polymers **P4-P9** were measured in both solution and solid states, and the optical properties are summarized in Table 3.2. As shown in Figure 3.1, the intensities of the short-wavelength absorption peaks (at ca. 300 nm) in THF solutions of **P4-P6** increase with the generation number of the dendrons, which are attributed to the absorption of the peripheral OXD units. Similarly, the absorption band of **P7-P9** solutions (in THF) at ca. 295 nm are originated from the combined absorption band of OXD and CAZ pendent groups. The additional absorption bands of polymers **P4-P9** at 384-391nm are assigned to the $\pi-\pi^*$ transition contributed from the conjugated backbones of the polyfluorenes. The absorption spectra of the polymers in solid films are similar (a little red-shifted) to those in THF solutions. Optical band gaps (E_g) determined from the absorption edge of **P4-P9** in solid films are found to be about 2.94 eV.

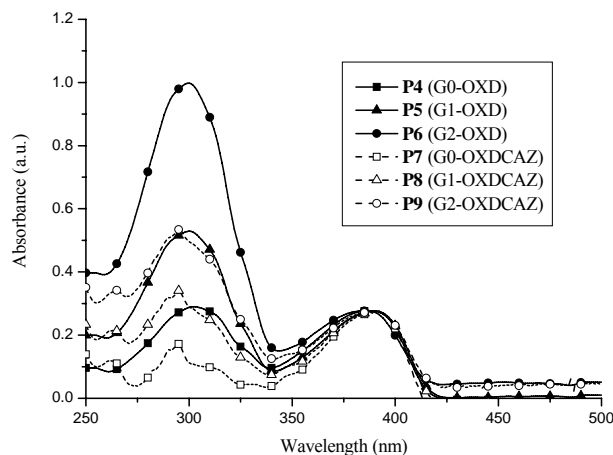


Figure 3.1. Absorption spectra of polymers **P4-P9** in THF solutions, normalized at the absorption peak of the polymer backbone.

As shown in Figure 3.2, the PL spectra of polymers in THF solutions are quite similar to one another. All polymers emit blue light at 417 nm with vibronic bands at 441 nm (except **P6**, which reveals two sharp bands at 415 and 439 nm). The slightly blue-shifted spectrum of **P6** could be explained by the incorporation of the attachment of G2-bulky OXD dendrons onto the side chains of the fluorene units, which twist the polyfluorene backbones to decrease the effective conjugation length to some extent. The PL spectra of polymer solid films were prepared by spin-coating from their THF solutions onto quartz plates. In comparison to the corresponding dilute solutions, the emission spectra of **P4-P9** in solid films show a slight red-shift of 8-11 nm (Figure 3.3). Similar to the solution state, the PL spectrum of **P6** in the solid state is slightly blue-shifted relative to the other polymers. It is worth noticing that the PL spectra of **P4** and **P7** have a long tail extending to longer wavelength regions (the “onsets” of the longer wavelength region is at 610 nm) and show a shoulder at ca. 520 nm.

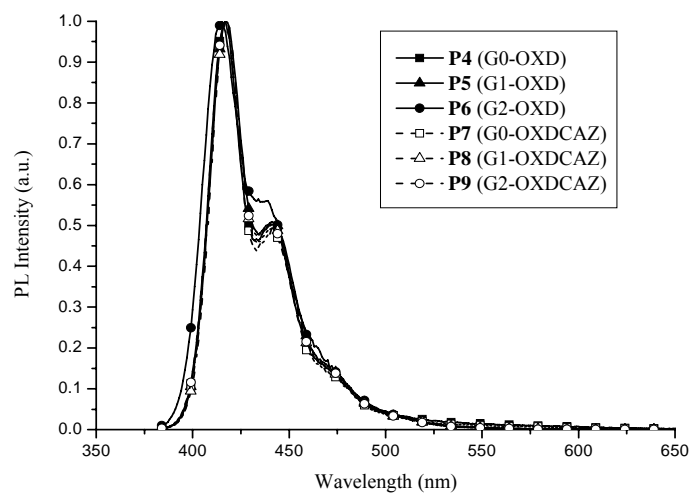


Figure 3.2. Normalized PL spectra of polymers **P4-P9** excited at the maximum absorption of backbones in THF solutions.

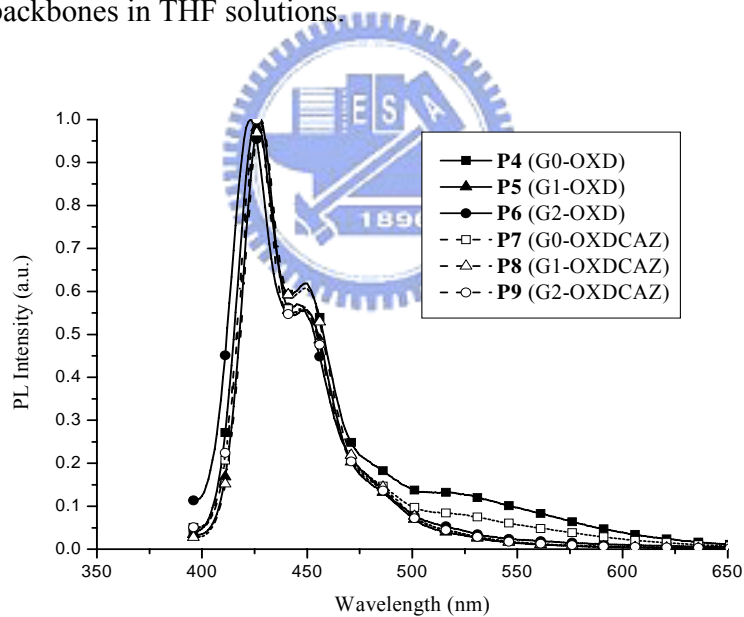


Figure 3.3. Normalized PL spectra of polymers **P4-P9** excited at the maximum absorption of backbones in solid films.

To examine the effects of the size of side chains on the thermal stability of the dendronized copolymers **P4-P9**, the polymer films were heated on a hot plate at 150 °C for 1 h under air. The results are illustrated in Figure 3.4. The annealing of the G0 polymers (**P4** and **P7**) compared with Figure 3.3 result the more significant emission bands between 500 and 600 nm. This spectral feature is attributed to the interchain excimer formation and/or keto defects, which is commonly observed in 9,9-disubstituted polyfluorenes.^{25, 26, 52} The incomplete suppression of long wavelength emission band were also seen in similar dendronized polyfluorenes with smaller dendrons.^{29(a)} In the case of G1 polymers (**P5** and **P8**), the appearance of the long wavelength tail are much less pronounced. The PL spectra of the G2 polymers (**P6** and **P9**), however, remain almost intact and no long wavelength emission are detected after thermal treatment. For comparison, the same experiment was conducted for the film of **PF** homopolymer (poly-2,7-(9,9-dihexylfluorene)). Annealing of the **PF** film led the most significant emission band between 500 and 600 nm. It is apparent that the thermal stability of dendronized copolymers **P4-P9** is improved over that of **PF**, which is due to the incorporation of bulky dendrons into the C-9 position of the fluorene units. **P5**, **P6**, **P8**, and **P9** with larger dendrons do not show any sign of aggregation or excimer formation. These results clearly indicate that the steric hindrance of larger dendritic substituents suppresses the intermolecular π - π stacking of the polymers and eliminate undesirable red-shifts in the emission spectra.

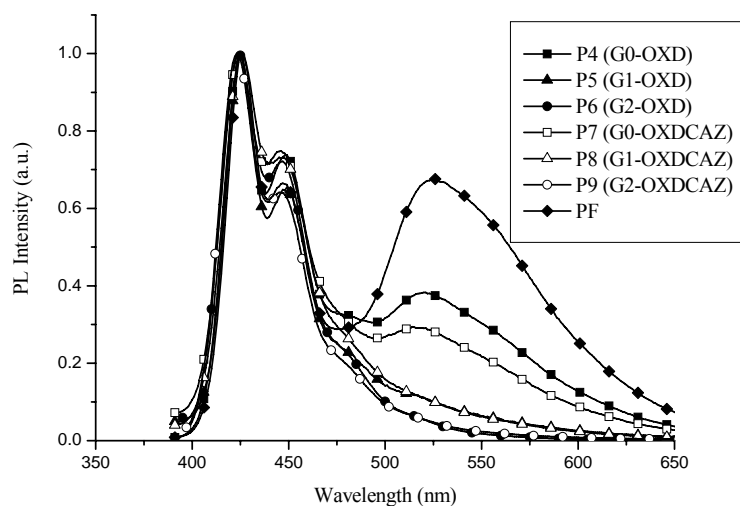
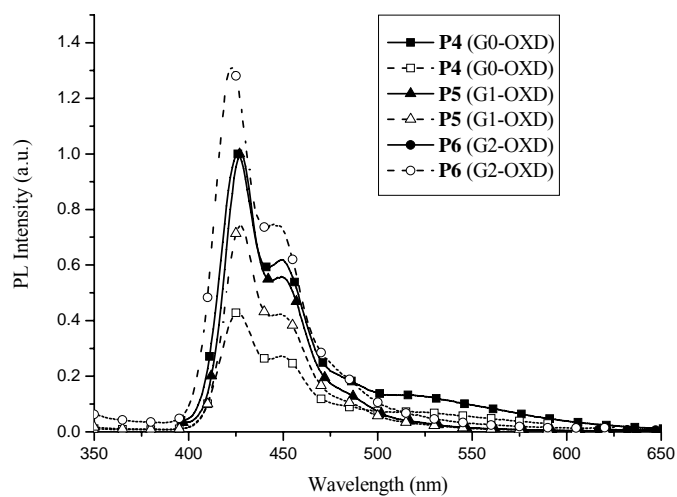


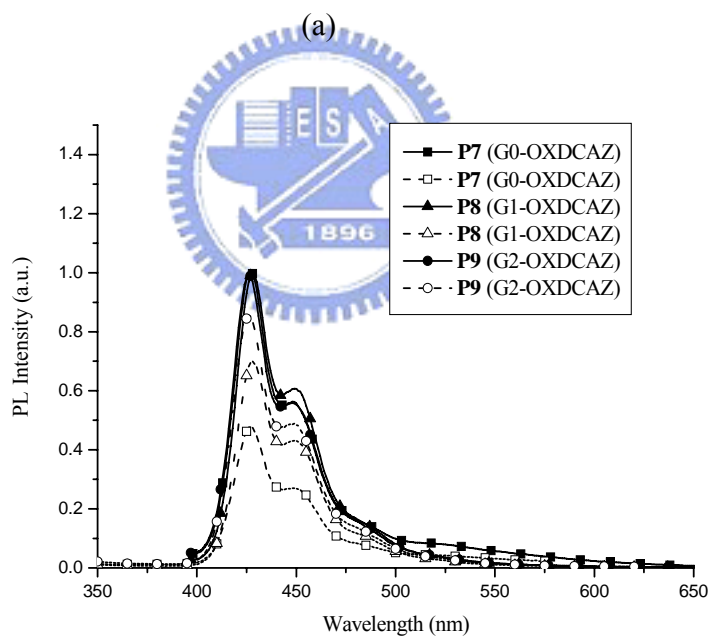
Figure 3.4. Normalized PL spectra of polymers excited at the maximum absorption of the polymer backbones after annealing at 150 °C for 1 h under air.

It is already known that OXD and CAZ units can act as energy-transfer donors (light antennae) for the light-emitting cores (as energy-transfer acceptors). In fact, the photoexcitations of OXD or CAZ units predominantly created identical emissions as those excited at the absorption of polyfluorene backbones. No characteristic emission features of OXD or CAZ side chains were observed in Figure 3.5, which indicate that both pendant groups (as energy-transfer donors) and polymer backbones (as energy-transfer acceptors) contribute the major emissions of the polyfluorenes. As shown in Figure 3.5, the intensity of the sensitized emission (excited at peripheral OXD units ca. 303 nm) of **P6** is 31% higher than the direct backbone emission (excited at the maximum absorption of the polymer backbone ca. 390 nm), which is the only enhanced result of the sensitized emission due to the largest number of dendritic OXD pendants (energy-transfer

donors) in the highest generation of dendrons. The result clearly indicates that the photoluminescence of dendronized polymers by the light antenna design is more efficient than direct excitation at the absorption maximum of the polymer backbone. The PL quantum yields (Φ_{PL}) of polymers **P4-P9** excited at the maximum absorption of backbones in solutions were measured with 9,10-diphenylanthracene as a reference standard (cyclohexane, $\Phi_{\text{PL}} = 0.90$),⁴⁶ where the highest quantum yield reaches 1.0. The PL quantum yields in solid films were measured using the same standard in poly(methyl methacrylate),⁴⁷ and the results are listed in Table 3.2. The PL efficiencies of copolymers **P4-P6** show a trend similar to those of copolymers **P7-P9**, where the polymers incorporating smaller G0-substituted dendrons exhibit relatively higher degrees of aggregation and larger tendencies of excimer formation, and thus to possess relatively lower PL efficiencies. The G1-substituted polymers, however, exhibit the highest PL efficiencies with respect to their G0- and G2-analogues. The lower quantum yields of G2-analogues (**P6** and **P9**) with the highest generation of dendrons are probably due to the lower degrees of polymerization and slight twists of backbones in polyfluorene backbones, which lead to the quenching effect of polyfluorenes.



(a)



(b)

Figure 3.5. Normalized PL spectra of polymers (a) **P4-P6** and (b) **P7-P9** in solid films, which were excited at the maximum absorption of the peripheral OXD pendants (open symbols) and at the maximum absorption of the polymer backbone (solid symbols).

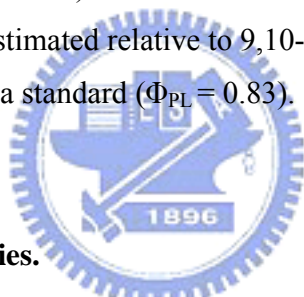
Table 3.2 Absorption and PL Emission Spectral Data of Polymers in THF Solutions and Solid Films.

Polymer	$\lambda_{\text{abs,sol}}^a$ (nm)	Band gap (eV)	$\lambda_{\text{PL,sol}}^a$ (nm)	$\lambda_{\text{PL, film}}^a$ (nm)	$\Phi_{\text{PL,sol}}^b$	$\Phi_{\text{PL,film}}^c$
P4 (G0-OXD)	302, 387	2.94	417, 441	426, 449	0.73	0.34
P5 (G1-OXD)	300, 391	2.94	417, 441	427, 449	0.98	0.55
P6 (G2-OXD)	299, 384	2.94	415, 439	423, 445	0.77	0.16
P7 (G0-OXDCAZ)	295, 391	2.94	417, 441	427, 448	0.97	0.30
P8 (G1-OXDCAZ)	295, 391	2.94	417, 441	428, 449	1.00	0.52
P9 (G2-OXDCAZ)	295, 388	2.94	417, 441	426, 448	0.86	0.24

^a The data in parentheses are the wavelengths of shoulders and subpeaks.

^b Solution fluorescence quantum efficiency were measured in THF, relative to 9,10-diphenylanthracene ($\Phi_{\text{PL}} = 0.90$).

^c PL quantum efficiency were estimated relative to 9,10-diphenylanthracene in poly-(methyl methacrylate) as a standard ($\Phi_{\text{PL}} = 0.83$).



3.3.3 Electrochemical Properties.

Cyclic voltammetry (CV) measurements were carried out in a conventional three-electrode cell. The measured oxidation potentials and HOMO and LUMO energy values are summarized in Table 3.3. As depicted in Figure 3.6, polymers **P4-P6** show the onset potentials of oxidation between 1.32 and 1.38 V in the anodic scans. The onset potentials are similar to the reported value of poly(2,7-(9,9-dioctyl)-fluorene)s (1.4 V)⁵³ and the onset potentials are due to the oxidation of the polyfluorene backbones. On the contrary, copolymers **P7-P9** have lower onset potentials of oxidation between 1.23 and 1.26 V, which are attributed to the introduction of CAZ groups.⁵⁴ It implies that the CAZ units reduce the hole-injection barrier by 0.08-0.14 eV thus to facilitate the capability of hole injection from ITO electrodes. Similarly, the high electron affinity of OXD units is

helpful in electron injection. The HOMO energy values of **P4-P9** were calculated relative to ferrocene (Fc), which has a value of -4.8 eV with respect to zero vacuum level. It can be visualized that the generation variety of the OXD dendrons has little effect on the oxidation potentials. The redox wave broadening or shifted effects on higher generations of dendrons, which were referred as the shell effect,⁵⁵ can be observed in G2-substituted polymers **P6** and **P9**.

Table 3.3 Oxidation Potentials and Calculated HOMO Energies of Polymers

polymer	$E_{\text{ox/onset}}$ (V)	HOMO (eV)
P4 (G0-OXD)	1.37	-5.72
P5 (G1-OXD)	1.38	-5.73
P6 (G2-OXD)	1.32	-5.67
P7 (G0-OXDCAZ)	1.23	-5.58
P8 (G1-OXDCAZ)	1.26	-5.61
P9 (G2-OXDCAZ)	1.24	-5.59

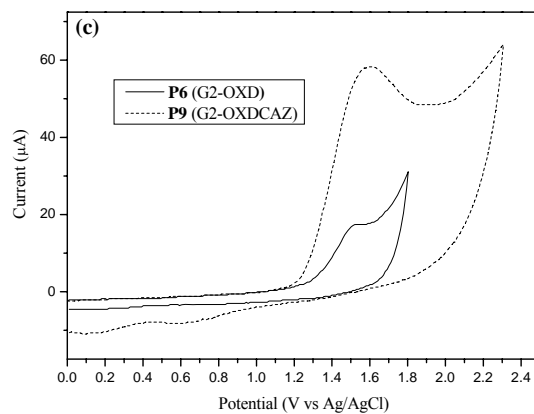
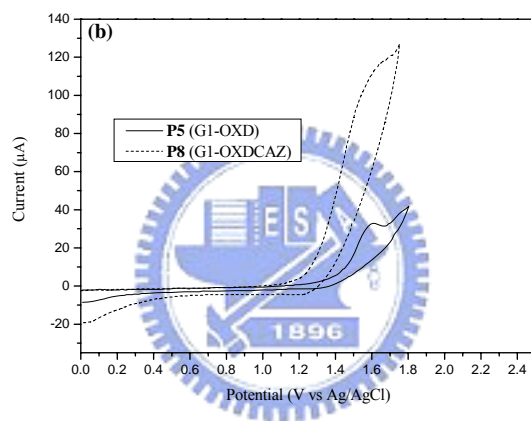
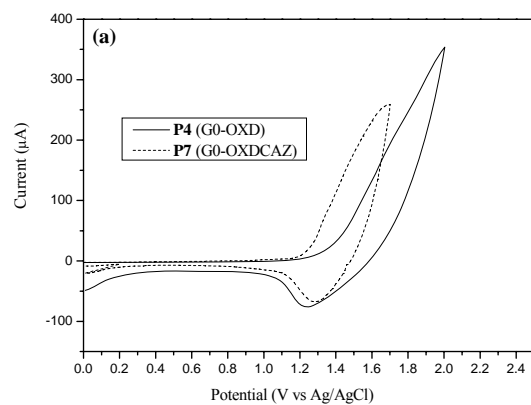


Figure 3.6. Cyclic voltammograms of the polymers: (a) **P4** and **P7**, (b) **P5** and **P8**, (c) **P6** and **P9**.

3.3.4 Electroluminescent Properties.

To evaluate these novel dendron-functionalized luminescent materials, double-layer light emitting devices using the dendronized polymers **P4-P9** as the active layer with the configuration of ITO/PEDOT/polymer/LiF/Al have been fabricated and investigated. The performance data of these devices are collected in Table 3.4. As a result, the emission wavelengths and spectral features of the EL spectra (Figure 3.7) are very similar to those of the corresponding PL spectra in solid films, which suggest that their EL emissions originate from the polyfluorene backbones. Both **P4** and **P7** show significantly broadened emissions to agree with their PL spectra, which might be due to excimer formation by aggregation in the solid state or fluorenone defects introduced during device fabrication and operation.^{26(c), 29(a), 5(a)} However, the green emission has been efficiently suppressed in **P5, P6, P8**, and **P9**, which might be due to the hindrance of the exciton migration to reduce oxidized ketonic defects by the bulky OXD dendrons and thereby to increase the color stability of these devices.^{29(b)} The PLED device made of **P7** (Figure 3.8) has the maximum brightness of 2446 cd/m² at a bias voltage of 12 V and a power efficiency of 0.24 cd/A at 100 mA/cm². The turn-on voltages of PLED devices based on G2-substituted polymers were a few volts higher than those of PLED devices based on G0- and G1-substituted polymers as shown in Table 3.4. Such unfavorable results are presumably due to a dominant shielding effect of G2-dendritic wedges, which deteriorates the charge transporting properties for the higher generations of the dendrimers.⁵⁶ The device performance characteristics of G0 dendritic PF-based PLEDs are generally better than those of corresponding G1 and G2 dendritic PF-based devices, the opposite result compared with the optical properties of **P4-P9** might be due to the two

different characteristic mechanisms of EL and PL performances.

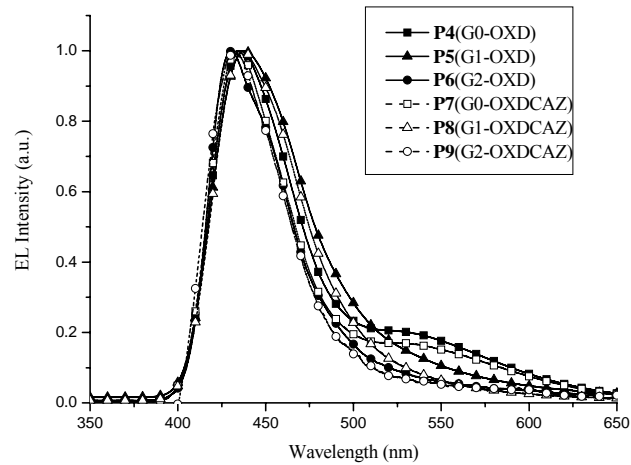


Figure 3.7. Normalized EL spectra of the devices with the configuration of ITO/PEDOT/polymer/LiF/Al at 12V.

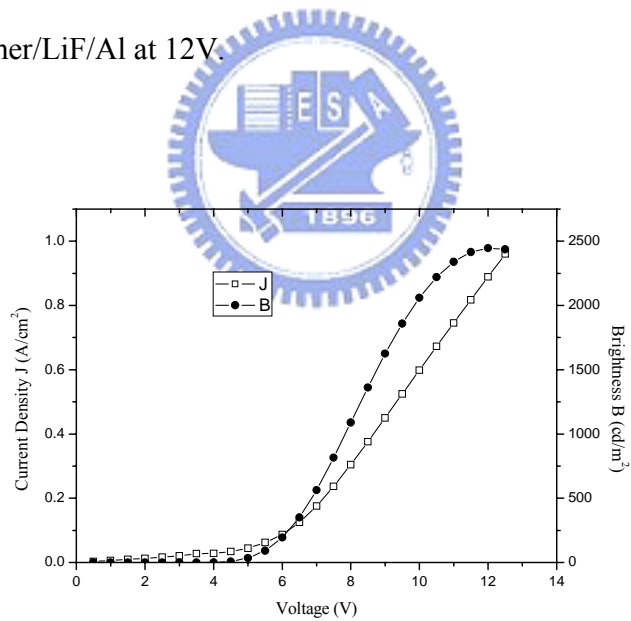


Figure 3.8. Current density-voltage-brightness (J - V - B) characteristics of the PLED device containing **P7** with the configuration of ITO/PEDOT/**P7**/LiF/Al.

Table 3.4 EL Data of PLED Devices ^a

Polymer	$\lambda_{\text{max,EL}}$ (nm)	V_{on}^b (V)	Luminance Efficiency ^c (lm/W)	Power Efficiency ^c (cd/A)	Max. Brightness (cd/m ²)
P4 (G0-OXD)	436	5.0	0.90	0.31	1480 (10V)
P5 (G1-OXD)	438	7.5	0.34	0.08	380 (14V)
P6 (G2-OXD)	432	9.0	0.10	0.05	520 (15V)
P7 (G0-OXDCAZ)	434	4.5	0.24	0.12	2446 (12V)
P8 (G1-OXDCAZ)	438	7.0	0.10	0.02	119 (15V)
P9 (G2-OXDCAZ)	432	8.5	0.05	0.02	92 (15V)

^a Device structure: ITO/PEDOT/Polymer/LiF/Al.

^b V_{on} is the turn-on voltage of light.

^c Measured at 100 mA/cm².



3.4 Conclusion

A series of novel polyfluorenes containing three generations of dendronized side chains, including Fréchet-type poly(aryl ether) dendrons and functional peripheral groups such as OXD units were synthesized. The resulting polymers possess good thermal stability and excellent solubility in common organic solvents. The G1- and G2-substituted polymers may narrow down the emission spectra by reducing the emission spectral tail (extending to longer wavelength regions). The improvement of the emission spectral quality is attributed to less molecular packing caused by the steric hindrance of bulky dendritic side chains. The PLEDs with the configuration of ITO/PEDOT/polymer/LiF/Al were fabricated, and emitted blue light. The poor device performance of the more bulky dendronized polyfluorene-based PLEDs are presumably due to a large excess of the electron-affinitive OXD moieties in the higher generations of dendrons, which could act as electron traps and lead to the reduction of charge balance.

Chapter 4

H-Bonded Effects on Novel Supramolecular Dendrimers Containing Electron-Transporting Donor dendron and Single/Double H-Bonded Acceptor Emitters

4.1 Introduction

The luminescent quantum efficiencies of π -conjugated materials are substantially lower in the solid state than those in the solution state because of intermolecular interactions, such as aggregation and excimer formation, which lead to a self-quenching process of excitons.^{25, 57} A very attractive way to solve this problem is to encase chromophores within dendritic architectures.⁵⁸ By connecting bulky dendrons around a central dye moiety, it has been used to prevent the self-aggregation of chromophores in the solid state⁵⁹ and also define the color of the light emission.⁶⁰ Furthermore, chromophore-cored dendrimers may be potentially useful as multifunctional emissive materials in OLED devices. For example, the proper charge transporting functionalities are incorporated at the periphery of the dendritic wedges. This may result in the improvement of imbalanced charge characters in organic luminescent materials.⁶¹ In light-harvesting antennae, the peripheral donor units can collect photons, and transfer excitation energy through bonds to the cores or focal points of the acceptors, thus to enhance luminescence efficiencies considerably. In addition, a special benefit is that the amorphous phase of chromophores can be significantly induced by well-defined dendritic structures which prevent from crystallization of chromophores to develop high quality films by spin-coating technique. It is important because melting and recrystallization, caused by heat or

short-circuit currents, often result in device damages.⁶²

Another route to overcome the π - π stacking phenomenon is the utilization of branching systems. In a previous report, oligo(*p*-phenylene vinylene)s (OPVs) have been oriented in a tetrahedral framework to minimize the intramolecular stacking.⁶³ These tetrahedral arrays do not crystallize and thus form stable amorphous phases. However, it is very difficult to obtain branched systems because of their complicated synthetic routes and low yields. Supramolecules as well as supramolecular polymers can be prepared from two complementary components that are appropriately substituted with functional H-bonded donor and acceptor groups.⁶⁴ The simpler synthetic molecules through supramolecular self-assembly often possess specific and useful chemical, physical, or optical properties due to the collective behavior of each other. Upon hydrogen-bonded (H-bonded) complexation with dendritic acceptors, the dendritic supramolecules showed a significantly higher PL emission than those individual emitting OPV donors alone, due to the three-dimensional orientation of the OPV emitting molecules.⁶⁵

In our previous work,⁶⁶ we have completed several series of H-bonded liquid crystalline trimers and H-bonded polymer networks, which were constructed by complexation of two complementary components containing various bifunctional photoluminescent (PL) acceptor cores and monofunctional proton donors (or donor polymers). These supramolecular trimers and H-bonded polymer networks demonstrate that different wavelengths of PL emissions and liquid crystalline phases can be achieved by introducing non-photoluminescent proton donors (or donor polymers).

In this report, the design, synthesis, and optical properties of highly efficient light emitting H-bonded dendrimers with single/double H-bonds, i.e. asymmetric/symmetric supramolecules as shown in Figure 2, are presented. A new

strategy involving two complementary segments which contain monofunctional/bifunctional photoluminescent acceptor cores and dendritic donor wedges (bearing OXD segments) are explored. The key structural elements in the dendritic H-donors are various generations of functional poly(aryl ether) dendrons bearing outward OXD arms and a focal point of benzoic acid. This self-assembly of dendritic framework is expected to be effective for the construction of light-harvest of OXD arms and site-isolation of emitting cores. The absorption, emission spectra, as well as energy transfer of the H-bonded dendrimers are also studied to gain insight into the effect of dendritic wedges on the photoluminescent cores. Significantly, by choosing different generations of H-donors, the color of PL emission can be tuned. Even more, stronger fluorescence emission from OXD excitation can be obtained by reduced aggregation and energy transfer from OXD wedges in these supramolecular dendrimers. On the other hand, dendritic donor cores of poly(alkyl aryl ether), were also synthesized to form another chromophore-shelled dendrimers by complexation with the same emitting acceptors (as the peripheral emitting shells) in comparison with the previous chromophore-cored dendrimers. Hopefully, this study is expected to be helpful and constructive for the forthcoming researches about light-emitting dendrimers.

4.2 Experimental Section

4.2.1 Measurements

¹H NMR spectra were recorded on a Varian Unity 300 MHz spectrometer using CDCl₃ or DMSO-*d*₆ solvent with tetramethylsilane as reference. Elemental analyses were performed on HERAEUS CHN-OS RAPID elemental analyzer. MALDI-TOF spectra were measured on a Biflex III (Bruker) time-of-flight mass spectrometer utilizing a 5-methoxysalicylic acid matrix. Fourier transform infrared (FTIR) spectra were performed a Nicolet 360 FT-IR spectrometer. Phase transition temperatures were determined by differential scanning calorimetry (Perkin Elmer Diamond) with a heating and cooling rate of 10 °C/min and polarizing optical microscopy (Leica DMLP) equipped with a hot stage. UV-visible absorption spectra were recorded in dilute THF solutions (10⁻⁶ M) on a HP G1103A spectrophotometer, and photoluminescence (PL) spectra were obtained on a Hitachi F-4500 spectrophotometer. Thin films of UV-vis and PL measurements were spin-coated on a quartz substrate from THF solution with a concentration of 1 wt %. The fluorescence quantum yields (Φ_{PL}) of the chromophores and H-bonded dendrimers were determined relative to a standard film of 9,10-diphenylanthracene dispersed in PMMA ($\Phi = 0.83$).⁴⁷

4.2.2 Materials

Chemicals and solvents were reagent grades and purchased from Aldrich, ACROS, TCI, and Lancaster Chemical Co. Dichloromethane and THF were distilled to keep anhydrous before use. The other chemicals were used without further purification. Compounds **15** were done by following the previous literature procedure.⁶⁷ The synthetic procedures of all donor dendrimers of various generations containing OXD moieties are described in Schemes 4.1-4.2. Besides, Scheme 4.3 shows dendritic

donor cores, which are H-bonded with emitting acceptor shells. All mono-pyridyl and bis-pyridyl acceptor chromophores **PBBOC₈-OC₈**, **PBBCN-OC₈**, **PBP-OC₈**, and **PBBBP-Me-OC₈** are shown in Figure 4.1.

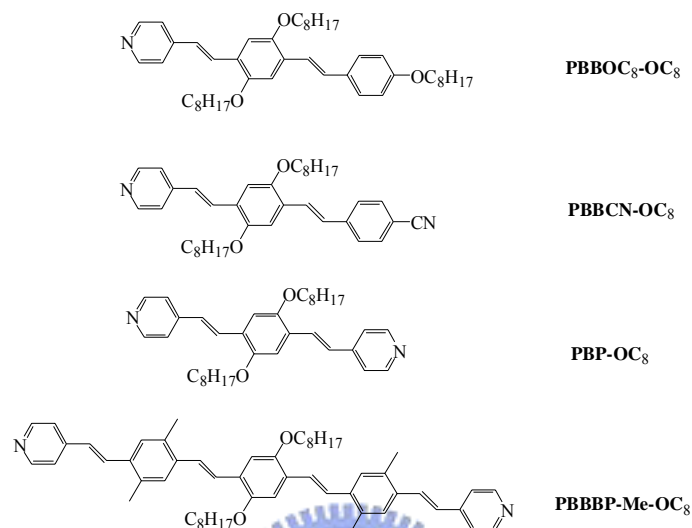


Figure 4.1 Mono-pyridyl (single H-bonded) and bis-pyridyl (double H-bonded) acceptors used in dendritic supramolecules.

General Synthetic Procedures of Dendritic Benzoic Acid Methyl Esters (G1COOCH₃, G2COOCH₃, and G3COOCH₃). A mixture of **2**, **4**, or **6** (2.1 equiv), 3,5-dihydroxybenzoate (1 equiv), K₂CO₃ (2.5 equiv), and 18-crown-6 (0.2 equiv) in dry THF was heated to reflux and stirred under nitrogen for 24 h. The mixture was evaporated to dry under reduced pressure, and the residue was partitioned between water and CH₂Cl₂. Later on, the aqueous layer was extracted with CH₂Cl₂, and the organic layer was dried over MgSO₄. Consequently, the crude products **G1COOCH₃**, **G2COOCH₃**, and **G3COOCH₃** were purified as outlined in the following text.

G1COOCH₃. **G1COOCH₃** was purified by column chromatography with EA/CH₂Cl₂ (1:10) to get a white solid. Yield: 63%. ¹H NMR (ppm, CDCl₃): δ 0.86-0.95 (m, 12H), 1.23-1.54 (m, 16H), 1.70-1.76 (m, 2H), 3.90-3.91 (overlap, 7H),

5.15 (s, 4H), 6.81 (s, 1H), 7.00 (d, $J = 9$ Hz, 4H), 7.30 (s, 2H), 7.57 (d, $J = 8.4$ Hz, 4H), 8.04 (d, $J = 9$ Hz, 4H), 8.13 (d, $J = 8.4$ Hz, 4H).

G2COOCH₃. **G2COOCH₃** was purified by column chromatography with EA/CH₂Cl₂ (1:8) to get a white solid. Yield: 73%. ¹H NMR (ppm, CDCl₃): δ 0.92-0.97 (m, 24H), 1.33-1.53 (m, 32H), 1.74-1.81 (m, 4H), 3.88-3.92 (overlap, 11H), 5.02(s, 4H), 5.10 (s, 8H), 6.57 (s, 2H), 6.69(s, 4H), 6.74 (s,1H), 7.00 (d, $J = 8.4$ Hz, 8H), 7.26 (s, 2H), 7.55 (d, $J = 8.1$ Hz, 8H), 8.04 (d, $J = 8.1$ Hz, 8H), 8.10 (d, $J = 7.5$ Hz, 8H).

G3COOCH₃. **G3COOCH₃** was purified by column chromatography with THF/CH₂Cl₂ (1:8) to get a white solid. Yield: 70%. ¹H NMR (ppm, CDCl₃): δ 0.91-0.96 (m, 48H), 1.32-1.54 (m, 64H), 1.70-1.76 (m, 8H), 3.85(s, 3H), 3.89 (d, $J = 5.7$ Hz, 16H), 4.96-5.04 (overlap, 28H), 6.50 (s, 2H), 6.52 (s, 4H), 6.62(s, 4H), 6.65 (s, 8H), 6.71 (s, 1H), 6.98 (d, $J = 9$ Hz, 16H), 7.23 (s, 2H), 7.50 (d, $J = 8.1$ Hz, 16H), 8.00 (d, $J = 9$ Hz, 16H), 8.06 (d, $J = 8.4$ Hz, 16H).

G1COOH . To a solution of **G1COOCH₃** (1.0 equiv) in THF, KOH (5 equiv) dissolved in water was added. A small amount of Methanol was then added to the two-phase mixture to afford a homogeneous solution. The reaction was heated at reflux for 24 h. After the solution was cooled to room temperature, hydrochloric acid was added to precipitate the product **G1COOH**, which was isolated by filtration, washed with water and dried overnight in a vacuum oven. Yield: 80%. ¹H NMR (ppm, DMSO-*d*₆): δ 0.85-0.90 (m, 12H), 1.28-1.45 (m, 16H), 1.68-1.74 (m, 2H), 3.92 (d, $J = 4.8$ Hz, 4H), 5.26 (s, 4H), 6.97 (s, 1H), 7.12 (d, $J = 8.4$ Hz, 4H), 7.19 (s, 2H), 7.65 (d, $J = 8.1$ Hz, 4H), 8.00 (d, $J = 8.7$ Hz, 4H), 8.09 (d, $J = 7.8$ Hz, 4H), 13.10 (broad, COOH). MS (MALDI-TOF): m/z [MH⁺] 880.53, calcd m/z [M⁺] 879.05. Anal. Calcd. for C₅₃H₅₈N₄O₈: C 72.42, H 6.65, N 6.37 Found: C 72.04, H 6.74, N 6.42.

G2COOH. This compound was prepared from **G2COOCH₃** by the same

synthesized procedure as that of **G1COOH**. Yield: 85%. ^1H NMR (ppm, CDCl_3): δ 0.90-0.95 (m, 24H), 1.32-1.53 (m, 32H), 1.71-1.75 (m, 4H), 3.86 (d, $J = 5.4$ Hz, 8H), 5.00 (overlap, 12H), 6.50 (s, 2H), 6.65(s, 4H), 6.75 (s,1H), 6.96 (d, $J = 8.7$ Hz, 8H), 7.31 (s, 2H), 7.49 (d, $J = 8.1$ Hz, 8H), 7.99 (d, $J = 8.7$ Hz, 8H), 8.05 (d, $J = 8.1$ Hz, 8H). MS (MALDI-TOF): m/z [MH^+] 1848.88, calcd m/z [M^+] 1848.22. Anal. Calcd. for $\text{C}_{113}\text{H}_{122}\text{N}_8\text{O}_{16}$: C 73.43, H 6.65, N 6.06 Found: C 73.09, H 6.93, N 6.11.

G3COOH. This compound was prepared from **G3COOCH₃** by the same synthesized procedure of **G1COOH**. Yield: 82%. ^1H NMR (ppm, CDCl_3): δ 0.90-0.95 (m, 48H), 1.26-1.55 (m, 64H), 1.71-1.75 (m, 8H), 3.86 (d, $J = 5.4$ Hz, 16H), 4.91-4.98 (overlap, 28H), 6.50 (overlap, 6H), 6.56-6.70 (overlap, 13H), 6.95 (d, $J = 8.7$ Hz, 16H), 7.27 (s, 2H), 7.47 (d, $J = 8.4$ Hz, 16H), 7.97 (d, $J = 9$ Hz, 16H), 8.02 (d, $J = 8.4$ Hz, 16H). MS (MALDI-TOF): m/z [MH^+] 3787.14, calcd m/z [M^+] 3786.57. Anal. Calcd. for $\text{C}_{233}\text{H}_{250}\text{N}_{16}\text{O}_{32}$: C 73.91, H 6.65, N 5.92. Found: C 73.63, H 6.51, N 6.04.

16. Sodium hydride (3 equiv) in anhydrous THF was slowly added into a stirred solution of compound **15** (1 equiv) in dry THF under nitrogen. After 10 min of stirring, 1,6-dibromo-hexane (5 equiv) was added rapidly. After being stirred overnight, the reaction mixture was quenched with water. The mixture was evaporated to dry under reduced pressure, and the residue was partitioned between water and CH_2Cl_2 . Then, the aqueous layer was extracted with CH_2Cl_2 , and the organic layer was dried over MgSO_4 . Finally, the crude product was purified by column chromatography with CH_2Cl_2 /Hexane (1:2) to get a white oil. Yield: 72%. ^1H NMR (ppm, CDCl_3): δ 1.26-1.44 (m, 4H), 1.57-1.63 (m, 2H), 1.79-1.89 (m, 2H), 3.36-3.45 (m, overlap, 4H), 4.41 (s, 2H), 5.08 (s, 4H), 6.46 (s, 1H), 6.56 (s, 2H), 7.51 (d, $J = 8.1$ Hz, 4H), 7.65 (d, $J = 8.1$ Hz, 4H).

17. The previous procedure was followed using sodium hydride (3 equiv),

compound **15** (1 equiv), and 1,6-dibromo-decane (5 equiv). The crude product was purified by column chromatography with CH₂Cl₂/Hexane (1:2) to get a white oil. Yield: 67%. ¹H NMR (ppm, CDCl₃): δ 1.27 (m, 12H), 1.55-1.57 (m, 2H), 1.82-1.87 (m, 2H), 3.35-3.44 (m, overlap, 4H), 4.41 (s, 2H), 5.08 (s, 4H), 6.46 (s, 1H), 6.57 (s, 2H), 7.51 (d, *J* = 7.8 Hz, 4H), 7.66 (d, *J* = 8.1 Hz, 4H).

General Synthetic Procedures of Dendritic Trialkylated Donor Cores (18 and 19). A mixture of **16** or **17** (3.1 equiv), 1,1,1-tris(4'-hydroxyphenyl)ethane (1.0 equiv), K₂CO₃ (4.0 equiv), and 18-crown-6 (0.3 equiv) in dry THF was heated to reflux and stirred vigorously under nitrogen for 24 h. The mixture was evaporated to dry under reduced pressure, and the residue was partitioned between water and CH₂Cl₂. Then, the aqueous layer was extracted with CH₂Cl₂, and the organic layer was dried over MgSO₄. Consequently, the crude products **18** or **19** were purified as outlined in the following text.

18. Compound **18** was purified by column chromatography with EA/CH₂Cl₂ (1:10) to get a slight yellow oil. Yield: 51%. ¹H NMR (ppm, CDCl₃): δ 1.26-1.43 (m, 12H), 1.57-1.63 (m, 6H), 1.72-1.78 (m, 6H), 2.03 (s, 3H), 3.43 (t, 6H), 3.90 (t, 6H), 4.41 (s, 6H), 5.07 (s, 12H), 6.45 (s, 3H), 6.57 (s, 6H), 6.73 (d, *J* = 9 Hz, 6H), 6.94 (d, *J* = 8.4 Hz, 6H), 7.50 (d, *J* = 8.1 Hz, 12H), 7.65 (d, *J* = 8.4 Hz, 12H).

19. Compound **19** was purified by column chromatography with EA/CH₂Cl₂ (1:10) to get a slight yellow oil. Yield: 42%. ¹H NMR (ppm, CDCl₃): δ 1.23-1.40 (m, 36H), 1.55-1.59 (m, 6H), 1.70-1.75 (m, 6H), 2.07 (s, 3H), 3.42 (t, 6H), 3.88 (t, 6H), 4.41 (s, 6H), 5.08 (s, 12H), 6.45 (s, 3H), 6.57 (s, 6H), 6.74 (d, *J* = 9 Hz, 6H), 6.95 (d, *J* = 9 Hz, 6H), 7.50 (d, *J* = 8.4 Hz, 12H), 7.65 (d, *J* = 8.4 Hz, 12H).

G1-C₆-(COOH)₆. This compound was prepared from **18** by the same synthesized procedure of **G1-COOH**. Yield: 77%. ¹H NMR (ppm, DMSO-*d*₆): δ 1.34 (m, 12H), 1.47-1.49 (m, 6H), 1.65 (m, 6H), 1.96 (s, 3H), 3.33 (t, 6H), 3.86 (t, 6H), 4.35 (s, 6H),

5.14 (s, 12H), 6.57 (overlap, 9H), 6.76 (d, $J = 8.7$ Hz, 6H), 6.85 (d, $J = 8.7$ Hz, 6H), 7.51 (d, $J = 8.1$ Hz, 12H), 7.94 (d, $J = 7.8$ Hz, 12H), 12.94 (broad, COOH). MS (MALDI-TOF): m/z [$M^+ + K$] 1817.14, calcd m/z [$M^+ + K$] 1816.08. Anal. Calcd. for $C_{107}H_{108}O_{24}$: C 72.28, H 6.12. Found: C 71.95, H 6.31.

G1-C₁₀-(COOH)₆. This compound was prepared from **19** by the same synthesized procedure of **G1COOH**. Yield: 80%. ¹H NMR (ppm, DMSO-*d*₆): δ 1.21 (m, 36 H), 1.44 (m, 6H), 1.61 (m, 6H), 1.97 (s, 3H), 3.31 (t, 6H), 3.84 (t, 6H), 4.33 (s, 6H), 5.14 (s, 12H), 6.57 (overlap, 9H), 6.75 (d, $J = 8.7$ Hz, 6H), 6.86 (d, $J = 9$ Hz, 6H), 7.51 (d, $J = 8.1$ Hz, 12H), 7.94 (d, $J = 8.1$ Hz, 12H), 12.94 (broad, COOH). MS (MALDI-TOF): m/z [$M^+ + K$] 1985.31, calcd m/z [$M^+ + K$] 1984.40. Anal. Calcd. for $C_{119}H_{132}O_{24}$: C 73.44, H 6.84. Found: C 73.14, H 6.76.

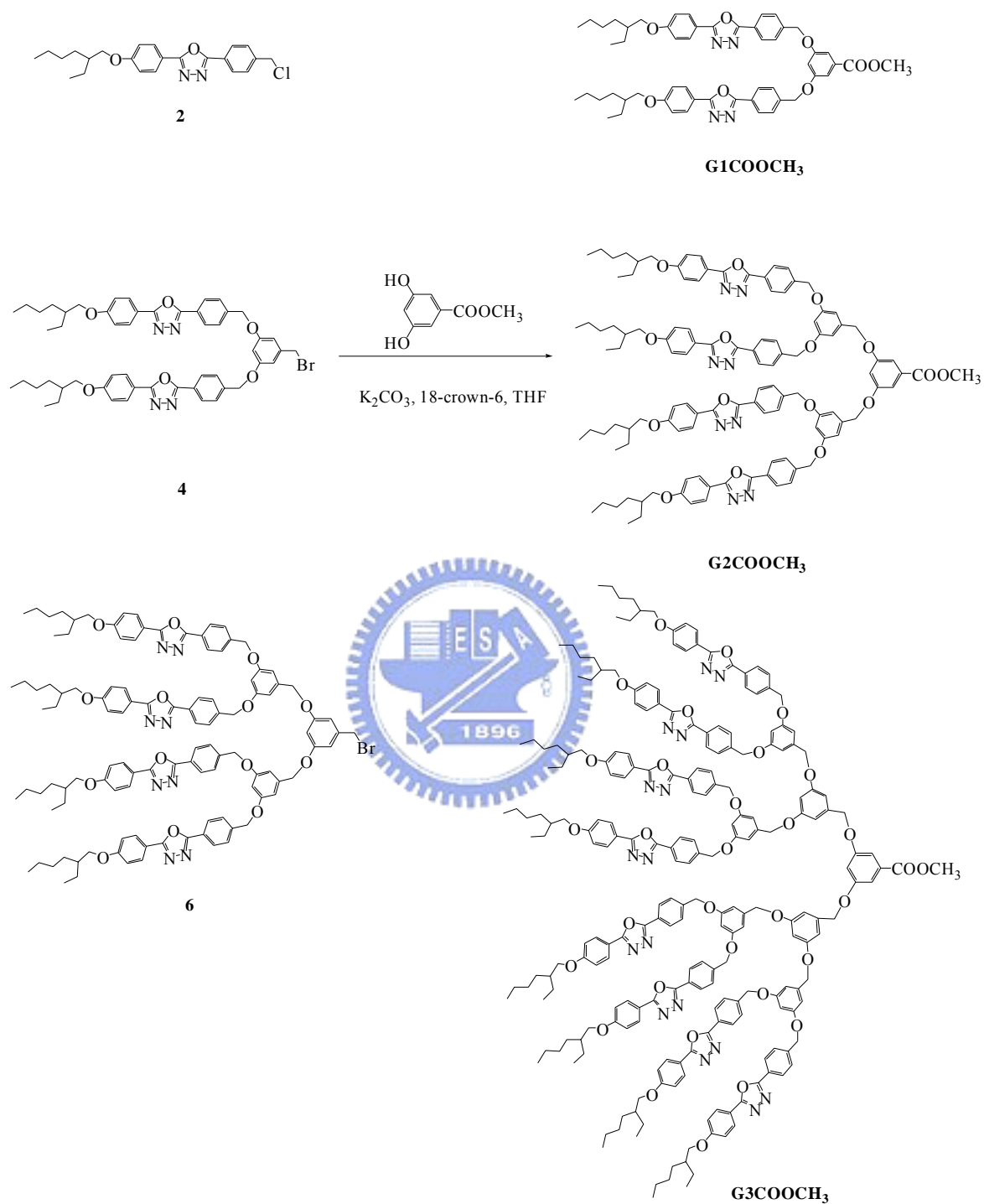
4.2.3 Preparation of H-bonded complexes

All H-bonded complexes are made up of appropriate (fully H-bonded) molar ratios of acceptor and donor moieties in THF. Thus, symmetric dendritic supramolecules were produced by complexation of double H-bonded acceptor emitters **PBP-OC₈** and **PBBBP-Me-OC₈** with dendritic donors **G1COOH**, **G2COOH**, and **G3COOH** in the molar ratio of 1 : 2, respectively; and asymmetric dendritic supramolecules were generated by complexation of single H-bonded acceptor emitters **PBBOC₈-OC₈** and **PBBCN-OC₈** with dendritic donors **G1COOH**, **G2COOH**, and **G3COOH** in the molar ratio of 1 : 1, respectively. Furthermore, the single H-bonded acceptor emitters **PBBOC₈-OC₈** and **PBBCN-OC₈** were complexed with another type of dendritic donor cores **G1-C₆-(COOH)₆** and **G1-C₁₀-(COOH)₆** in the molar ratio of 6 : 1 to form exterior emitting shells. In addition, the double H-bonded acceptor emitters **PBP-OC₈** and **PBBBP-Me-OC₈** (as H-bonded crosslinkers) were also complexed with dendritic donor cores **G1-C₆-(COOH)₆** and **G1-C₁₀-(COOH)₆** in the molar ratio

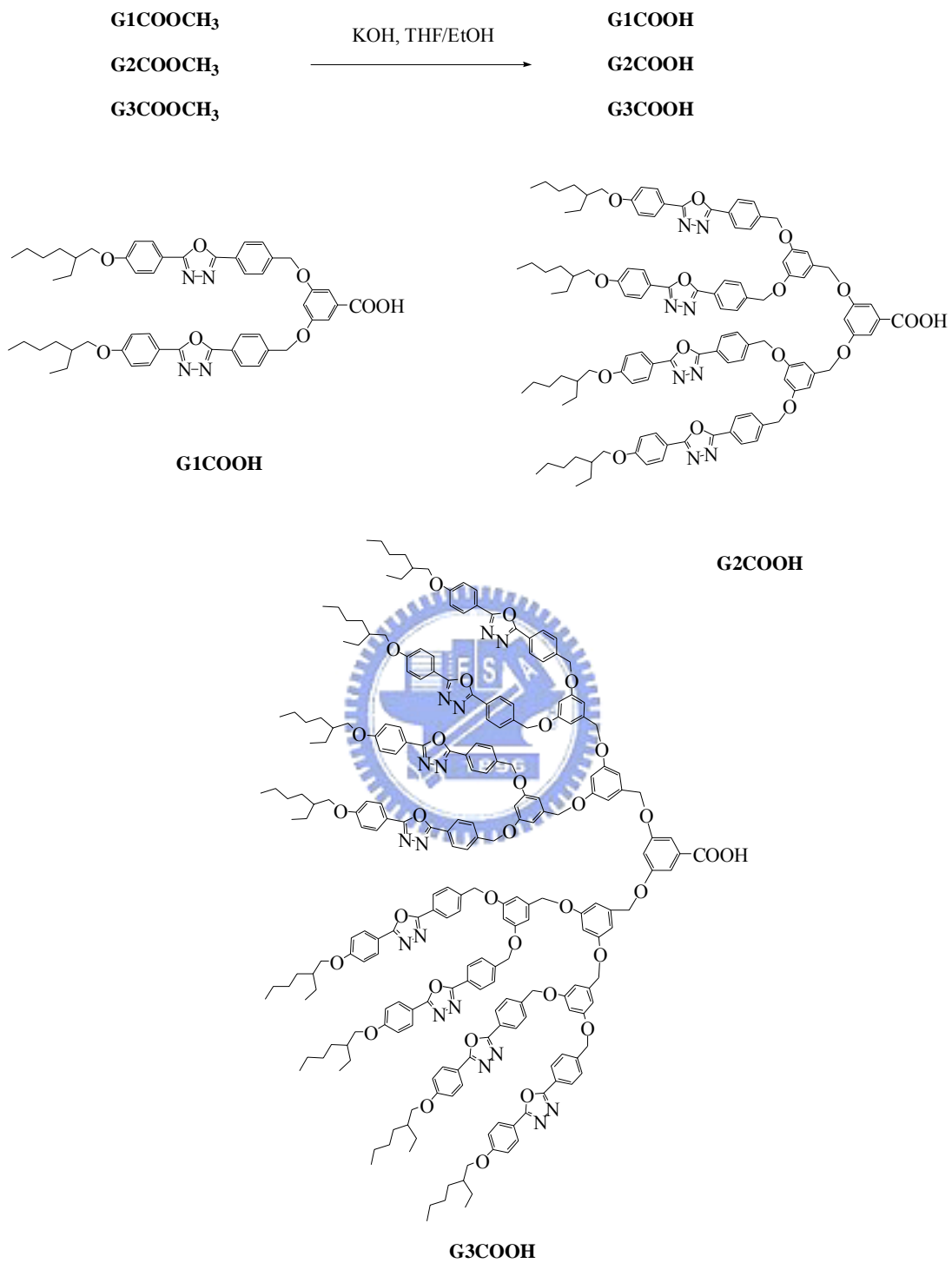
of 6 : 2 to form crosslinked H-bonded emitting shells. All H-bonded dendrimers were prepared by slow evaporation of THF solution containing the mixtures of the acceptor and donor moieties, followed by drying in vacuo.



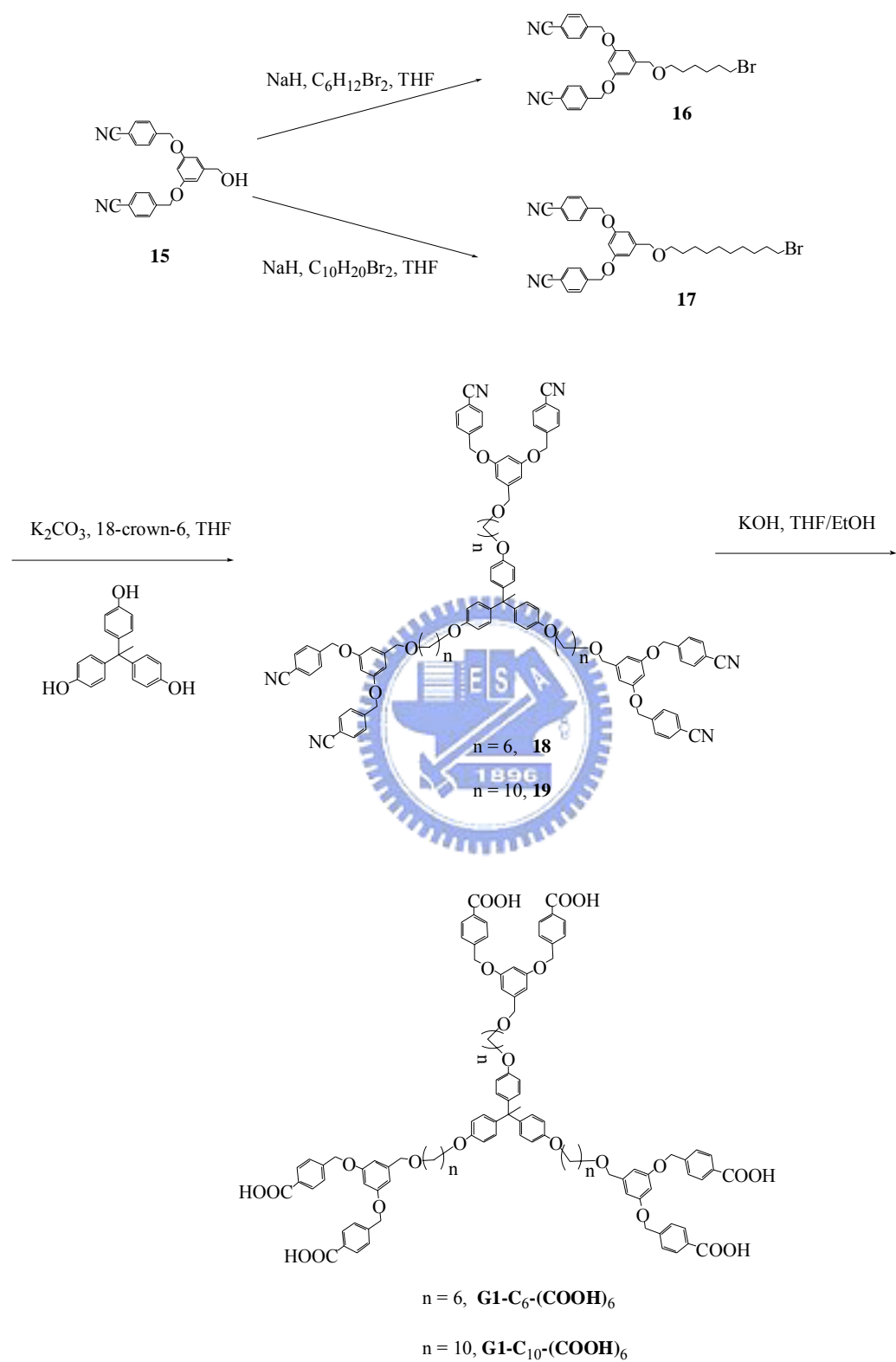
Scheme 4.1



Scheme 4.2



Scheme 4.3



4.3 Results and Discussion

4.3.1 Synthesis and Characterization

As shown in Schemes 4.1-4.3, all H-bonded donors were synthesized via a previously reported convergent method.⁶⁸ In the presence of K_2CO_3 with THF at reflux, 3,5-dihydroxy-benzoic acid methyl ester reacted with various corresponding generations of dendrons (**2**, **4**, and **6**) to obtain **G1COOCH₃**, **G2COOCH₃**, and **G3COOCH₃**, which were followed by hydrolysis reaction with KOH in methanol/THF at reflux to give **G1COOH**, **G2COOH**, and **G3COOH**. Another series of dendrimers (**18** and **19**) were prepared by coupling dendritic wedges to a polyfunctional core and followed by hydrolysis reaction to give **G1-C₆-(COOH)₆** and **G1-C₁₀-(COOH)₆** as shown in Scheme 4.3. The polyfunctional core chosen in this case was 1,1,1-tris(4'-hydroxyphenyl)ethane, and the resulting molecules were characterized by NMR spectroscopy, elemental analysis, and MALDI-TOF mass spectroscopy.

The existence of hydrogen bonds in the H-bonded complexes can be characterized by IR spectra. Therefore, the IR spectra of **PBBCN-OC₈**, **G1COOH**, and H-bonded complex of **PBBCN-OC₈/G1COOH** shown in Figure 4.2 are compared to analyze the hydrogen bonds. In contrast to the O-H band of pure **G1COOH** (H-bonded dimer) at 2604 cm^{-1} , the weaker O-H band observed at 1911 and 2500 cm^{-1} in the H-bonded complex **PBBCN-OC₈/G1COOH** is indicative of stronger hydrogen bonding between the pyridyl group of **PBBCN-OC₈** and the carboxylic acid of **G1COOH** in the H-bonded complex. On the other hand, a C=O stretching vibration appeared at 1710 cm^{-1} in the H-bonded complex **PBBCN-OC₈/G1COOH**, which show that the carbonyl group was in a less associated state than that in pure **G1COOH** (H-bonded dimer) with weaker C=O stretching vibration appeared at 1695 cm^{-1} . Both results suggest that hydrogen bonds formed between **PBBCN-OC₈** and **G1COOH** in the

solid state of the H-bonded complex **PBBCN-OC₈/G1COOH**. The other H-bonded complexes discussed in this study should have similar consequences as the demonstrated complexes.⁶⁹ The three-dimensional dendritic scaffolding of H-bonded dendrimer design provides the desired amorphous films without crystallization and leads to good film qualities by spin-coating. The resulting supramolecular H-bonded assemblies were investigated with respect to their thermal and photophysical properties.

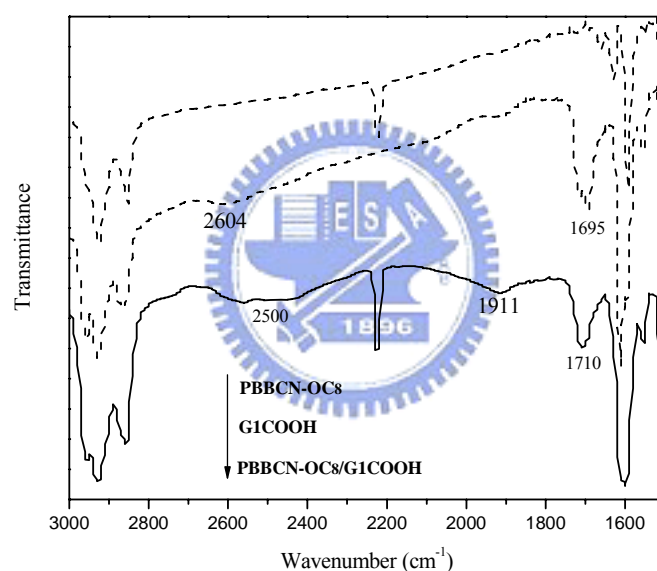


Figure 4.2 IR spectra of H-bonded moieties **PBBCN-OC₈**, **G1COOH**, and H-bonded complex **PBBCN-OC₈/G1COOH**.

4.3.2 Thermal Properties

To elucidate the H-bonding effect on the thermal properties of the H-bonded dendrimers, all compounds were characterized by differential scanning calorimetry (DSC). Polarizing optical microscopy (POM) demonstrated that no phase separation took place between donors and acceptors in the H-bonded dendrimers. In addition, the third-generation (G3) of H-bonded dendrimers containing **G3COOH** have higher isotropization temperatures (T_i) than the lower generations of H-bonded dendrimers. As shown in Table 4.1, it is observed that dendritic donors **G1COOH**, **G2COOH**, and **G3COOH** possess the glass transition temperatures (T_g) at 51, 63, and 72 °C, respectively. Due to higher molecular weights in the higher generations of dendrimers, the glass transition temperatures of the H-bonded dendrimers with higher generations were observed to increase monotonically. The behavior is consistent with the trends of the glass transition temperatures in earlier studied dendrimers.⁷⁰ As for the acceptor, **PBP-OC₈** exhibits a melting temperature at 137 °C without T_g , indicating the crystalline nature of the molecule. However, H-bonds have a strong effect on the thermal properties by the introduction of OXD dendritic donors (bearing benzoic acids) to the emitting acceptor **PBP-OC₈** via H-bonded self-assembly. Symmetric H-bonded dendrimers **PBP-OC₈/G1COOH**, **PBP-OC₈/G2COOH**, and **PBP-OC₈/G3COOH** reveal distinct glass transition temperatures at 26, 48, and 65 °C, respectively, which are lower than their corresponding dendrimeric donors (owing to the formation of H-bonded dimers by two dendritic acids). Similar phenomena were observed in the other H-bonded dendrimers (see Table 4.1). The incorporation of OXD dendrons into the supramolecular structures shows no melting (only observed in POM) and crystallization peaks in DSC measurements, but T_g only. This clearly indicates that the OXD bulky wedges in these H-bonded dendrimers effectively suppress the crystallization and reduce the chain aggregation of the emitting cores.

Another interesting trend is that all generations of dendritic analogues have the same order of transition temperatures in T_g and T_i for the H-bonded dendrimers containing the following emitting acceptors: **PBBBBP-Me-OC₈** > **PBP-OC₈** > **PBBCN-OC₈** > **PBBOC₈-OC₈**. The result of higher T_g and T_i in symmetric dendritic supramolecules (H-bonded trimers) containing **PBBBBP-Me-OC₈** and **PBP-OC₈** than asymmetric dendritic supramolecules (H-bonded dimers) containing **PBBCN-OC₈** and **PBBOC₈-OC₈** may be explained by the higher molecular weights of H-bonded trimers in the symmetric dendritic supramolecules. Higher T_g and T_i in H-bonded dendrimer containing **PBBBBP-Me-OC₈** than that containing **PBP-OC₈** is due to the longer central core of **PBBBBP-Me-OC₈**. Besides, higher T_g and T_i in H-bonded dendrimer containing **PBBCN-OC₈** than that containing **PBBOC₈-OC₈** is because of the dipole-dipole interaction of CN groups in **PBBCN-OC₈**. In the reverse H-bonded dendrimers (containing emitting shells), e.g. **PBBBBP-Me-OC₈**, **PBP-OC₈**, **PBBCN-OC₈**, and **PBBOC₈-OC₈** were complexed with dendritic donor cores **G1-C₆-(COOH)₆** and **G1-C₁₀-(COOH)₆** in proper ratios, no phase transition peaks were found, which is probably due to the flexible chains of the polyfunctional cores in the H-bonded dendritic donors. Similar behavior in polypropylene dendrimers containing trialkoxybenzene wedges as mesogenic units was reported in the literature.⁷¹

Table 4.1. Transition Temperatures of H-Bonded Donors, Acceptors, and Dendritic

Complexes		
Compound or H-Bonded Complex	T_g (°C)	T_i (°C)
G1COOH	51	175 ^b
G2COOH	63	121 ^b
G3COOH	72	129 ^b
G1-C₆-(COOH)₆	--- ^a	135 ^b
G1-C₁₀-(COOH)₆	--- ^a	130 ^b
PBBOC₈-OC₈	--- ^a	73
PBBOC₈-OC₈/G1COOH	9	92 ^b
PBBOC₈-OC₈/G2COOH	37	86 ^b
PBBOC₈-OC₈/G3COOH	61	98 ^b
PBBOC₈-OC₈/G1-C₆-(COOH)₆	--- ^a	85 ^b
PBBOC₈-OC₈/G1-C₁₀-(COOH)₆	--- ^a	81 ^b
PBBCN-OC₈	--- ^a	119
PBBCN-OC₈/G1COOH	17	123 ^b
PBBCN-OC₈/G2COOH	43	110 ^b
PBBCN-OC₈/G3COOH	66	128 ^b
PBBCN-OC₈/G1-C₆-(COOH)₆	--- ^a	92 ^b
PBBCN-OC₈/G1-C₁₀-(COOH)₆	--- ^a	88 ^b
PBP-OC₈	--- ^a	137
PBP-OC₈/G1COOH	26	127 ^b
PBP-OC₈/G2COOH	48	120 ^b
PBP-OC₈/G3COOH	65	135 ^b
PBP-OC₈/G1-C₆-(COOH)₆	--- ^a	111 ^b
PBP-OC₈/G1-C₁₀-(COOH)₆	--- ^a	98 ^b
PBBBP-Me-OC₈	--- ^a	164
PBBBP-Me-OC₈/G1COOH	33	142 ^b
PBBBP-Me-OC₈/G2COOH	55	134 ^b
PBBBP-Me-OC₈/G3COOH	69	148 ^b
PBBBP-Me-OC₈/G1-C₆-(COOH)₆	--- ^a	141 ^b
PBBBP-Me-OC₈/G1-C₁₀-(COOH)₆	--- ^a	127 ^b

^a Not observed in DSC measurements.

^b The isotropization temperatures were determined by polarizing optical microscopy (POM).

4.3.3 Optical Properties

The absorption and PL spectral data of the pure chromophores (in THF and solid films) and all H-bonded dendrimers in solid films are summarized in Table 4.2. The series of H-bonded dendrimers show very similar absorption and emission characteristics in the solid films. Figure 4.3 shows absorption spectra of uncomplexed H-bond donors and **PBBCN-OC₈** in THF solutions. Figure 4.4 shows various asymmetric H-bonded dendrimers containing single H-bonded acceptor emitter **PBBCN-OC₈** in solid films. In the asymmetric supramolecular complexes bearing dendritically mono-encapsulated chromophores, i.e. **PBBCN-OC₈/G1COOH**, **PBBCN-OC₈/G2COOH**, and **PBBCN-OC₈/G3COOH**, the absorption peak at 305 nm was attributed to the transition absorption of OXD groups and the longer absorption peak at 423 nm was attributed to the characteristic absorption of emitter **PBBCN-OC₈**. By increasing the generation of the dendritic donors in the H-bonded complexes, the absorbance of OXD units at 305 nm is proportional to the generation number of the dendrimers.

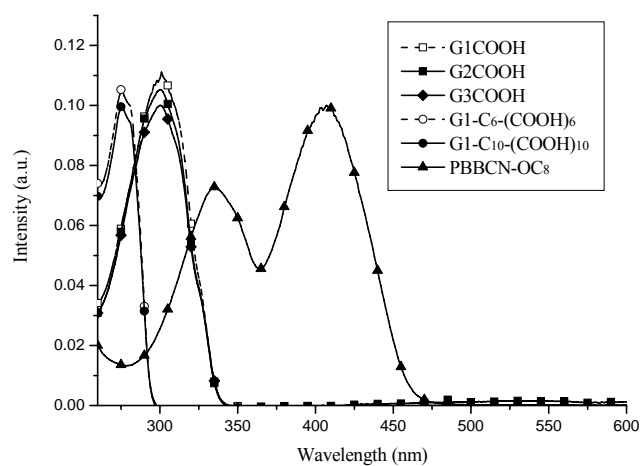


Figure 4.3 UV-vis absorption spectra of uncomplexed H-bond donors and **PBBCN-OC₈** in THF solutions.

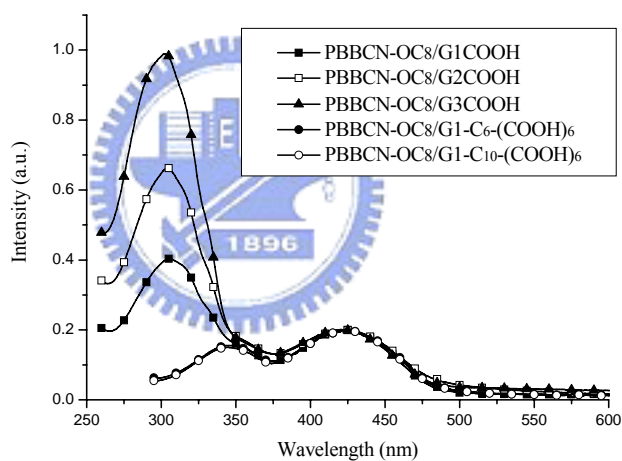


Figure 4.4 UV-vis absorption spectra of **PBBCN-OC₈** and its H-bonded dendrimers in solid films, which are normalized at the absorption peak of **PBBCN-OC₈** at 423 nm.

In view of Figure 4.5, the PL emission spectrum of **PBBCN-OC₈** showed a characteristic peak at 470 nm in THF, which is red-shifted to 512 nm in solid films due to the formation of π - π stacking and molecular aggregation. In contrast to the single H-bonded acceptor emitter **PBBCN-OC₈** alone, the asymmetric supramolecular dendrimers **PBBCN-OC₈/G1COOH**, **PBBCN-OC₈/G2COOH**, and **PBBCN-OC₈/G3COOH** exhibit red-shifted PL emissions with values of λ_{max} at 554, 541, and 531 nm excited at 423 nm, respectively. This result is similar to our previous work,⁶⁶ where the photoluminescent H-bonded trimers containing bifunctional bis-pyridyl acceptors complexed with monofunctional carboxylic acids show red-shifted PL spectra as the acceptor emitters are H-bonded to donors with smaller *pKa* values. As well known that pH values of aqueous solutions may affect photoluminescence properties of polyelectrolytes containing pyridine units. Therefore, the H-bonded dendritic donors **G1COOH**, **G2COOH**, and **G3COOH** bearing benzoic acid groups can be regarded as acidic solvents, so the PL spectra reveal red-shifted PL emissions compared with that of emitter **PBBCN-OC₈** in THF. Interestingly, different generations of asymmetric H-bonded dendrimers containing single H-bonded acceptor emitter **PBBCN-OC₈** appeared to have different degrees of red-shifted PL emissions. The red-shifts of PL emissions in asymmetric H-bonded dendrimers **PBBCN-OC₈/G1COOH**, **PBBCN-OC₈/G2COOH**, and **PBBCN-OC₈/G3COOH** are 84, 71, and 61 nm, respectively, where the higher generations of the H-bonded dendrimers have smaller red-shifted PL emissions than the lower generations of the H-bonded dendrimers. It clearly indicates that larger dendritic wedges have higher site-isolation or dendron dilution effect than smaller dendritic ones, so the higher generations of dendrimers efficiently reduce the aggregation extent of the emitting cores. The opposite type of H-bonded dendritic complexes containing poly(alkyl aryl ether) dendrimer (dendritic donor core)

complexed with single H-bonded acceptor emitter **PBBCN-OC₈** at the periphery, i.e. **PBBCN-OC₈/G1-C₆-(COOH)₆** and **PBBCN-OC₈/G1-C₁₀-(COOH)₆**, also both exhibit red-shifted emission peaks at 556 and 550 nm, respectively, compared with that of **PBBCN-OC₈** in THF. With respect to **PBBCN-OC₈/G1-C₆-(COOH)₆**, the relative 6 nm blue-shift of PL emission in **PBBCN-OC₈/G1-C₁₀-(COOH)₆** may be explained by that the longer flexible alkyl chains (as solid solvents) in the dendritic donor cores result in higher dilution effect for emitting acceptors. It is worthy noticing that the PL emission spectra of **PBBCN-OC₈/G1-C₆-(COOH)₆** and **PBBCN-OC₈/G1-C₁₀-(COOH)₆** are similar to that of **PBBCN-OC₈/G1COOH**, which means that poly(alkyl aryl ether) dendritic acid cores in the reverse form of the previous H-bonded dendrimers affect PL emission behavior of **PBBCN-OC₈** in a similar way as the lower generation of **G1COOH**.

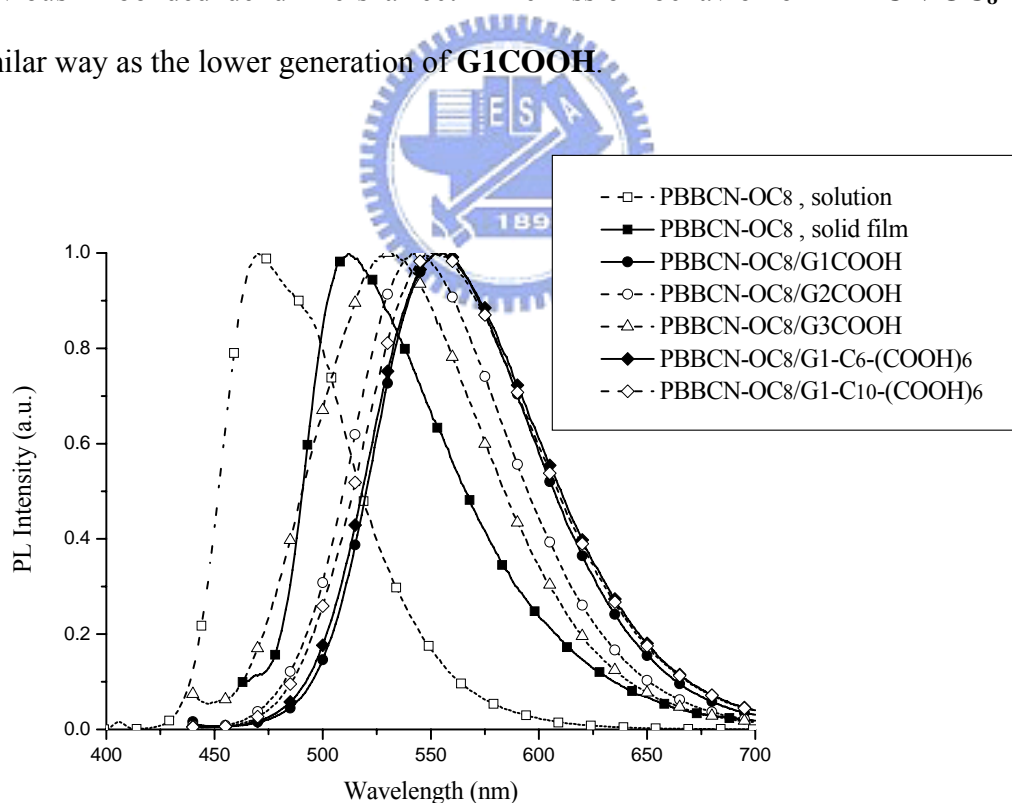


Figure 4.5 Normalized PL spectra of mono-pyridyl (single H-bonded) acceptor emitter **PBBCN-OC₈** and its H-bonded dendrimers.

Figure 4.6 shows the PL emission characteristics of emitter **PBP-OC₈** and its double H-bonded dendrimers with symmetric structures. All PL emission data are summarized in Table 4.2, which demonstrate similar trends as those of single H-bonded acceptor emitter **PBBCN-OC₈** and its asymmetric H-bonded dendrimers. Compared with single H-bonded dendrimers, no further red-shifted PL emissions were observed in the double H-bonded dendrimers due to the weaker H-bonded effect of the second H-bonds on the conjugated structures of double H-bonded acceptors and the double dilution effect from double amount of donor acids.

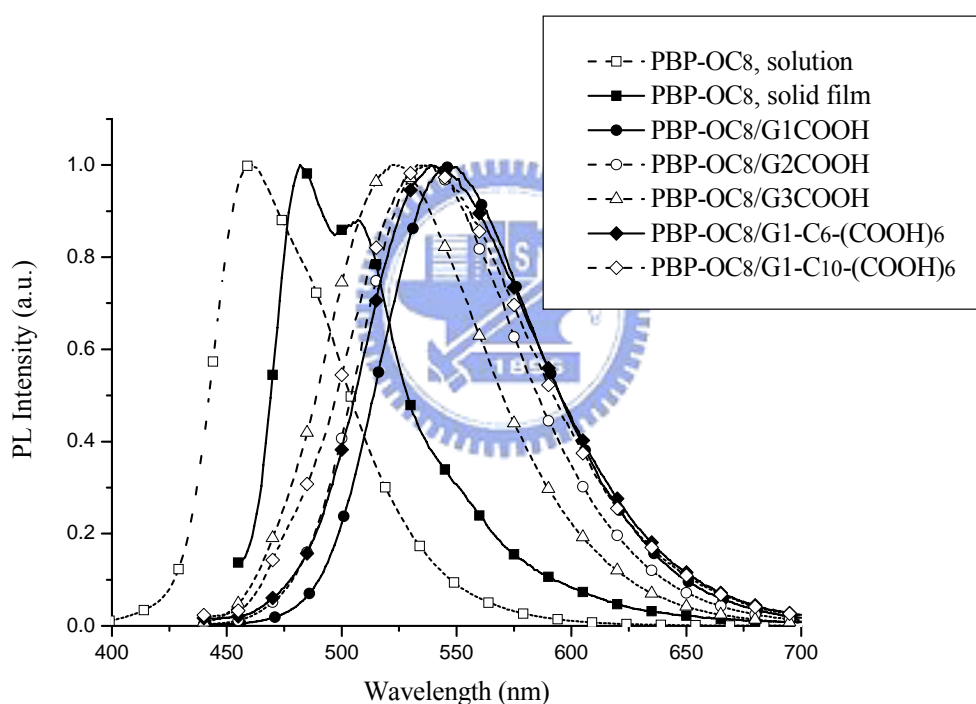


Figure 4.6 Normalized PL spectra of bis-pyridyl (double H-bonded) acceptor emitter **PBP-OC₈** and its H-bonded dendrimers.

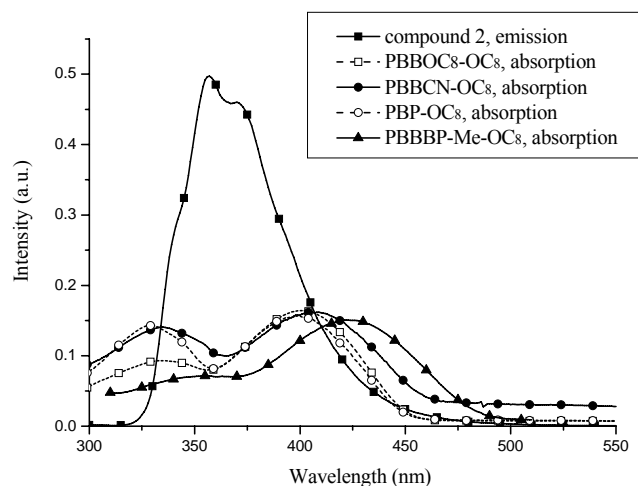


Figure 4.7 UV-vis absorption spectra of (single/double H-bonded) acceptor emitters **PBOC₈-OC₈**, **PBBCN-OC₈**, **PBP-OC₈**, and **PBBBP-Me-OC₈** and PL spectrum of compound **2** (containing an OXD unit) in THF. It indicates that an overlap exists between the emission band of the donor and the absorption bands of the acceptor emitters, resulting in energy transfer from OXD units to the emitting core.

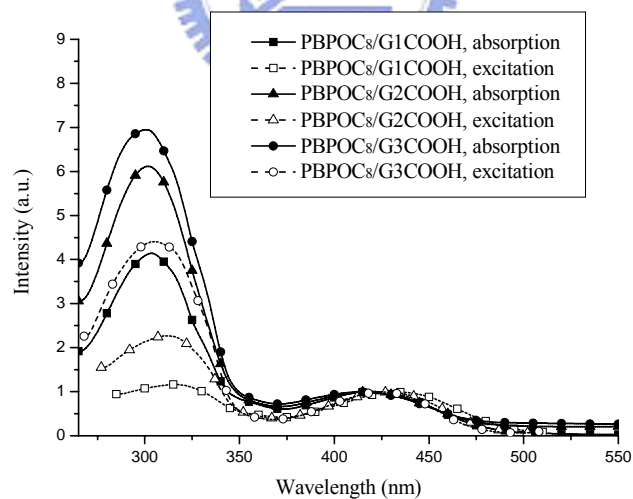


Figure 4.8 UV-vis absorption and corrected excitation spectra of symmetric H-bonded dendrimers (with different generations of donor dendrimers) **PBP-OC₈/G1COOH**, **PBP-OC₈/G2COOH**, and **PBP-OC₈/G3COOH** monitored at the core of double H-bonded acceptor emitter **PBP-OC₈**.

Due to significant overlap in the absorption spectra of the representative chromophores (H-bonded acceptors) and the emission spectrum of model compound **2** in Figure 4.7, the energy transfer from the OXD dendritic groups to the central emitters can be expected, which was also probed by photoluminescent excitation (PLE) spectra of H-bonded dendrimers containing **PBP-OC₈** as shown in Figure 4.8. Similar spectral features of PLE spectra appear to match those of the corresponding absorption spectra, where both peaks (ca. 300 and 425 nm) exists, indicating that the peripheral OXD units in such supramolecular dendrimers possess light-harvesting capability. Hence, the functionalized OXD dendron units or the emitting core **PBP-OC₈** can be independently addressed by changing the excitation wavelength. By excitation of the dendrons and the cores selectively, it provides a window to study the photoinduced energy transfer between H-bonded donors and acceptors.

As shown in Figure 4.9, when the dendritic OXD groups were excited at 305 nm, the symmetric H-bonded dendrimers containing **PBP-OC₈**, i.e. **PBP-OC₈/G1COOH**, **PBP-OC₈/G2COOH**, and **PBP-OC₈/G3COOH**, emit fluorescence at wavelengths of 545, 539, and 522 nm, respectively. The photoexcitation of H-bonded dendrimers at the maximum absorption wavelength of OXD units apparently generated identical predominant emission peaks as those excited at the maximum absorption of **PBP-OC₈**. Whereas, no luminescence was detected from the major emission of OXD dendron, and thus the energy transfer of OXD emission from the dendritic wedges to the central emitting cores is confirmed. In addition, the values of relative fluorescent intensities (RFI) were calculated from the intensity ratio of core emissions by respective excitations at the maximum absorption peaks of the OXD dendrons and the emitting cores (ca. 300 and 425 nm, respectively). The values of RFI from H-bonded G1 to G3 dendrimers are 1.27, 2.33, and 4.50, respectively. The results indicate that the intensity of the sensitized emission (by energy transfer from OXD dendritic

absorption at 300 nm) is even stronger than that of the direct core emission (by core absorption at 425 nm) in the H-bonded dendrimers. Therefore, sensitization by the telechelic antennae is more efficient than direct excitation at the maximum absorption of the chromophore. The increasing tendency from H-bonded G1 to G3 dendrimers unambiguously suggests that the more number of grafted OXD units (higher generations) in the dendrons, the higher capability of light-harvest. However, in contrast to symmetric H-bonded (G1-G3) dendrimers containing double H-bonded acceptor emitter **PBP-OC₈**, where all RFI values are larger than 1 in all generations of H-bonded dendrimers, the enhancement of the core emission in the asymmetric H-bonded dendrimers containing single H-bonded acceptor emitter **PBBCN-OC₈** (as excited at the maximum absorption of OXD dendron) only occurred in the third generation of H-bonded dendrimers **PBBCN-OC₈/G3COOH** as shown in Figure 4.10. One of the major reasons should be attributed to that single H-bonded acceptor emitter **PBBCN-OC₈** is complexed only with one H-bonded donor (energy-transfer donor) in the molar ratio of 1:1 to result in the relatively lower enhancement of fluorescent intensity, as compared with double H-bonded acceptor emitter **PBP-OC₈** complexed with two H-bonded donor (energy-transfer donor) in the molar ratio of 1:2.

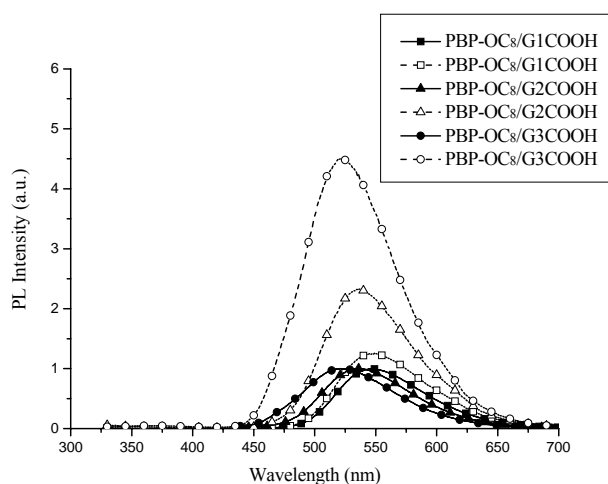


Figure 4.9 PL spectra of symmetric dendritic supramolecules containing double H-bonded acceptor emitter **PBP-OC₈** in thin films, which were excited at the dendritic peripheral OXD units (at 305 nm for open symbols) and at the maximum absorption of the emitting core **PBP-OC₈** in H-bonded G1-G3 dendrimers (at 418, 415, 408 nm, respectively, for solid symbols).

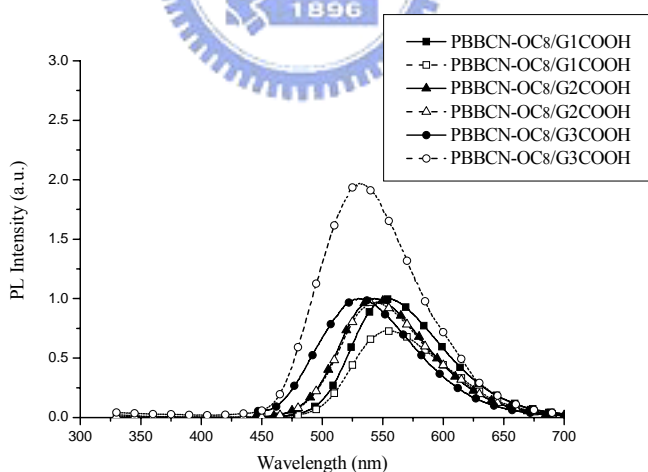


Figure 4.10 PL spectra of asymmetric dendritic supramolecules containing single H-bonded acceptor emitter **PBBCN-OC₈** in thin films, which were excited at the dendritic peripheral OXD units (at 305 nm for open symbols) and at the maximum absorption of the emitting core **PBBCN-OC₈** in H-bonded G1-G3 dendrimers (at 424, 423, 419 nm, respectively, for solid symbols).

The possible behavior of supramolecular aggregation might be explained as shown in Figure 4.11. To balance the contribution of the number of OXD units in asymmetric/symmetric H-bonded dendrimers, the complexation of G1 donors with double H-bonded acceptor emitters should be comparable with the complexation of G2 donors with single H-bonded acceptor emitters as shown in Figure 4.11(b)-(d), which all possess 4 OXD units in each asymmetric/symmetric H-bonded dendrimer. Interestingly, comparing asymmetric H-bonded dendrimers with 4 OXD units on one donor side of asymmetric ones and 2 OXD units on both donor sides of symmetric ones (or with 8 OXD units on one donor side of asymmetric ones and 4 OXD units on both donor sides of symmetric ones), both series of RFI values exhibit the trends in H-bonded dendrimers containing: **PBP-OC₈** > **PBBOC₈-OC₈** > **PBBCN-OC₈** as the acceptor emitters **PBP-OC₈**, **PBBOC₈-OC₈**, and **PBBCN-OC₈** were complexed with dendritic donors bearing the same number of OXD units. In terms of energy transfer, RFI values (with 4 OXD units in each H-bonded complex) are equal to 1.27, 1.14, and 0.97 in **PBP-OC₈/G1COOH**, **PBBOC₈-OC₈/G2COOH**, and **PBBCN-OC₈/G2COOH**, respectively; and RFI values (with 8 OXD units in each H-bonded complex) are 2.33, 2.16, and 1.97 in **PBP-OC₈/G2COOH**, **PBBOC₈-OC₈/G3COOH**, and **PBBCN-OC₈/G3COOH**, respectively. This should be attributed to the best acceptor emitter separation by donor dendrons on both sides of the symmetric H-bonded dendrimers containing double H-bonded acceptor emitter **PBP-OC₈**. Moreover, comparing asymmetric H-bonded dendrimers containing single H-bonded acceptor emitters **PBBOC₈-OC₈** and **PBBCN-OC₈**, both acceptor emitters are encapsulated by single-side dendrons, but, as shown in Figure 4.1(d), **PBBCN-OC₈** in H-bonded dendrimers is further aggregated by the dipole-dipole interaction of CN groups. However, comparing symmetric H-bonded dendrimers **PBP-OC₈/G1COOH** and **PBP-OC₈/G2COOH** in Figure 4.11(a)-(b), not only the

number of the OXD units but also the distance between OXD units and the central acceptor emitter is major concern for the energy transfer regarding the RFI value. In general, the energy transfer is highly dependent on a number of factors,⁷² including the extent of aggregation, the relative orientation of the transition dipoles, the extent of the spectral overlap, and the distance between the donor and acceptor moieties. For instance, the overlap extent between the absorption spectra of the representative chromophores **PBP-OC₈**, **PBBOC₈-OC₈**, and **PBBCN-OC₈** and the emission spectrum of model compound **2** are approximately similar in Figure 4.7. In corresponding study of the H-bonded dendrimers containing double H-bonded acceptor emitter **PBBBP-Me-OC₈** with longer conjugation length (Figure 4.12), **PBBBP-Me-OC₈/G2COOH** and **PBBBP-Me-OC₈/G3COOH** excited at the peripheral dendritic OXD units exhibit higher fluorescent intensities than those excited at direct **PBBBP-Me-OC₈** absorption, except for the lowest generation of H-bonded dendrimer **PBBBP-Me-OC₈/G1COOH**. Compared with H-bonded dendrimers containing acceptor emitter **PBP-OC₈**, the less spectral overlap in the emission of OXD dendrons and the absorption of **PBBBP-Me-OC₈** in Figure 4.7 seems to explain the main reason for lower energy transfer (i.e. lower RFI values) of OXD units to chromophores in H-bonded counterparts containing acceptor emitter **PBBBP-Me-OC₈**.

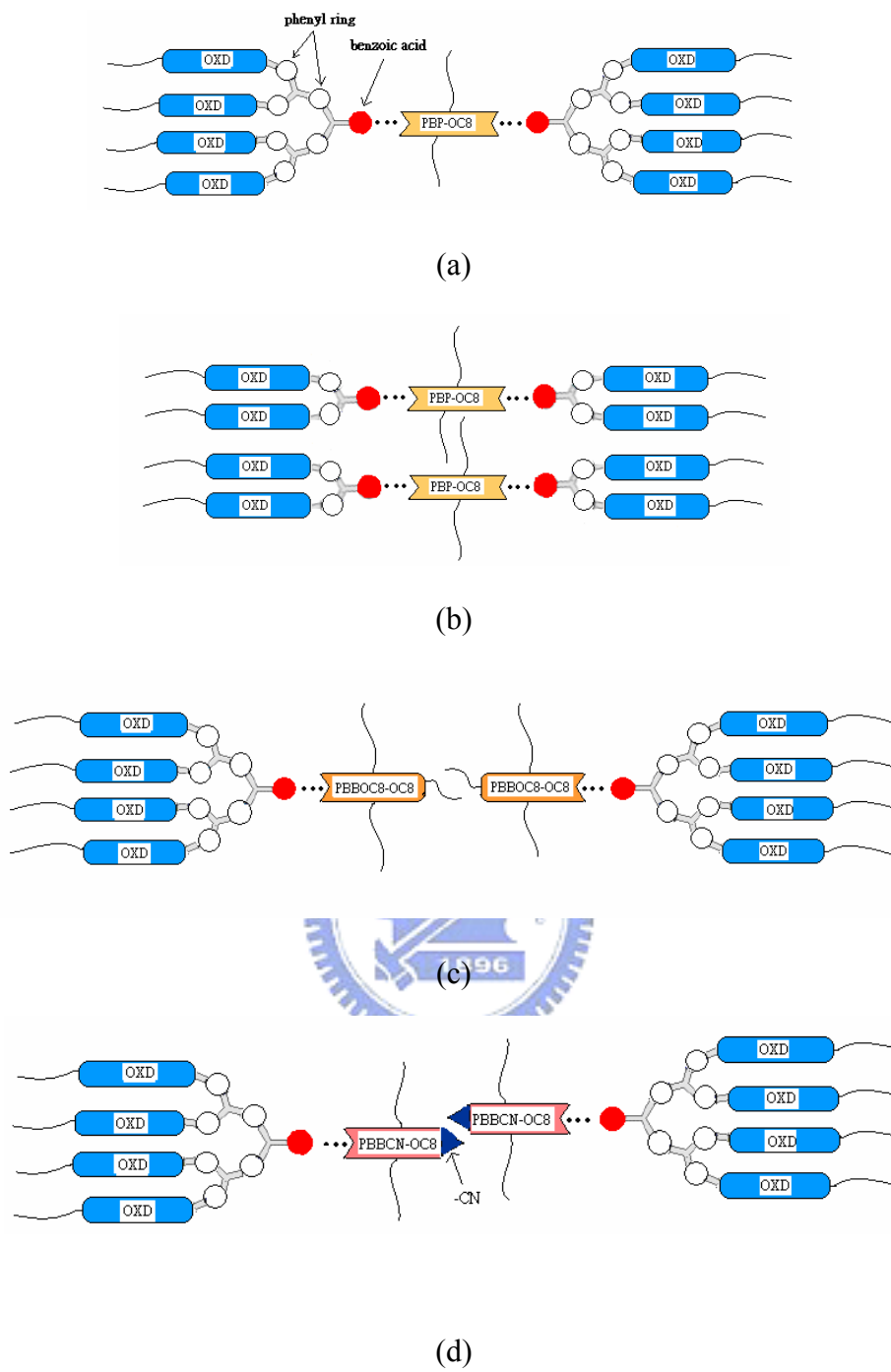


Figure 4.11 Schematic representation of double H-bonded encapsulation of symmetric dendrimers: (a) **PBP-OC₈/G2COOH** and (b) **PBP-OC₈/G1COOH**; and single H-bonded encapsulation of asymmetric dendrimers: (c) **PBBOC₈-OC₈/G2COOH** and (d) **PBBCN-OC₈/G2COOH**.

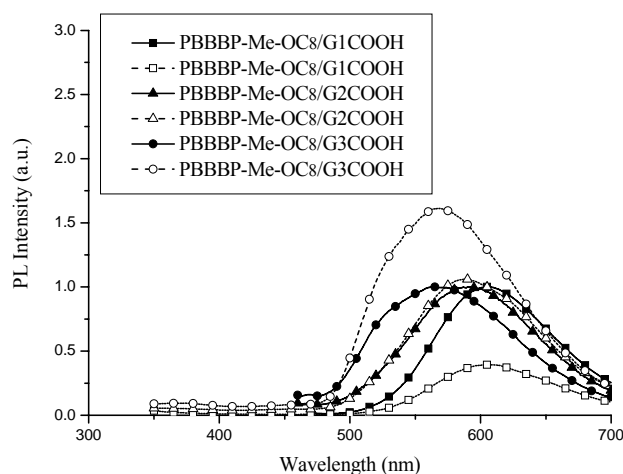


Figure 4.12 PL spectra of symmetric dendritic supramolecules containing double H-bonded acceptor emitter **PBBBP-Me-OC₈** in thin films as they were excited at the maximum absorption of the dendritic peripheral OXD units (at 305 nm for open symbols) and at the maximum absorption of the emitting core **PBBBP-Me-OC₈** in H-bonded G1-G3 dendrimers (at 450, 446, 439 nm, respectively, for solid symbols).

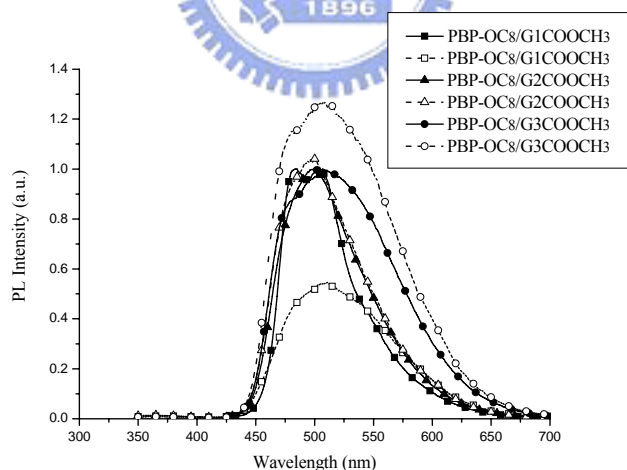


Figure 4.13 PL spectra of the simple mixture (without H-bonds) of **PBP-OC₈/G1COOCH₃**, **PBP-OC₈/G2COOCH₃**, and **PBP-OC₈/G3COOCH₃** in thin films excited at the dendritic peripheral OXD units (at 305 nm for open symbols) and at the maximum absorption of the emitting core **PBP-OC₈** in (at 425 nm for solid symbols).

In all H-bonded dendrimers containing emitting cores, the PL efficiencies are higher than pure chromophores and the values are much enhanced (the maximum value of 4 times larger) in the higher generation of H-bonded dendrimers, which is in accordance with the results obtained previously.⁷³ This improvement of PL efficiencies should be attributed to the bulky OXD dendrons refraining from the aggregation of chromophores. These results consistently indicate that the dendritic wedges play an important role of shielding/isolating effects among the cores. However, the PL efficiencies are not obviously improved by the complexation of chromophores with functionalized poly(alkyl aryl ether) donor dendrimers containing peripheral carboxylic acid units to form exterior emitting shells (reverse to the previous system with emitting cores). Therefore, the supramolecular anchoring of chromophores on the dendritic surface by H-bonds to form exterior emitting shells seems to be inefficient to solve the intermolecular aggregation of chromophores.

To evaluate the H-bonding effect on the efficiency of energy transfer within H-bonded dendrimers, analogous dendritic mixtures without H-bonds were prepared by the esterification of the dendritic acids and then mixing with corresponding chromophores. Due to lacking of H-bonds between two components, the simple mixtures of **PBP-OC₈/G1COOCH₃**, **PBP-OC₈/G2COOCH₃**, and **PBP-OC₈/G3COOCH₃** (molar ratio = 1:2, shown in Figure 4.13) showed similar emission spectra in contrast to **PBP-OC₈** in solid films (Figure 4.6). These mixed systems (without H-bonds) reveal lower ratio (the ratio of the core emissions excited at dendritic OXD units and at the core) of PL emission enhancement in comparison with those of H-bonded dendritic counterparts. Hence, **PBPOC₈/G1COOCH₃**, **PBP-OC₈/G2COOCH₃**, and **PBP-OC₈/G3COOCH₃** have the relative fluorescent intensities (RFI) values of 0.55, 1.04, and 1.27, respectively. Therefore, they exhibited lower fluorescence quantum yields and RFI values than their H-bonded dendritic

counterparts. The results indicate that better energy-transfer properties and higher fluorescence quantum yields are obtained as the dendritic donors are H-bonded to the emitting acceptors, where the better energy transfer is caused by higher pairing ratio and closer molecular distance between donors and acceptors through H-bonds.



Table 4.2 Photophysical Properties of H-Bonded Acceptors and Dendritic Complexes

Compound or H-Bonded Complex	$\lambda_{\text{PL,sol}}$ (nm)	$\lambda_{\text{PL,film}}$ (nm)	$\Phi_{\text{PL,film}}$	RFI ^a
PBBOC₈-OC₈	463	468,(495)	0.09	
PBBOC₈-OC₈/G1COOH		569	0.11	0.87
PBBOC₈-OC₈/G2COOH		562	0.19	1.14
PBBOC₈-OC₈/G3COOH		555	0.23	2.16
PBBOC₈-OC₈/G1-C₆-(COOH)₆		570	0.07	
PBBOC₈-OC₈/G1-C₁₀-(COOH)₆		558	0.07	
PBBCN-OC₈	470	512	0.08	
PBBCN-OC₈/G1COOH		556	0.20	0.73
PBBCN-OC₈/G2COOH		543	0.26	0.97
PBBCN-OC₈/G3COOH		532	0.32	1.97
PBBCN-OC₈/G1-C₆-(COOH)₆		556	0.13	
PBBCN-OC₈/G1-C₁₀-(COOH)₆		550	0.13	
PBP-OC₈	460	482,(506)	0.08	
PBP-OC₈/G1COOH		545	0.20	1.27
PBP-OC₈/G2COOH		539	0.26	2.33
PBP-OC₈/G3COOH		522	0.33	4.50
PBP-OC₈/G1-C₆-(COOH)₆		539	0.18	
PBP-OC₈/G1-C₁₀-(COOH)₆		533	0.16	
PBP-OC₈/G1COOCH₃		482,(506)	0.13	0.55
PBP-OC₈/G2COOCH₃		499	0.18	1.04
PBP-OC₈/G3COOCH₃		506	0.19	1.27
PBBBP-Me-OC₈	511	535,(567)	0.10	
PBBBP-Me-OC₈/G1COOH		607	0.16	0.39
PBBBP-Me-OC₈/G2COOH		588	0.22	1.06
PBBBP-Me-OC₈/G3COOH		568	0.32	1.61
PBBBP-Me-OC₈/G1-C₆-(COOH)₆		610	0.09	
PBBBP-Me-OC₈/G1-C₁₀-(COOH)₆		602	0.10	



^a The relative fluorescent intensities (RFI) were calculated by the ratio of the core emission intensities excited at the OXD unit and the core absorption peaks.

4.4 Conclusions

In summary, several series of novel H-bonded dendrimers were constructed by encapsulation of chromophores with dendrimers or by complexation of functionalized poly(alkyl aryl ether) dendrimers with peripheral chromophores via supramolecular self-assembly. Various degrees of red-shifted PL emissions are expected in the H-bonded dendrimers as benzoic acids are H-bonded to the H-bonded acceptor emitters. The emission wavelengths of the mono-/bis-pyridyl (single/double H-bonded) chromophores can be easily adjusted by their surrounding H-donors. As a result, the larger (higher generation) dendritic size can afford stronger site-isolation and dendron-dilution effect, and thus the better energy-transfer and higher fluorescence quantum efficiencies can be achieved. Moreover, the peripheral OXD dendrons have specific capabilities of light-antennae and enhanced core luminescence by energy transfer from OXD dendrons. Overall, the energy transfer in the dendritic supramolecules depends on the types of H-bonded acceptors and donors, including single/double (asymmetric/symmetric) H-bonded structures, dipole moments, dendritic generations, and the overlap ratio of the OXD emission spectra and the emitter absorption spectra. Owing to the efficient shielding effect and energy transfer of the donor dendrimers, high fluorescence quantum yields of these supramolecules have the potential to be utilized in molecular electro-optical devices.

Chapter 5

Synthesis and Characterization of Kinked and Hyperbranched Carbazole/Fluorene-Based Copolymers

5.1 Introduction

Over the last few years, carbazole-based molecules and polymers are good hole-transporting materials due to the electron-donating capabilities associated with the nitrogen in the carbazole.⁷⁴ Several studies of random and alternating fluorene/carbazole copolymers have been designed and synthesized to be used as a light-emitting layer in blue light-emitting diodes.⁷⁵ It is demonstrated that the incorporation of 3,6-carbazole units into the fluorene polymer chains will effectively raise the HOMO energy levels and improve the luminescent stability by interfering with the packing order to suppress the aggregation and excimer formation. However, the maxima of UV-vis absorption and PL emission were significantly blue-shifted compared with PF homopolymers, indicating that by copolymerization of PFs with 3,6-linked carbazole units the effective conjugation lengths of the copolymers have been reduced to some extent. In general, these copolymers showed decreased PL efficiencies compared with PF homopolymers in previous researches.

In this study, a series of carbazole/fluorene-based copolymers (**P10-P15**) were prepared by the Suzuki coupling reaction, and the influences of the functionalized carbazole units on thermal, photophysical, electrochemical, and electroluminescent properties of the resulting polymers were investigated. The noticeable difference between our investigation and those of previous researches is that the properties of polyfluorenes were improved by introducing minimal carbazole derivatives (**21-23**)

into poly(2,7-9,9-dihexylfluorene)s to avoid breaking the delocalization of π -electrons seriously along the polymer backbones. To suppress the aggregation phenomena and reduce the excimer formation, “kinked” and “hyperbranched” disordered structures were introduced into the conjugated polyfluorene backbones. Scheme 1 shows the chemical structures and the synthetic procedures of multifunctional carbazole derivatives (**21-23**). The introduction of hole-transporting dibromocarbazole (**21**) groups into the PF chains can suppress the chain aggregation by the formation of kinked linkages and improve the mismatch of energy levels between the anode and PF. In addition, the hyperbranched approach has proven to be an effective method for the design of amorphous nonaggregation in optoelectronic materials.^{31, 76} It has been well established that the solubility was poor in common organic solvents for hyperbranched polymers with higher contents of branched units by step-growth polymerization. Therefore, a small amount of tribromocarbazole (**22**) or tetrabromocarbazole (**23**) units are suitable as branched units to make the PF polymers with hyperbranched architecture. Thus, PF copolymers with kinked and hyperbranched structures derived from a series of carbazole-based compounds are expected to improve the material properties of polyfluorenes, which can be eventually useful for PLED device applications.

5.2 Experimental Section

5.2.1 Measurements

¹H NMR spectra were recorded on a Varian Unity 300 MHz spectrometer using CDCl₃ or 1,4-dioxane solvent. Elemental analyses were performed on a HERAEUS CHN-OS RAPID elemental analyzer. Phase transition temperatures were determined by differential scanning calorimetry (Perkin Elmer Diamond) with a heating and cooling rate of 10 °C/min. Thermogravimetric analysis (TGA) was conducted on a Du Pont Thermal Analyst 2100 system with a TGA 2950 thermogravimetric analyzer under a heating rate of 20 °C/min. Gel permeation chromatography (GPC) analysis was conducted on a Water 1515 separation module using polystyrene as a standard and THF as an eluant. UV-visible absorption spectra were recorded in dilute chloroform solutions (10⁻⁶ M) on a HP G1103A spectrophotometer, and photoluminescence (PL) spectra were obtained on a Hitachi F-4500 spectrophotometer. Thin films of UV-vis and PL measurements were spin-coated on a quartz substrate from chloroform solutions with a concentration of 1 wt %. Electrochemistry measurements were performed using an Autolab PGSTAT30 potentiostat/galvanostat with a standard three-electrode electrochemical cell in a 0.1 M tetrabutylammonium hexafluorophosphate (TBAPF₆) solutions (in acetonitrile) at room temperature with a scanning rate of 100 mV/s. A platinum working electrode, a platinum wire counter electrode, and an Ag/AgCl reference electrode were used. The onset potentials were determined from the intersection of two tangents drawn at the rising current and background current of the cyclic voltammogram (CV).

5.2.2 EL Device Fabrication

The devices were fabricated on ITO substrates that had been ultrasonicated and sequentially washed in detergent, methanol, 2-propanol, and acetone, and further

treated with O₃ plasma for 10 min before use. Thin layers of PEDOT (40 nm) on the anode and polymers (from 1 wt % of polymers in chloroform solutions) were consecutively spin-coated on the ITO surface, after which a thin layer of LiF(0.5 nm)/Al(200 nm) was deposited on the polymer films by thermal evaporation under a vacuum of 10⁻⁶ Torr. All measurements of the EL devices were carried out in air at room temperature. The luminance-current-voltage characteristics were recorded on a power source meter (Keithley 2400) and a photometer (MINOLTA CS-100A).

5.2.3 Materials

Compounds 9-(4-bromophenyl)-9*H*-carbazole (**20**)⁷⁷, 2,7-bis(4,4,5,5-tetramethyl-1,3,2-dioxaborolan-2-yl)-9,9-dihexylfluorene (**10**)³⁸, and 2,7-dibromo-9,9-dihexylfluorene (**24**)³⁸ were synthesized according to the literature procedures. Chemicals and solvents were reagent grades and purchased from Aldrich, ACROS, TCI, and Lancaster Chemical Co. Dichloromethane and THF were distilled to keep anhydrous before use. The other chemicals were used without further purification. The synthetic routes of monomers **21-23** and polymers are shown in Schemes 5.1 and 5.2, and their synthetic procedures are shown as follows:

9,9'-Bis-(4-bromophenyl)-9*H*,9'*H*-[3,3']bicarbazolyl (21**).** To a stirred solution containing 2.93 g (9.1 mmol) of 9-(4-bromophenyl)-9*H*-carbazole (**20**) in 70 ml of chloroform under nitrogen, 3.0 g (18.5 mmol) of iron(III) chloride was added. 75 ml of water was added after stirring for 40 h at room temperature. The mixture was extracted with CH₂Cl₂ and the organic layer was dried over MgSO₄, filtered and concentrated. The mixture was purified by column chromatography with EA/Hexane (1:10) to get a white solid. Yield: 70 %, ¹H-NMR (ppm, CDCl₃): δ 7.30-7.39 (m, 4H), 7.41-7.52 (m, 8H), 7.73-7.78 (m, 6H), 8.23 (d, 2H, *J* = 7.5 Hz), 8.43 (d, 2H, *J* = 1.2 Hz). MS (FAB): *m/z* [M⁺] 642, calcd *m/z* [M⁺] 642.38. Anal. Calcd. for C₃₆H₂₂Br₂N₂:

C 67.31, H 3.45, N 4.36. Found: C 67.28, H 3.68, N 4.42.

3,6-Dibromo-9-(4-bromophenyl)-9H-carbazole (22). In a flask covered with aluminum foil, a stirred solution containing 2 g (6.2 mmol) of 9-(4-bromophenyl)-9H-carbazole (**20**) in 200 ml of THF was cooled to 0 °C. 2.2 g (12.4 mmol) of N-bromosuccinimide (NBS) was added in small portions. The mixture was allowed to warm up to react at room temperature overnight. Then, the solvent was evaporated and the crude product was purified by extraction with CH₂Cl₂ and water. The combined organic phases were dried over MgSO₄. After removal of the solvent, the crude product was further purified by column chromatography on silica gel eluted with CH₂Cl₂/Hexane (1:10) and crystallization (acetone), respectively, to afford compound **3** as a white crystal. Yield: 65 %, ¹H-NMR (ppm, CDCl₃): δ 7.22 (d, 2H, *J* = 8.7 Hz), 7.38 (d, 2H, *J* = 8.4 Hz), 7.51 (dd, 2H, *J* = 1.5 Hz, *J* = 8.7 Hz), 7.74 (d, 2H, *J* = 9.0 Hz), 8.19 (d, 2H, *J* = 1.8 Hz). MS (EI): *m/z* [M⁺] 480, calcd *m/z* [M⁺] 479.99. Anal. Calcd. for C₁₈H₁₀Br₃N: C 45.04, H 2.10, N 2.92. Found: C 45.49, H 2.40, N 3.19.

6,6'-Dibromo-9,9'-bis-(4-bromophenyl)-9H,9'H-[3,3']bicarbazolyl (23). The synthesis of compound **23** was also followed by the similar procedure of compound **22**. 2 g (3.1 mmol) of compound **21**, 1.1 g (6.2 mmol) of NBS, and 100 ml of THF were used. Compound **23** was purified by column chromatography with CH₂Cl₂/Hexane (1:10) to get a white solid. Yield: 73%. ¹H NMR (ppm, 1,4-Dioxane): δ 7.34 (d, 2H, *J* = 8.7 Hz), 7.48 (d, 2H, *J* = 8.4 Hz), 7.55 (dd, 2H, *J* = 2.1 Hz, *J* = 8.7 Hz), 7.60 (d, 4H, *J* = 8.4 Hz), 7.83-7.87 (m, 6H), 8.48 (d, 2H, *J* = 2.1 Hz), 8.55 (d, 2H, *J* = 1.2 Hz). MS (FAB): *m/z* [M⁺] 800, calcd *m/z* [M⁺] 800.17. Anal. Calcd. for C₃₆H₂₀Br₄N₂: C 54.04, H 2.52, N 3.50. Found: C 53.92, H 2.87, N 3.73.

General Procedure for the Synthesis of Polymers. The synthetic route of polymers is shown in Scheme 5.2. A general procedure of polymerization is

proceeded through the Suzuki coupling reaction. The monomers, alq336, and $[\text{Pd}(\text{PPh}_3)_4]$ were dissolved in toluene and 2 M K_2CO_3 (3 : 2 in volume). The mixture was degassed and stirred at 85 °C for 2 days. After cooling to room temperature, the reaction mixture was poured into 200 mL of methanol. A fibrous solid was obtained by filtration. The obtained solid was followed by the Soxhlet extraction with acetone for 24 h to remove the catalyst residues and oligomers. Since polymers **P12-P15** tend to produce insoluble cross-linking portions in the step-growth polymerization, the solid residues of **P12-P15** were further extracted with THF using a Soxhlet apparatus for 24 h, and the insoluble solid (cross-linking networks) was discarded. After removal of THF, the soluble polymer products were dried in a vacuum oven for 24 h.

PFDiCAZ. Monomer **21** (219 mg, 0.34 mmol), monomer **10** (200 mg, 0.34 mmol), K_2CO_3 (1.1 g), $[\text{Pd}(\text{PPh}_3)_4]$ (8 mg), toluene (6 mL), and H_2O (4 mL) were used in the reaction mixture. **PFDiCAZ** was obtained as a gray solid. Yield: 85 %, $^1\text{H-NMR}$ (ppm, CDCl_3): δ 0.78-0.83 (m, 10H), 1.14 (m, 12H), 2.16 (broad, 4H), 7.37 (t, 2H, $J = 6.6$ Hz), 7.50 (t, 2H, $J = 8.1$ Hz), 7.57 (d, 2H, $J = 8.4$ Hz), 7.64 (d, 2H, $J = 8.1$ Hz), 7.74 (m, 8H), 7.88 (t, 4H, $J = 9.0$ Hz), 7.97 (d, 4H, $J = 7.8$ Hz), 8.30 (d, 2H, $J = 7.8$ Hz), 8.53 (s, 2H).

P10. Monomer **21** (27.4 mg, 0.043 mmol), monomer **10** (150 mg, 0.26 mmol), monomer **24** (104.9 mg, 0.21 mmol), K_2CO_3 (1.1 g), $[\text{Pd}(\text{PPh}_3)_4]$ (8 mg), toluene (6 mL), and H_2O (4 mL) were used in the reaction mixture. **P10** was obtained as a slight yellow solid. Yield: 89 %, $^1\text{H-NMR}$ (ppm, CDCl_3): δ 0.78 (broad), 1.23 (broad), 2.12 (broad), 7.32-7.35 (broad), 7.47-7.49 (broad), 7.54-7.94 (broad), 8.27 (d, $J = 8.1$ Hz), 8.50 (s).

P11. Monomer **21** (14.9 mg, 0.023 mmol), monomer **10** (150 mg, 0.26 mmol), monomer **24** (114.5 mg, 0.23 mmol), K_2CO_3 (1.1 g), $[\text{Pd}(\text{PPh}_3)_4]$ (8 mg), toluene (6 mL), and H_2O (4 mL) were used in the reaction mixture. **P11** was obtained as a slight

yellow solid. Yield: 80 %, $^1\text{H-NMR}$ (ppm, CDCl_3): δ 0.79 (broad), 1.14 (broad), 2.13 (broad), 7.30-7.36 (broad), 7.68 (broad), 7.83 (broad), 8.28 (d), 8.52 (s).

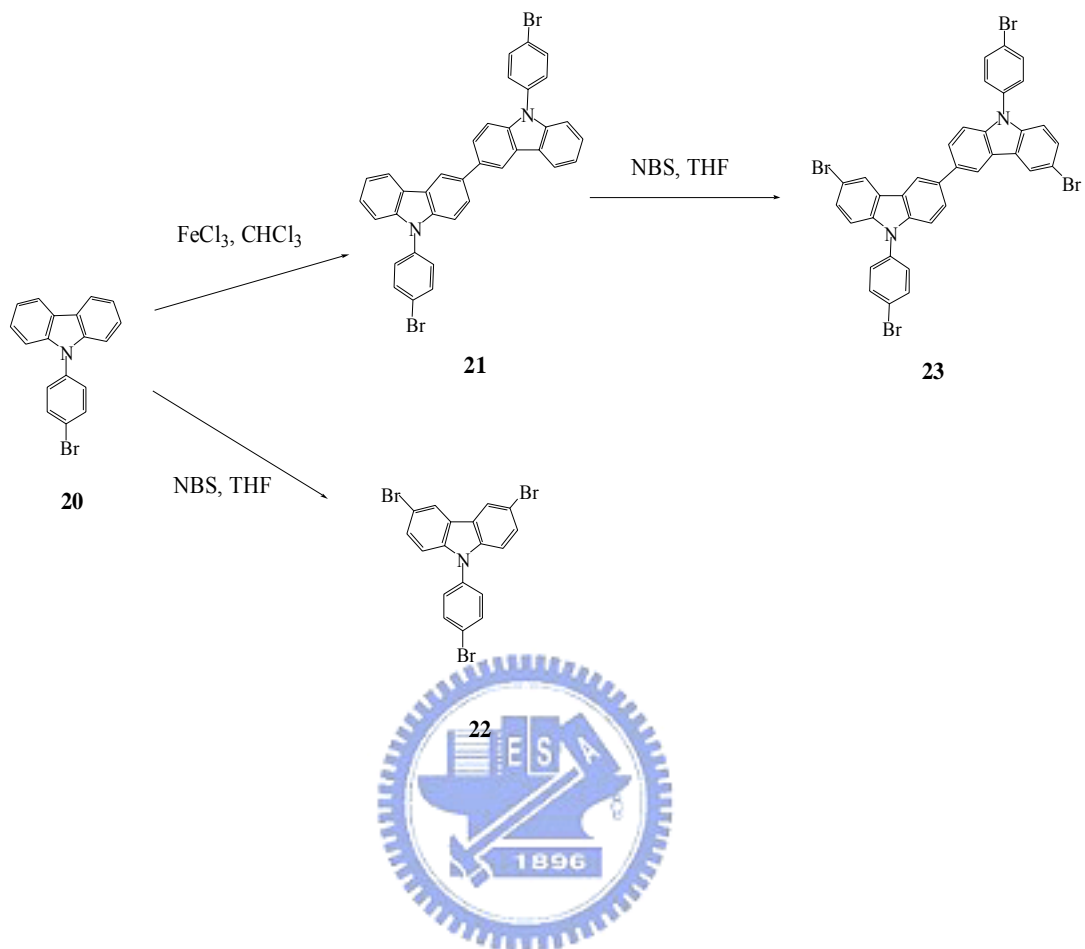
P12. Monomer **22** (18.9 mg, 0.039 mmol), monomer **10** (150 mg, 0.26 mmol), monomer **24** (96.9 mg, 0.20 mmol), K_2CO_3 (3.3 g), $[\text{Pd}(\text{PPh}_3)_4]$ (8 mg), toluene (18 mL), and H_2O (12 mL) were used in the reaction mixture. **P22** was obtained as a slight yellow solid. Yield: 62 %, $^1\text{H-NMR}$ (ppm, CDCl_3): δ 0.78 (broad), 1.12 (broad), 2.09 (broad), 7.22-7.28 (broad), 7.67 (broad), 7.82 (broad), 8.39 (s), 8.54 (s).

P13. Monomer **22** (10.7 mg, 0.022 mmol), monomer **10** (150 mg, 0.26 mmol), monomer **24** (109.5 mg, 0.22 mmol), K_2CO_3 (3.3 g), $[\text{Pd}(\text{PPh}_3)_4]$ (8 mg), toluene (18 mL), and H_2O (12 mL) were used in the reaction mixture. **P13** was obtained as a slight yellow solid. Yield: 74 %, $^1\text{H-NMR}$ (ppm, CDCl_3): δ 0.78 (broad), 1.13 (broad), 2.11 (broad), 7.27-7.30 (broad), 7.57 (broad), 7.82-7.85 (broad), 8.45 (s), 8.56 (s).

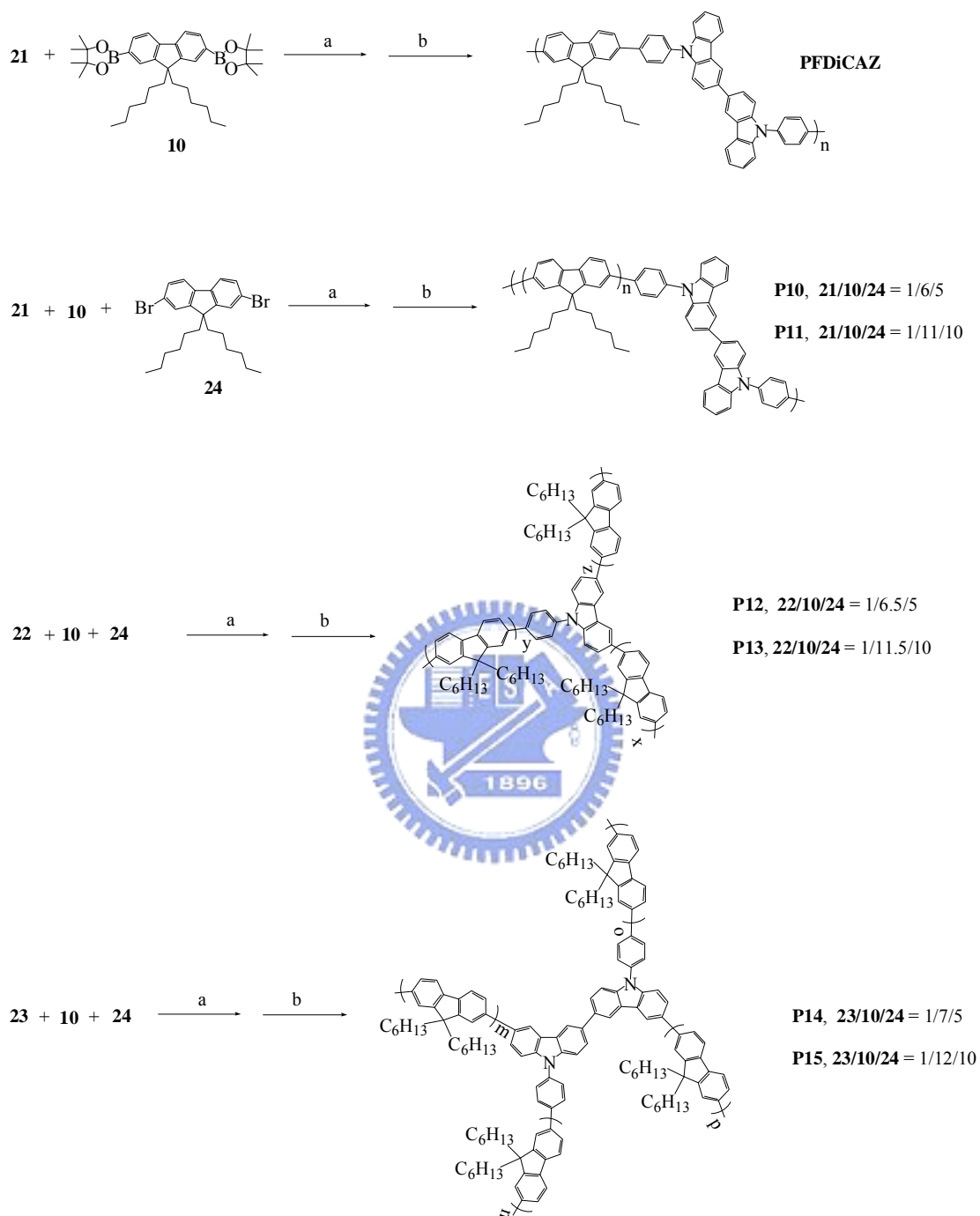
P14. Monomer **23** (29.2 mg, 0.037 mmol), monomer **10** (150 mg, 0.26 mmol), monomer **24** (90 mg, 0.18 mmol), K_2CO_3 (3.3 g), $[\text{Pd}(\text{PPh}_3)_4]$ (8 mg), toluene (18 mL), and H_2O (12 mL) were used in the reaction mixture. **P15** was obtained as a slight yellow solid. Yield: 43 %, $^1\text{H-NMR}$ (ppm, CDCl_3): δ 0.80 (broad), 1.22 (broad), 2.12 (broad), 7.26-7.36 (broad), 7.51-7.58 (broad), 7.68 (broad), 7.83-7.86 (broad), 8.59 (broad).

P15. Monomer **23** (17.1 mg, 0.021 mmol), monomer **10** (150 mg, 0.26 mmol), monomer **24** (104.9 mg, 0.21 mmol), K_2CO_3 (3.3 g), $[\text{Pd}(\text{PPh}_3)_4]$ (8 mg), toluene (18 mL), and H_2O (12 mL) were used in the reaction mixture. **P15** was obtained as a slight yellow solid. Yield: 55 %, $^1\text{H-NMR}$ (ppm, CDCl_3): δ 0.79 (broad), 1.21 (broad), 2.11 (broad), 7.30 (broad), 7.35 (broad), 7.67 (broad), 7.82 (broad), 8.58 (broad).

Scheme 5.1 Synthetic Routes of Monomers 20-23



Scheme 5.2 Synthetic Routes of Polymers



a = [Pd(PPh₃)₄], toluene, 2 M K₂CO₃

b = (i) Iodobenzene, (ii) Phenylboronic acid

5.3 Results and Discussion

5.3.1 Synthesis and Characterization

Scheme 5.1 shows the synthetic routes of monomers **21-23**. 9-(4-Bromophenyl)-9*H*-carbazole (**20**) was synthesized from carbazole as the starting material by a modified Ullmann reaction.^{77(b)} Two of compound **20** were linked via the 3- or 6-position of carbazoles to form dibromocarbazole monomer **21**. NBS was used to brominate compound **20** or **21** to produce tribromocarbazole monomer **22** or tetrabromocarbazole monomer **23**, respectively, with high yields. Monomers **21-23** were satisfactorily characterized by ¹H NMR, MS spectroscopy, and elemental analyses. The synthetic routes of **PFDiCAZ** and **P10-P15** are shown in Scheme 5.2. **PFDiCAZ**, **P10**, and **P11** were obtained by reaction of **21**, **10**, and **24** with different molar ratios in toluene containing Pd(PPh₃)₄ (1 mol %). The obtained polymers were further purified by washing with acetone in a Soxhlet apparatus for 24 h to remove oligomers and catalyst residues and were dried under reduced pressure at room temperature. After purification and drying, **PFDiCAZ**, **P10**, and **P11** were obtained as yellow fibrous solids in overall good yields. **P12** and **P13** were synthesized by reacting monomers **22**, **10**, and **24** with different molar ratios. The molar ratios of monomer **22** in copolymers were found to be key factors of the solubilities in hyperbranched **P12** and **P13**. The solubilities were poor in common organic solvents for hyperbranched polymers with higher contents of monomer **22**. The polymers with the molar ratios (monomer **22/10/24**) of 1:6.5:5 (**P12**) and 1:11.5:10 (**P13**) were approximately soluble in THF. **P12** and **P13** were purified by two-step extractions: first with acetone to remove catalyst residues and unreacted monomers (soluble in acetone), and then with THF to extract the soluble portions of hyperbranched polymers (insoluble cross-linking parts were discarded). The synthesis of **P14** and **P15** were also followed according to the synthetic procedures of **P12** and **P13** by

reacting monomers **23**, **10**, and **24** with different molar ratios. The obtained **PFDiCAZ** and **P10-P15** exhibited good solubilities in common organic solvents, e.g., toluene, THF, and chloroform.

Figure 5.1 shows ^1H NMR spectra of monomer **21**, **PFDiCAZ**, **P10**, and **P11** in CDCl_3 . ^1H NMR spectra of **PFDiCAZ**, **P10**, and **P11** showed doublet signals at $\delta = 8.3$ and singlet signals at $\delta = 8.5$, respectively, which were assigned to the proton signals of 9,9'-diphenyl-bicarbazolyl linkages. Comparing ^1H NMR spectra of **PFDiCAZ**, **P10**, and **P11**, it was found that the integrated signals of the kinked units increased with more amounts of monomer **21** added. The number-average molecular weights and the weight-average molecular weights of the polymers listed in Table 5.1 were 15100-24300, and 34500-66300, respectively, which were determined by means of gel permeation chromatography (GPC) using THF as eluant against polystyrene standards.

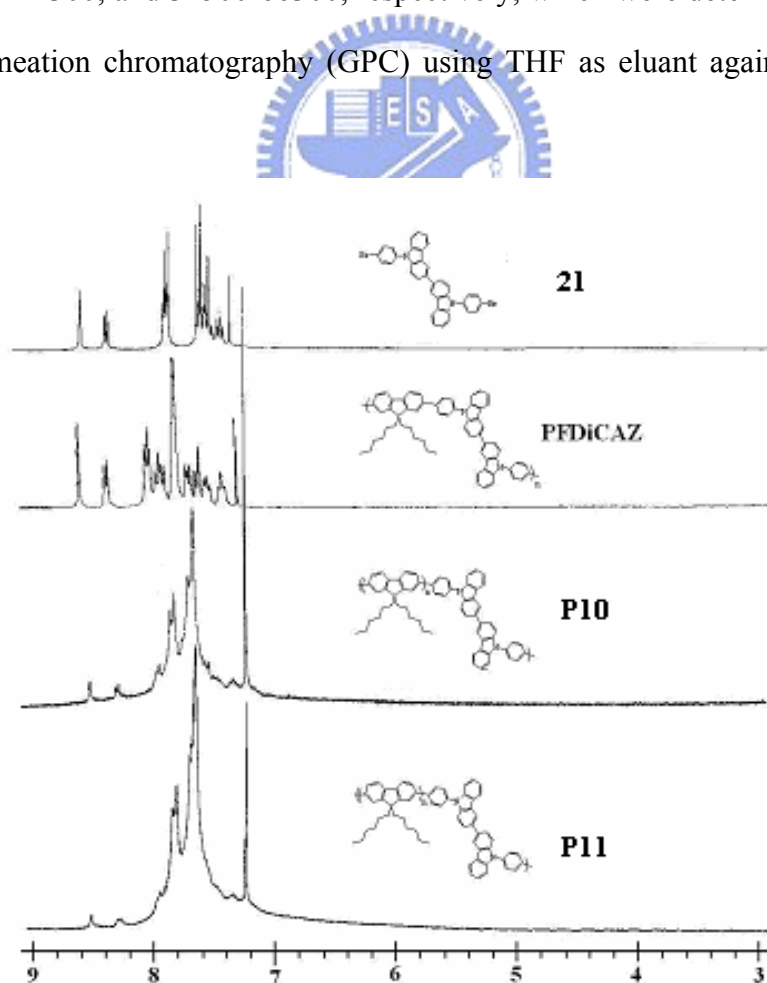


Figure 5.1 ^1H -NMR spectra of monomer **21**, **PFDiCAZ**, **P10**, and **P11**.

5.3.2 Thermal Properties

The thermal stability of the polymers was determined by thermogravimetric analysis (TGA) under nitrogen. As shown in Table 5.1, all of these polymers possess excellent thermal stability with 5% weight loss temperatures (T_{d5}) ranging from 407 to 466°C. These data reveal that all polymers have excellent thermal stability. Thermally induced phase transition properties of the polymers were also investigated by differential scanning calorimetry (DSC) under nitrogen. PF homopolymer had a crystallization temperature of 113 °C and a melting point of 159 °C, indicating the crystalline nature of this polymer as reported previously.⁷⁸ The incorporation of a series of carbazole units into the copolymers resulted in DSC traces that show no crystallization and melting peaks but only glass transition temperatures (T_g s). This clearly indicates that the presence of the kinked or hyperbranched structures in these copolymers effectively suppresses the crystallizability (or chain aggregation) of the polymer chains. The glass transition temperatures (T_g s) of **P10-P13** were ranged from 109 to 140 °C. Compared with **P11** possessing analogous kinked molecular architectures, **P10** with a higher kinked carbazole content has lower T_g , which is conceivable by reason of a higher kinked density of carbazole units in **P10**. Compared with **P13** possessing similar hyperbranched molecular architectures, **P12** with a higher hyperbranched carbazole content has higher T_g , which is plausible because of a higher hyperbranched density of carbazole units in **P12**. Hence, polymers with higher kinked density or lower hyperbranched density of carbazole units possess lower T_g relatively. No distinct glass transitions were observed for **PFDiCAZ**, **P14**, and **P15** in their DSC curves of the second heating. In addition, the measured values of T_{d5} and T_g s were higher than that of the linear polyfluorene.⁷⁹

Table 5.1 Molecular Weights and Thermal Properties of Polymers

Polymer	M_n^a	M_w^a	PDI	T_g^b (°C)	T_d^c (°C)
PFDiCAZ	23400	43600	1.87	n.d. ^d	466
P10	24300	39900	1.64	109	424
P11	21400	40600	1.90	115	420
P12	15100	34500	2.28	140	433
P13	21800	66300	3.04	120	449
P14	15500	49500	3.19	n.d. ^d	407
P15	17800	49500	2.78	n.d. ^d	407

^a Molecular weight determined by GPC in THF, based on polystyrene standards.

^b Glass transition temperature (°C) determined by DSC at a heating rate of 10 °C min⁻¹ under nitrogen.

^c Temperature (°C) at 5% weight loss measured by TGA at a heating rate of 20 °C min⁻¹ under nitrogen.

^d No noticeable T_g was observed.



5.3.3 Optical Properties

UV-vis absorption and PL emission data of the polymers are shown in Table 5.2 and Figures 5.2-5.5. **PFDiCAZ** (alternative copolymers) displayed an absorption maximum ($\lambda_{\text{Abs,sol}}$) at 351 nm in CHCl₃ solution, resulting in a substantially blue shift compared with that of PF homopolymer. This behavior is similar to the analogous alternating fluorene/carbazole copolymers,⁸⁰ which is due to the interruption of the delocalization of π -electrons along the polymer backbones by 9,9'-diphenyl-bicarbazolyl linkages. This effect also manifests itself in the solution PL spectrum, where the emission peak is blue-shifted to 402 nm as compared with that of PF. With considerable decreases in the amounts of 9,9'-diphenyl-bicarbazolyl moieties, **P10** and **P11** show their absorption peaks with the values of $\lambda_{\text{Abs,sol}} = 380$ nm for **P10** and $\lambda_{\text{Abs,sol}} = 388$ nm for **P11** (which are close to those of PF). In the case

of hyperbranched polymers, the absorption peaks in solutions appeared at 380 nm for **P12** and **P14**, and 388 nm for **P13** and **P15**, were similar to those of copolymers **P10** and **P11**. The result indicated that the absorption maxima are blue-shifted in analogous systems with the increasing contents of kinked or branching units. Compared with the absorption spectra of monodisperse oligofluorenes reported in the literature,⁸¹ the average conjugated lengths of the polymers can be estimated. According to this assumption, **P10**, **P12**, and **P14** should have comparable persistent conjugation lengths to that of an oligomer with 8 fluorene units. However, the average conjugated lengths of **P11**, **P13**, and **P15** are not conceivable but similar to those of PF homopolymers with high molecular weights. It has been reported that as the number of fluorene units is larger than five, the emission wavelengths of the oligofluorenes approach those of polyfluorenes with high molecular weights.⁸¹

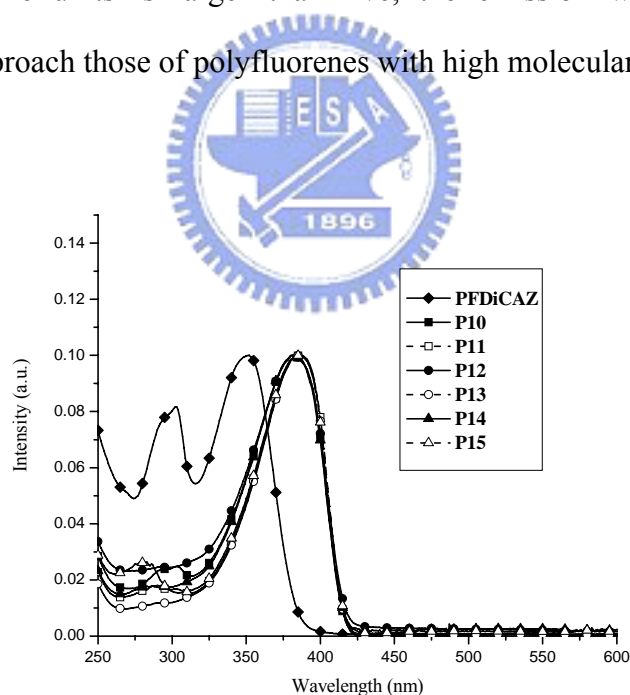


Figure 5.2 Normalized UV-vis absorption spectra of polymers in chloroform (10^{-6} M).

As shown in Figure 5.3, the PL spectra of **P10-P15** in CHCl_3 solutions are strikingly similar to each other, which show the maximum band around 417 nm along with a vibronic band at 440 nm. In general, the presence of well defined vibronic structures in the emission spectra indicates that the polymers have rigid and well-defined backbone structures.⁸² The similar emissions observed for these copolymers in comparison with that of PF homopolymer might suggest that the carbazole derivatives in the polymer backbones do not prevent efficient energy transfer from the short conjugated-emissions to the long ones in these copolymers. Therefore, as discussed above, the carbazole segments of the copolymers efficiently interrupt the conjugation of the polymer backbones, but most of the excitons migrate to the fluorene segments to emit light with lower energy. UV-vis and PL spectra of thin solid films were measured by spin-coating of solutions on quartz substrates. The optical band gaps (E_g) of **P10-P15** were determined to be around 2.9 eV from the UV-vis absorption spectra (solid films). As shown in Figure 5.4, the PL spectra of all polymers in the solid state showed 5-8 nm of red shifts and some broadening of the emission bands in comparison with their solution PL spectra. Unlike the PL spectrum of polyfluorene possessing an aggregation peak around 520 nm besides two excitonic emission peaks, the PL spectra of **P10-P15** only show peaks at 424 and 446 nm. The lack of the excimer emission in the solid films of **P10-P15** proves that even introducing a small amount of carbazole derivatives can influence the packing of the polymer chains in the solid state, and thus to enhance the quantum efficiency.

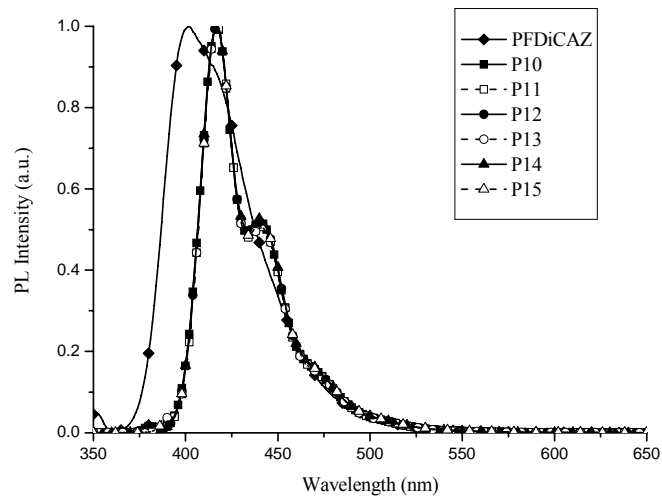


Figure 5.3. Normalized PL spectra of polymers excited at the maximum absorption of the polymer backbones in chloroform (10^{-6} M).

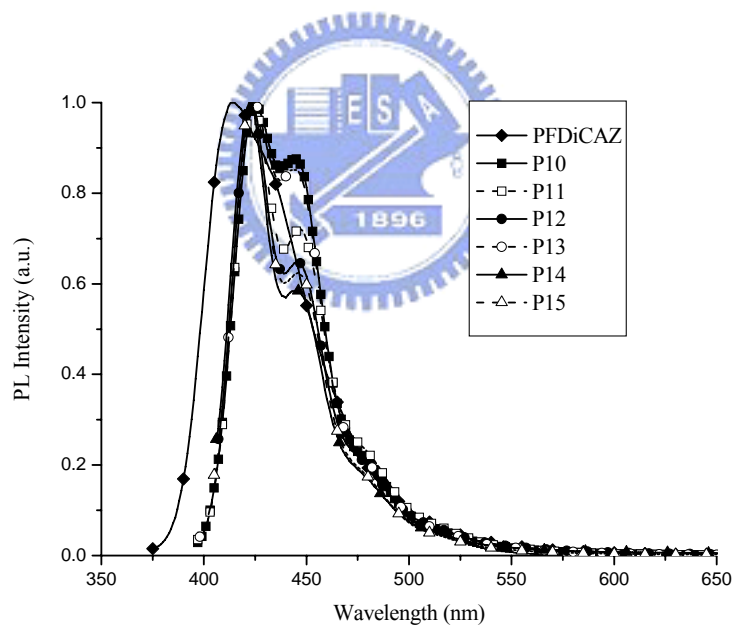


Figure 5.4. Normalized PL spectra of polymers excited at the maximum absorption of the polymer backbones in solid films.

To investigate luminescent stability of the polymers in the solid state, annealing experiments were performed on polymers **P10-P15**. Since the incorporation of the carbazole derivatives into PFs in this work suppressed the crystallizability of the polymers by lack of crystallization and melting peaks in the DSC measurements, it could be expected that these copolymers would be prone to have less chain aggregation and thus to possess improved fluorescent stabilities. After being spin-coated on a quartz substrate, the solid film was annealed at 200 °C for 1 h under nitrogen. Annealing at such a temperature, which is much higher than the glass transition temperature, can cause the movement of chain segments and increase the packing order. In fact, annealing of **PFDiCAZ** and **P10-P15** at 200 °C for 1 h under nitrogen resulted in no obvious changes in the PL spectra as compared with those of pristine (as-prepared) films. There was no additional band emerged to change the pure blue emission into another undesirable blue-green color. This clearly suggests that the formation of excimer aggregation in these copolymers is effectively suppressed even at temperatures much higher than their T_g 's. However, different results can be observed after annealing at 200 °C under air, since traces of defects formed via oxidation could also cause drastic spectral changes.²⁶ As shown in Figure 5.5, PL spectra of kinked polymers **P10** and **P11** show a little change at the peak of 445 nm by annealing at 200 °C for 0.5 h under air. In comparison with kinked polymers **P10** and **P11**, all hyperbranched polymers **P12-P15** have better thermal stability by annealing under air (but no difference under nitrogen). Besides, PL spectra of **P10-P13** showed a weak long wavelength emission tail around 520 nm after annealing under air. These changed features of PL spectra were attributed to the interchain excimer formation and/or keto defects, which are commonly observed in 9,9-disubstituted PFs after annealing.^{30(a), 52(b)} Nevertheless, the excimer peak increases very slowly compared with previously reported PF homopolymers.^{52(a)} It is

noteworthy that no green-blue band emission was observed in the thermal treatment of **P14** and **P15**. Apparently, the introduction of kinked or hyperbranched disorder in the conjugated polymer chains shows more stable PL spectra of these copolymers upon annealing, where the aggregation and excimer-formation of polymer chains can be avoided efficiently. Similar phenomenon regarding the effect of disorder on chromic behavior for other polyfluorene copolymers have also been reported by Leclerc,⁸³ which was attributed to the increased conformational flexibility of the copolymers to interchain interaction resulting in the incorporation of nonfluorene comonomer units.

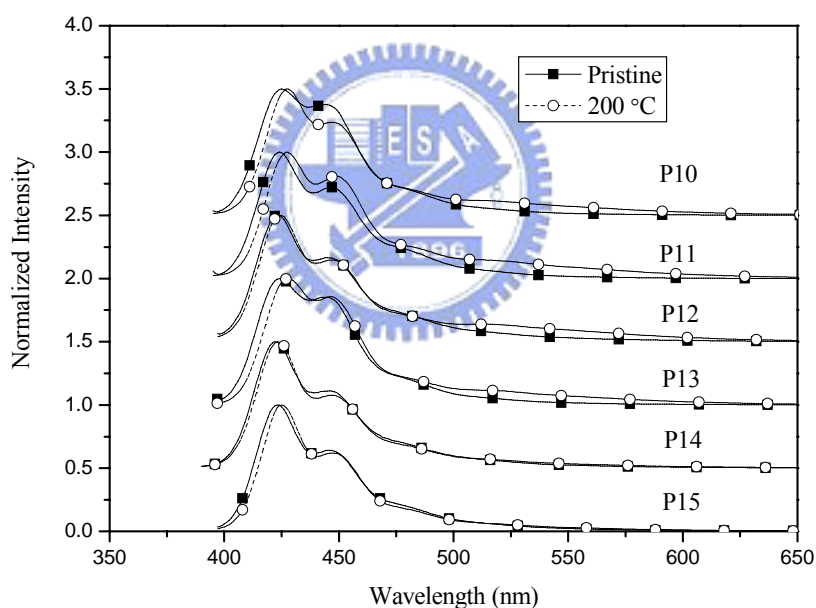


Figure 5.5. Normalized PL spectra of polymers excited at the maximum absorption of the polymer backbones in solid films: before annealing (pristine film) and annealing at 200 °C for 0.5 h under air.

The PL quantum yields (Φ_{PL}) of **PFDiCAZ** and **P10-P15** excited at the maximum absorption of the polymer backbones in solutions were measured with

9,10-diphenylanthracene as a reference standard (cyclohexane, $\Phi_{\text{PL}} = 0.90$).⁴⁶ Except **PFDiCAZ**, the quantum efficiencies of **P10-P15** reach 0.81-0.99, which are much higher than the hyperbranched polyfluorene in the previous report.⁸⁴ The high PL quantum yields (Φ_{PL}) of these polymers were attributed to the introduction of minimal carbazole derivatives into poly(2,7-9,9-dihexylfluorene) to avoid reducing the effective conjugation lengths of the copolymers seriously. Besides, The PL quantum yields (Φ_{PL}) of polymers **P10-P15** were also compared with that of PF homopolymer, i.e. poly-2,7-(9,9-dihexylfluorene). The values of Φ_{PL} for **P10-P15** are slightly lower than that of PF homopolymer. The measured data of PL quantum yields are listed in Table 5.2.

Table 5.2. Absorption and PL Emission Spectral Data of Polymers in Solution and Solid States

Polymer	$\lambda_{\text{Abs,sol}}^a$ (nm)	$\lambda_{\text{PL,sol}}^a$ (nm)	$\lambda_{\text{Abs,film}}$ (nm)	$\lambda_{\text{PL,film}}$ (nm)	Band Gap ^b (eV)	$\Phi_{\text{PL,sol}}^c$	$\Phi_{\text{PL,rel}}^d$
PFDiCAZ	351	402	355	414	3.1	0.47	0.44
P10	380	417, 440	379	425, 444	2.9	0.99	0.94
P11	388	417, 440	380	424, 447	2.9	0.94	0.88
P12	380	417, 440	388	423, 445	2.9	0.96	0.90
P13	388	417, 440	380	424, 444	2.9	0.81	0.76
P14	380	417, 441	388	422, 446	2.9	0.90	0.85
P15	388	417, 440	388	423, 446	2.9	0.88	0.83

^a Chloroform as solvent with a concentration of 10^{-6} M.

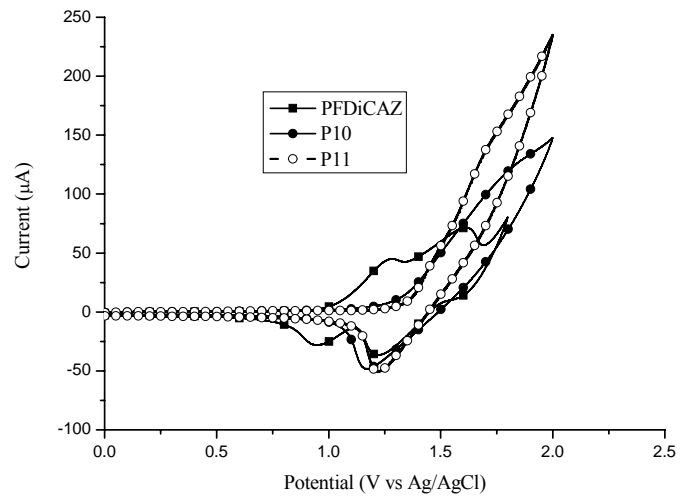
^b Band gaps were calculated from the onsets of UV-visible absorption spectra of **P10-P15** in solid films.

^c Solution fluorescence quantum efficiency measured in chloroform, relative to 9,10-diphenylanthracene in cyclohexane ($\Phi_{\text{PL}} = 0.9$).

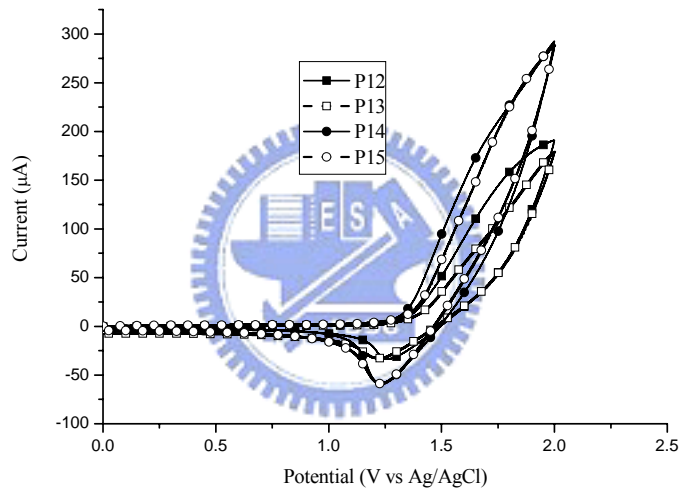
^d Relative fluorescence quantum efficiencies in solutions were estimated relative to the synthesized PF homopolymer, i.e. poly-2,7-(9,9-dihexylfluorene) as a reference, with $M_n = 26700$, $PDI = 1.94$, and $\Phi_{\text{PL,rel}} = 1$.

5.3.4 Electrochemical Characterization.

The electrochemical properties of the polymers were investigated by using cyclic voltammetry (CV), and their anodically scanned cyclic voltammograms are shown in Figure 5.6. **PFDiCAZ** (50% of the fluorene units was replaced by diphenylcarbazole units) exhibited reversible processes in the oxidation scan and had an oxidative onset potential at 0.96 V which was much lower than the reported value (1.4 V) of poly(9,9-dioctylfluorene) (POF).⁵³ The decrease of the oxidative onset potential indicated the introduction of the 9,9'-diphenyl-bicarbazolyl linkages facilitates better hole injection from the ITO anode. When the 9,9'-diphenyl-bicarbazolyl contents decreased substantially, the copolymers display a slightly higher onset potential of oxidation with values of 1.20 V for **P10** and 1.28 V for **P11**, but still lower than the value of POF. The similar effect was also observed in the previous report where only a small amount of carbazole units was incorporated into the polymers.⁸⁰ It is noticeable that the onset potential of oxidation in **P10** is slightly lower than that in **P11** due to the higher carbazole content in **P10**. In the meanwhile, similar trends were also observed in the oxidation processes of hyperbranched polymers **P12-P15**. The HOMO energy values of the polymers were estimated according to that (-4.8 eV) of ferrocene (Fc) with respect to zero vacuum level. Furthermore, the optical absorption edge was utilized to derive the band gap and calculate the LUMO energy values for the polymers.⁸⁵ The measured oxidation potentials along with HOMO and LUMO energy values of the polymers are summarized in Table 5.3. As a result, all of the polymers have higher HOMO energy levels than that of the POF, which means that better hole transporting capabilities can be expected in polymers **P10-P15**.



(a)



(b)

Figure 5.6 Cyclic voltammograms of the polymers: (a) **PFDiCAZ**, **P10**, and **P11**; (b) **P12**, **P13**, **P14**, and **P15**.

Table 5.3 Oxidation Potentials and HOMO and LUMO Energy Values of Polymers

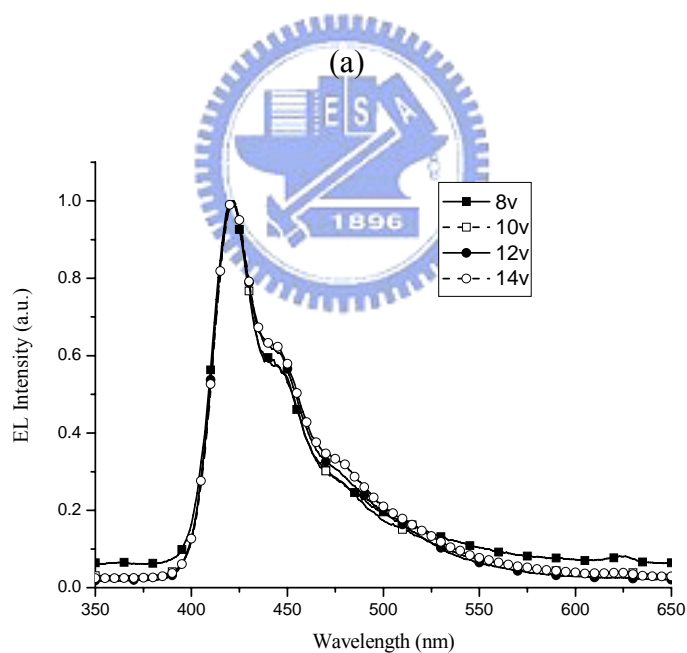
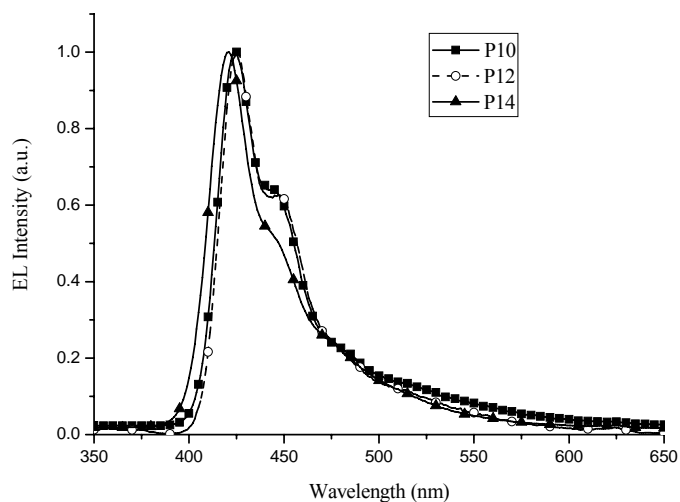
Polymer	$E_{\text{ox/onset}}$ (V)	HOMO (eV)	LUMO ^a (eV)
PFDiCAZ	0.96	-5.36	-2.26
P10	1.20	-5.60	-2.70
P11	1.32	-5.72	-2.82
P12	1.33	-5.73	-2.83
P13	1.36	-5.76	-2.86
P14	1.27	-5.67	-2.77
P15	1.36	-5.76	-2.86

^a LUMO energy values were deduced from HOMO energy values and optical band gaps.

5.3.5 Electroluminescence (EL) Properties.

Owing to the short conjugation length and low PL efficiency of **PFDiCAZ**, the applications of polymers **P10**, **P12**, and **P14** in PLED devices were surveyed in this study. The representative polymers **P10**, **P12**, and **P14** were used as emitting layers in double-layered PLED devices with a configuration of ITO/PEDOT:PSS/polymer/LiF/Al, and their EL data of PLED devices are shown in Table 5.4. As can be seen in Figure 5.7(a), the pure blue EL emissions with negligible emissions in the region of 500-600 nm (which commonly appears for PF-based PLEDs) can be achieved from **P10**, **P12**, and **P14**. In Figure 5.7(b), the EL spectra of **P12** are almost unchanged and without any low energy emission bands as the voltage was increased from 8 V to 14 V. The fwhm values of the EL spectra in **P10**, **P12**, and **P14** are 42, 42, and 39 nm, respectively. The narrow EL spectra of these polymers are almost identical to the PL spectra of the corresponding polymer films. Figure 5.8 shows the current and luminance of PLED device containing **P12** as a function of the applied voltage. The device emitted bright blue light starting about 6.0 V and reaches a brightness of 213 cd/m² at a bias voltage of 13 V. The results suggest that the improvement in EL device performance with these copolymers is due to the

introduction of kinked or hyperbranched disorder in the conjugated polymer chains. These preliminary data show the applicability of these novel polymers as PLED blue-emitters.



(b)

Figure 5.7 (a) Normalized EL spectra of **P10**, **P12**, and **P14** at 10 V. (b) Normalized EL spectra of ITO/PEDOT/**P12**/LiF/Al device at different voltages.

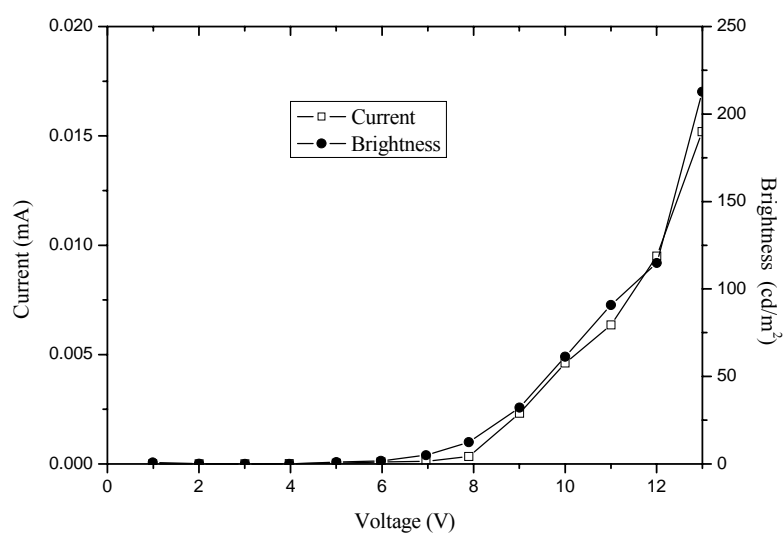


Figure 5.8 Current -voltage-brightness (I - V - B) characteristics of the PLED device containing **P12** with the configuration of ITO/PEDOT/**P12**/LiF/Al.

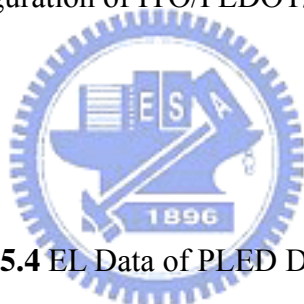


Table 5.4 EL Data of PLED Devices ^a

Polymer	λ_{EL} (nm)	fwhm (nm)	V_{on}^b (V)	Luminance Efficiency ^c (lm/W)	Power Efficiency ^c (cd/A)	Max. Brightness (cd/m ²)
P10	425	42	7	0.11	0.05	133 (14V)
P12	426	42	6	0.35	0.08	213 (13V)
P14	421	39	8	0.07	0.03	87 (13V)

^a Device structure: ITO/PEDOT/Polymer/LiF/Al.

^b V_{on} : the turn-on voltage of light.

^c Measured at 100 mA/cm².

5.4 Conclusion.

In summary, a series of novel kinked and hyperbranched carbazole/fluorene-based copolymers by one-pot Suzuki coupling were successfully synthesized. The polymers exhibited high thermal stability with their decomposition temperatures (T_d s) in the range of 407-466 °C. The PL quantum efficiencies of **P10-P15** in chloroform solutions were in the range of 0.81-0.99. The PL spectra of **P10-P15** in solid films exhibited similar spectral patterns (only with 5-8 nm of red shift in their emission maxima) in contrast to those measured in solutions. No long wavelength excimer-like emissions at 500-600 nm attributed to self-aggregation of polyfluorenes in the solid state were observed in these polymers. Thus, the polymers were less easy to self-aggregate in the solid state due to their kinked and hyperbranched structures. The polymer films exhibited very stable blue light emission even annealing at 200 °C for 1 hr under nitrogen. Besides, the tunability of hole-transporting properties and the stability of excellent luminescent properties were all demonstrated by these kinked and hyperbranched structures, which render them promising candidates for use as light-emitting materials in stable blue PLED devices. Thus, the possibility of improved luminescence properties in polyfluorene materials through carbazole copolymerization has been demonstrated.

Chapter 6

Conclusion

A series of poly(fluorene-*co-alt*-phenylene)s and polyfluorenes (PFs) containing various generations of dendritic oxadiazole (OXD) pendent wedges were synthesized by Suzuki polycondensation. The obtained polymers possess excellent solubility in common solvents and good thermal stability. Photophysical studies showed that the dendronized polymers appended with higher generations of OXD dendrons exhibit enhanced photoluminescence efficiencies and more narrow values of full width at half-maximum (fwhm). This is attributed to the shielding effect induced by the bulky dendritic OXD side chains, which prevent self-quenching and suppress the formation of aggregates/excimers. The energy transfer from OXD dendrons to polymer backbones is very efficient when excitation of the peripheral OXD dendrons results mainly in the polymer backbone emission alone. For device performance, the introduction of charge-transporting pendants can not only tune the HOMO and LUMO energy levels but also suppress the formation of aggregation. Double-layer light-emitting diode (LED) devices with the configuration of ITO/PEDOT/polymer/LiF/Al were fabricated and reported. The device with PF bearing G0 dendrons and CAZ pendants (G0-OXDCAZ) as an emitter shows a turn-on voltage of 4.5 V, and a bright luminescence of 2446 cd/m² at 12 V with a power efficiency of 0.24 cd/A at 100 mA/cm².

Novel asymmetric/symmetric dendritic supramolecules were constructed by two kinds of (single/double) H-bonded acceptor chromophores, encapsulated with (one or two) 1,3,4-oxadiazole (OXD) dendritic donors in proper acceptor/donor molar ratios. Due to shielding effect of bulky OXD dendritic shells in H-bonded donors, the dendritic supramolecules are able to prevent acceptor emitters from spatial

aggregation, and thus to induce glass-forming properties (with T_g) and show stronger emission intensities via H-bonds. Besides, the dendritic donors act as efficient light-harvesting antennae capable of transferring light energy from their peripheral OXD arms to their emitting acceptors, where the chromophore luminance induced by energy transfer is more efficient than that by direct excitation of the emitting cores. Compared with analogous dendritic mixtures without H-bonds. Therefore, compared with acceptor emitters, not only can the emission wavelength be tuned (up to 100 nm of red-shift) by H-bonds, but also much higher emission efficiencies of the H-bonded complexes were induced by reduced aggregation and energy transfer from the OXD donor dendrons.

A series of novel kinked and hyperbranched carbazole units were copolymerized by the Suzuki coupling polycondensation reaction to introduce disorder packing into the copolymer backbones. All of these polymers possess excellent thermal stability with onset decomposition temperatures at 407-466 °C and glass transition temperatures at 109-140 °C. Photoluminescent (PL) studies showed that these polymers were promising blue light-emitting materials, which exhibited high quantum efficiencies in solution. Long wavelength emissions at 500-600 nm, which were typical for PFs due to their self-aggregation in the solid state, were suppressed in these polymers. It was proven that HOMO energy levels of the copolymers can be enlarged by increasing the carbazole content in the electrochemical measurements; hence, the hole injection was greatly enhanced. Pure blue electroluminescence (EL) spectra with narrow fwhm (full width at the half-maximum) values (39-42 nm) and negligible low-energy excimer emission bands were successfully achieved, indicating that these copolymers could be good candidates for blue light-emitting materials.

References

- (1) Pope, M.; Kallmann, H. P.; Magnante, P. *J. Chem. Phys.* **1963**, *38*, 2042.
- (2) Tang, C. W.; VanSlyke, S. A. *Appl. Phys. Lett.* **1987**, *51*, 913.
- (3) Burroughes, J. H.; Bradley, D. D. C.; Brown, A. R.; Marks, R. N.; Mackay, K.; Friend, R. H.; Burns, P. L.; Holmes, A. B. *Nature* **1990**, *347*, 539.
- (4) (a) Tang, C. W.; VanSlyke, S. A.; Chen, C. H. *J. Appl. Phys.* **1989**, *65*, 3610. (b) Braun, D.; Heeger, A. *J. Appl. Phys. Lett.* **1991**, *58*, 1982. (c) Bernius, M. T.; Inbasekaran, M.; O'Brien, J.; Wu, W. *Adv. Mater.* **2000**, *12*, 1737. (d) Sheats, J. R.; Antoniadis, H.; Hueschen, M.; Leonard, W.; Miller, J.; Moon, R.; Roitman, D.; Stocking, A. *Science* **1996**, *273*, 884.
- (5) Reviews concerning OLEDs: (a) Kraft, A.; Grimsdale, A. C.; Holmes, A. B. *Angew. Chem., Int. Ed.* **1998**, *37*, 402. (b) Grell, M.; Bradley, D. D. C. *Adv. Mater.* **1999**, *11*, 895. (c) Friend, R. H.; Gymer, R. W.; Holmes, A. B.; Burroughes, J. H.; Marks, R. N.; Taliani, C.; Bradley, D. D. C.; Dos Santos, D. A.; Brédas, J. L.; Lögdlund M.; Salaneck, W. R. *Nature* **1999**, *397*, 121. (d) Greiner, A. *Polym. Adv. Technol.* **1998**, *9*, 371.
- (6) (a) Roncali, J. *Chem. Rev.* **1997**, *97*, 173. (b) Feast, W. J.; Tsibouklis, J.; Pouwer, K. L.; Groenendaal, L.; Meijer, E. W. *Polymer*, **1996**, *37*, 5017. (c) Chan, H. S. O.; Ng, S. C. *Prog. Polym. Sci.* **1998**, *23*, 1167. (d) Handbook of Organic Conductive Molecules and Polymers, ed. H. S. Nalwa, John Wiley & Sons, Chichester, **1997**. (e) Handbook of Conducting Polymers, eds. T. A. Skotheim, R. L. Elsenbaumer and J. R. Reynolds, Marcel Dekker, New York, **1998**.
- (7) (a) Tour, J. M. *Chem. Rev.* **1996**, *96*, 537. (b) Electronic Materials: The Oligomer Approach, eds. G. Wegner and K. Müllen, Wiley-VCH, Weinheim, **1998**. (c) Martin, R. E.; Diederich, F. *Angew. Chem., Int. Ed.* **1999**, *38*, 1350.

- (8) (a) Thelakkat, M. Schmidt, H.-W. *Polym. Adv. Technol.* **1998**, *9*, 429. (b) Tsutsui, T.; Aminaka, E.-I.; Fujita, Y.; Hamada, Y.; Saito, S. *Synth. Met.* **1993**, *55-57*, 4157. (c) Tsutsui, T. *MRS Bull.*, **1997**, *22*, 39. (c) Hamada, Y.; Adachi, C.; Tsutsui, T.; Saito, S. *Jpn. J. Appl. Phys.* **1992**, *31*, 1812.
- (9) Adachi, C.; Tsutsui, T.; Saito, S. *Appl. Phys. Lett.* **1989**, *55*, 1489.
- (10) (a) Berggren, M.; Granström, M.; Inganäs, O.; Andersson, M. *Adv. Mater.* **1995**, *7*, 900. (b) Granström, M. *Polym. Adv. Technol.* **1997**, *8*, 424. (c) Andersson, M. R.; Thomas, O.; Mammo, W.; Svensson, M.; Theander, M.; Inganäs, O. *J. Mater. Chem.* **1999**, *9*, 1933. (d) Yang, Y.; Jiang, H.; Liu, S.; Zhou, X.; Wu, F.; Tian, W.; Ma, Y.; Shen, J. *Synth. Met.* **1997**, *91*, 335.
- (11) (a) Kim, S. T.; Hwang, D.-H.; Li, X. C.; Grüner, J.; Friend, R. H.; Holmes, A. B.; Shim, H. K. *Adv. Mater.* **1996**, *8*, 979. (b) Edwards, A.; Blumstengel, S.; Sokolik, I.; Yun, H.; Okamoto, Y.; Dorsinville, R. *Synth. Met.* **1997**, *84*, 639. (c) Hong, Z.; Wang, D.; Ma, D.; Zhao, X.; Jing, X.; Wang, F. *Synth. Met.* **1997**, *91*, 321. (d) Ma, D.-G.; Wang, D.-K.; Hong, Z.-Y.; Zhao, X.-J.; Jing, X.-B.; Wang, F.-S.; Li, B.; Zhang, H.-J.; Wang, S.-B. *Chin. J. Chem.* **1998**, *16*, 1.
- (12) (a) Cao, Y.; Parker, I. D.; Yu, G.; Zhang, C.; Heeger, A. J. *Nature* **1999**, *397*, 414. (b) Yoshida, M.; Kawahara, H.; Fujii, A.; Ohmori, Y.; Yoshino, K. *Jpn. J. Appl. Phys.* **1995**, *34*, L1237.
- (13) Tak, Y.-H.; Bässler, H.; Leuninger, J.; Müllen, K. *J. Phys. Chem. B*, **1998**, *102*, 4887.
- (14) Kido, J.; Ontaki, C.; Hongawa, K.; Oknyama, K.; Nagai, K. *Jpn. J. Appl. Phys.* **1993**, *32*, L917.
- (15) (a) Yakushchenko, I. K.; Kaplunov, M. G.; Efimov, O. N.; Belov, M. Y.; Shamaev, S. N. *Phys. Chem. Chem. Phys.* **1999**, *1*, 1783. (c) Kido, J.; Kimura, M.; Nagai, K. *Science* **1995**, *267*, 1332.

- (16) (a) Segura, J. L. *Acta Polym.* **1998**, *49*, 319. (b) Chen, C. H.; Shi, J.; Tang, C. W. *Macromol. Symp.* **1997**, *125*, 1.
- (17) (a) Tsutsui, T.; Aminaka, E.; Lin, C. P.; Kim, D.-U. *Phil. Trans. R. Soc. Lond. A* **1997**, *355*, 801. (c) Suganma, N.; Adachi, C.; Koyama, T.; Taniguchi, Y.; Shiraishi, H. *Appl. Phys. Lett.* **1999**, *74*, 1206.
- (18) (a) Thelakkat, M.; Fink, R.; Haubner, F.; Schmidt, H.-W. *Macromol. Symp.* **1997**, *125*, 157. (b) Thayumanavan, S.; Barlow, S.; Marder, S. R. *Chem. Mater.* **1997**, *9*, 3231. (c) O'Brien, D. F.; Burrows, P. E.; Forrest, S. R.; Koene, B. E.; Loy, D. E.; Thompson, M. E. *Adv. Mater.* **1998**, *10*, 1108.
- (19) (a) Alam, M. M.; Tonzola, C. J.; Jenekhe, S. A. *Macromolecules* **2003**, *36*, 6577. (b) Moons, E. *J. Phys.: Condens. Matter* **2002**, *14*, 12235. (c) Bates, F. S. *Science* **1991**, *251*, 895.
- (20) (a) Antoniadis, H.; Inbasekaran, M.; Woo, E. P. *Appl. Phys. Lett.* **1998**, *73*, 3055. (b) Doi, H.; Kinoshita, M.; Okumoto, K.; Shirota, Y. *Chem. Mater.* **2003**, *15*, 1080. (c) Thomas, K. R. J.; Lin, J. T.; Velusamy, M.; Tao, Y.-T.; Chuen, C.-H. *Adv. Funct. Mater.* **2004**, *14*, 83.
- (21) (a) Liu, M. S.; Jiang, X.; Liu, S.; Herguth, P.; Jen, A. K.-Y. *Macromolecules* **2002**, *35*, 3532. (b) Li, X.-C.; Liu, Y.; Liu, M. S.; Jen, A. K.-Y. *Chem. Mater.* **1999**, *11*, 1568. (c) Jin, Y.; Ju, J.; Kim, J.; Lee, S.; Kim, J. Y.; Park, S. H.; Son, S.-M.; Jin, S.-H.; Lee, K.; Suh, H. *Macromolecules* **2003**, *36*, 6970.
- (22) (a) Wu, F.-I.; Reddy, S.; Shu, C.-F.; Liu, M. S.; Jen, A. K.-Y. *Chem. Mater.* **2003**, *15*, 269. (b) Shu, C.-F.; Dodda, R.; Wu, F.-Y.; Liu, M. S.; Jen, A. K.-Y. *Macromolecules* **2003**, *36*, 6698.
- (23) (a) Grice, A. W.; Bradley, D. D. C.; Bernius, M. T.; Inbasekaran, M.; Wu, W. W.; Woo, E. P. *Appl. Phys. Lett.* **1998**, *73*, 629. (b) Pei, Q.; Yang, Y. *J. Am. Chem. Soc.* **1996**, *118*, 7416. (c) Leclerc, M. *J. Polym. Sci., Part A: Polym. Chem.* **2001**,

22, 1365.

- (24) (a) Huber, J.; Müllen, K.; Salbeck, J.; Schenk, H.; Scherf, U.; Stehlin, T.; Stern, R. *Acta Polym.* **1994**, *45*, 244. (b) Lemmer, U.; Heun, S.; Mahrt, R. F.; Scherf, U.; Hopmeier, M.; Sieger, U.; Göbel, E. O.; Müllen, K.; Bässler, H. *Chem. Phys. Lett.* **1995**, *240*, 373. (c) Grell, M.; Bradley, D. D. C.; Ungar, G.; Hill, J.; Whitehead, K. *S. Macromolecules* **1999**, *32*, 5810.
- (25) Jenekhe, S. A.; Osaheni, J. A. *Science* **1994**, *265*, 765.
- (26) (a) List, E. J. W.; Güntner, R.; Scanducci de Freitas, P.; Scherf, U. *Adv. Mater.* **2002**, *14*, 374. (b) Gong, X.; Iyer, P. K.; Moses, D.; Bazan, G. C.; Heeger, A. J.; Xiao, S. S. *Adv. Funct. Mater.* **2003**, *13*, 325. (c) Scherf, U.; List, E. J. M. *Adv. Mater.* **2002**, *14*, 477.
- 27 (a) Kim, J. H.; Park, J. H.; Lee, H. *Chem. Mater.* **2003**, *15*, 3414. (b) Grell, M.; Knoll, W.; Lupo, D.; Meisel, A.; Miteva, T.; Neher, D.; Nothofer, H. G.; Scherf, U.; Yasuda, A. *Adv. Mater.* **1999**, *11*, 671. (c) List, E. J. W.; Partee, J.; Shinar, J.; Scherf, U.; Müllen, K.; Graupner, W.; Petritsch, K.; Zojer, E.; Leising, G. *Phys. Rev. B* **2000**, *61*, 10807. (d) Sung, H. H.; Lin, H. C. *J. Polym. Sci., Part A: Polym. Chem.* **2005**, *43*, 2700.
- (28) (a) Pschirer, N. G.; Bunz, U. H. F. *Macromolecules* **2000**, *33*, 3961. (b) Schmitt, C.; Nothofer, H. G.; Falcou, A.; Scherf, U. *Macromol. Rapid Commun.* **2001**, *22*, 624. (c) Lee, J. I. G.; Daver, M. H.; Miller, R. D. *Synth. Met.* **1999**, *102*, 1087. (e) Liu, B.; Yu, W. L.; Lai, Y. H.; Huang, W. *Macromolecules* **2000**, *33*, 8945.
- (29) (a) Setayesh, S.; Grimsdale, A. C.; Weil, T.; Enkelmann, V.; Müllen, K.; Meghdadi, F.; List, E. J. W.; Leising, G. *J. Am. Chem. Soc.* **2001**, *123*, 946. (b) Pogantsch, A.; Wenzl, F. P.; List, E. J. W.; Leising, G.; Grimsdale, A. C.; Müllen, K. *Adv. Mater.* **2002**, *14*, 1061. (c) Marsitzky, D.; Vestberg, R.; Blainey, P.; Tang, B. T.; Hawker, C. J.; Carter, K. R. *J. Am. Chem. Soc.* **2001**, *123*, 6965. (d) Tang,

- H. Z.; Fujiki, M.; Zhang, Z. B.; Torimitsu, K.; Motonaga, M. *Chem. Commun.* **2001**, 2426. (e) Chou, C. H.; Shu, C. F. *Macromolecules* **2002**, *35*, 9673.
- (30) (a) Lee, J. I.; Klarner, G.; Miller, R. D. *Chem. Mater.* **1999**, *11*, 1083. (b) Klarner, G.; Lee, J. I.; Davey, M. H.; Miller, R. D. *Adv. Mater.* **1999**, *11*, 115. (c) Xiao, S.; Nguyen, M.; Gong, X.; Cao, Y.; Wu, H.; Moses, D.; Heeger, A. J. *Adv. Funct. Mater.* **2003**, *13*, 25.
- (31) (a) Li, J.; Bo, Z. S. *Macromolecules* **2004**, *37*, 2013. (b) Xin, Y.; Wen, G. A.; Zeng, W. J.; Zhao, L.; Zhu, X. R.; Fan, Q. L.; Feng, J. C.; Wang, L. H.; Wei, W.; Peng, B.; Cao, Y.; Huang, W. *Macromolecules* **2005**, *38*, 6755.
- (32) Wu, W.; Bernius, M.; Dibbs, M.; Inbasekaran, M.; Woo, E.; Wujkowski, L. *Polym. Prepr.* **2000**, *41*, 821.
- (33) (a) Liu, M. S.; Jiang, X.; Herguth, P.; Jen, A. K. Y. *Chem. Mater.* **2001**, *13*, 3820. (b) Kim, J. L.; Kim, J. K.; Cho, H. N.; Kim, D. Y.; Kim, C. Y.; Hong, S. *Macromolecules* **2000**, *33*, 5880. (c) Liu, S.; Jiang, X.; Ma, H.; Liu, M. S.; Jen, A. K. Y. *Macromolecules* **2000**, *33*, 3514.
- (34) (a) Song, S. Y.; Jang, M. S.; Shim, H. K.; Song, I. S.; Kim, W. H. *Synth. Met.* **1999**, *102*, 1116. (b) Peng, Z.; Bao, Z.; Galvin, M. E. *Adv. Mater.* **1998**, *10*, 680. (c) Zhan, X. W.; Liu, Y. Q.; Wu, X.; Wang, S.; Zhu, D. B. *Macromolecules* **2002**, *35*, 2529.
- (35) (a) Chen, Z. K.; Meng, H.; Lai, Y. H.; Huang, W. *Macromolecules* **1999**, *32*, 4351. (b) Bao, Z.; Peng, Z.; Galvin, M. E.; Chandross, E. A. *Chem. Mater.* **1998**, *10*, 1201. (c) Chung, S. J.; Kwon, K. Y.; Lee, S. W.; Jin, J. I.; Lee, C. H.; Lee, C. E.; Park, Y. *Adv. Mater.* **1998**, *10*, 1112.
- (36) (a) Lee, D. W.; Kwon, K. Y.; Jin, J. L.; Park, Y.; Kim, Y. R.; Hwang, I. W. *Chem. Mater.* **2001**, *13*, 565. (b) Sung, H. H.; Lin, H. C. *Macromolecules* **2004**, *37*, 7945. (c) Sung, H. H.; Lin, H. C. *J. Polym. Sci. Part A: Polym. Chem.* **2005**, *43*, 2700. (d)

- Jin, S. H.; Kim, M. Y.; Kim, J. Y.; Lee, K.; Gal, Y. S. *J. Am. Chem. Soc.* **2004**, *126*, 2474.
- (37) (a) Pan, J.; Zhu, W.; Li, S.; Zeng, W.; Cao, Y.; Tian, H. *Polymer* **2005**, *46*, 7658. (b) Pan, J.; Zhu, W.; Li, S.; Xu, J.; Tian, H. *Eur. J. Org. Chem.* **2006**, 986. (c) Du, P.; Zhu, W. H.; Xie, Y. Q.; Zhao, F.; Ku, C. F.; Cao, Y.; Chang, C. P.; Tian, H. *Macromolecules* **2004**, *37*, 4387. (d) Tseng, Y. H.; Wu, F. I.; Shih, P. I.; Shu, C. F. *J. Polym. Sci. Part A: Polym. Chem.* **2005**, *43*, 5147.
- (38) Ranger, M.; Rondeau, D.; Leclerc, M. *Macromolecules* **1997**, *30*, 7686.
- (39) Bo, Z.; Zhang, C.; Severin, N.; Jurgen, P. R.; Schlüter, A. D. *Macromolecules* **2000**, *33*, 2688.
- (40) (a) Frahn, J.; Karakaya, B.; Schäfer, A.; Schlüter, A. D. *Tetrahedron* **1997**, *53*, 15459. (b) Schlüter, S.; Frahn, J.; Schlüter, A. D. *Macromol. Chem. Phys.* **2000**, *201*, 139.
- (41) Tolman, C. A.; Seidel, W. C.; Gerlach, D. H. *J. Am. Chem. Soc.* **1972**, *94*, 2669.
- (42) Tokito, S.; Tanaka, H.; Noda, K.; Okada, A.; Taga, Y. *Appl. Phys. Lett.* **1997**, *70*, 1929.
- (43) Zeng, G.; Yu, W. L.; Chua, S.; Huang, W. *Macromolecules* **2002**, *35*, 6907.
- (44) Haugland, R. P.; Yguerabide, J.; Stryer, L. *Proc Natl Acad Sci U.S.A.* **1969**, *63*, 23.
- (45) (a) Adronov, A.; Gilat, S. L.; Fréchet, J. M. J.; Ohta, K.; Neuwahl, F. V. R.; Fleming, G. R. *J. Am. Chem. Soc.* **2000**, *122*, 1175. (b) Adronov, A.; Malenfant, P. R. L.; Fréchet, J. M. *J. Chem. Mater.* **2000**, *12*, 1463. (c) Weil, T.; Reuther, E.; Müllen, K. *Angew Chem, Int Ed.* **2002**, *41*, 1900. (d) Du, P.; Zhu, W. H.; Xie, Y. Q.; Zhao, F.; Ku, C. F.; Cao, Y.; Chang, C. P.; Tian, H. *Macromolecules* **2004**, *37*, 4387.
- (46) Eaton, D. *Pure Appl. Chem.* **1998**, *60*, 1107.

- (47) Guilbault, G. G., Ed. *Practical Fluorescence*; Marcel Dekker, Inc.: New York, 1990; Chapter 1.
- (48) Pommerehne, J.; Vestweber, H.; Guss, W.; Mahrt, R. F.; Bässler, H.; Porsch, M.; Daub, J. *Adv. Mater.* **1995**, *7*, 551.
- (49) Yu, W.-L.; Cao, Y.; Pei, J.; Huang, W.; Heeger, A. J. *Appl. Phys. Lett.* **1999**, *75*, 3270.
- (50) (a) Kwok, C. C.; Wong, M. S. *Macromolecules* **2001**, *34*, 6821. (b) Kwok, C. C.; Wong, M. S. *Chem. Mater.* **2002**, *14*, 3158.
- (51) Fu, Y. Q.; Li, Y.; Li, J.; Yan, S.; Bo, Z. S. *Macromolecules* **2004**, *37*, 6395.
- (52) (a) Bliznyuk, V. N.; Carter, S. A.; Scott, J. C.; Klärmer, G.; Miller, R. D.; Miller, D. C. *Macromolecules* **1999**, *32*, 361. (b) Sims, M.; Bradley, D. D. C.; Ariu, M.; Koeberg, M.; Asimakis, A.; Grell, M.; Lidzey D. G. *Adv. Funct. Mater.* **2004**, *14*, 765.
- (53) Janietz, S.; Bradley, D. D. C.; Grell, M.; Giebeler, C.; Inbasekaran, M.; Woo, E. *P. Appl. Phys. Lett.* **1998**, *73*, 2453.
- (54) Xia, C.; Advincula, R. C. *Chem. Mater.* **2001**, *13*, 1682.
- (55) Satoh, N.; Cho, J. S.; Higuchi, M.; Yamamoto, K. *J. Am. Chem. Soc.* **2003**, *125*, 8104.
- (56) Lupton, J. M.; Samuel, I. D. W.; Beavington, R.; Burn, P. L.; Bässler, H. *Adv. Mater.* **2001**, *13*, 258.
- (57) Joswick, M. D.; Cambell, I. H.; Barashkov, N. N.; Ferraris, J. P. *J. Appl. Phys.* **1996**, *80*, 2883.
- (58) (a) Weil, T.; Reuther, E.; Müllen, K. *Angew. Chem., Int. Ed.* **2002**, *41*, 1900. (b) Herrmann, A.; Weil, T.; Sinigersky, V.; Wiesler, U. -M.; Vosch, T.; Hofkens, J.; De Schryver, F. C.; Müllen, K. *Chem. Eur. J.* **2001**, *7*, 4844.
- (59) (a) Gronheid, R.; Hofkens, J.; Kohn, F.; Weil, T.; Reuther, E.; Müllen, K.; De

- Schryver, F. C. *J. Am. Chem. Soc.* **2002**, *124*, 2418. (b) Liu, D.; De Feyter, S.; Cotlet, M.; Stefan, A.; Wiesler, U.-M.; Herrmann, A.; Grebel-Koehler, D.; Qu, J.; Müllen, K.; De Schryver, F. C. *Macromolecules* **2003**, *36*, 5918.
- (60) Kwon, T. W.; Alam, M. M.; Jenekhe, S. A. *Chem. Mater.* **2004**, *16*, 4657.
- (61) (a) Wang, P. W.; Liu, Y. J.; Devadoss, C.; Bharathi, P.; Moore, J. S. *Adv. Mater.* **1996**, *8*, 237. (b) Halim, M.; Pillow, J. N. G.; Samuel, D. W.; Burn, P. L. *Adv. Mater.* **1999**, *11*, 371.
- (62) (a) Kuwabara, Y.; Ogawa, H.; Inada, H.; Noma, N.; Shirota, Y. *Adv. Mater.* **1994**, *6*, 677. (b) Bettenhausen, J.; Greczmiel, M.; Jandke, M.; Strohmriegl, P. *Synth. Met.* **1997**, *91*, 223. (c) Bettenhausen, J.; Strohmriegl, P. *Adv. Mater.* **1996**, *8*, 507.
- (63) Oldham, W. J., Jr.; Lachicotte, R. J.; Bazan, G. C. *J. Am. Chem. Soc.* **1998**, *120*, 2987.
- (64) (a) Paleos, C. M.; Tsiourvas, D. *Angew. Chem., Int. Ed. Eng.* **1995**, *34*, 1696. (b) Kato, T.; Mizoshita, N.; Kanie, K. *Macromol. Rapid Commun.* **2001**, *22*, 797. (c) Beginn, U. *Prog. Polym. Sci.* **2003**, *28*, 1049.
- (65) Precup-Blaga, F. S.; Garcia-Martinez, J. C.; Schenning, A. P. H. J.; Meijer, E. W. *J. Am. Chem. Soc.* **2003**, *125*, 12953.
- (66) (a) Lin, H. C.; Sheu, H. Y.; Chang, C. L.; Tsai, C. *J. Mater. Chem.* **2001**, *11*, 2958. (b) Lin, H. C.; Tsai, C. M.; Huang, G. H.; Tao, Y. T. *Macromolecules* **2006**, *39*, 557.
- (67) Fréchet, J. M. J.; Wooley, K. L.; Hawker, C. J. *J. Am. Chem. Soc.* **1993**, *115*, 11496.
- (68) Hawker, C. J.; Fréchet, J. M. J. *J. Am. Chem. Soc.* **1990**, *112*, 7638.
- (69) (a) Kumar, U.; Kato, T.; Fréchet, J. M. J. *J. Am. Chem. Soc.* **1992**, *114*, 663. (b) Odinkov, S. E.; Mashkovshky, A. A.; Glazunov, V. P.; Iogansen, A. V.; Rassadin, B. V. *Spectrochim. Acta* **1976**, *32A*, 1355. (c) Kato, T.; Kihara, H.;

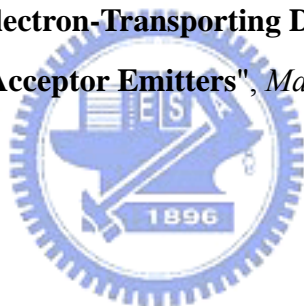
- Uryu, T.; Fujishima, A.; Fréchet, J. M. J. *Macromolecules* **1992**, *25*, 6836.
- (70) (a) Farrington, P. J.; Craig, J. H.; Fréchet, J. M. J.; Mackay, M. E. *Macromolecules* **1998**, *31*, 5043. (b) Stutz, H. J. *Polym. Sci., Part B: Polym. Phys.* **1995**, *33*, 333. (c) Wooley, K. L.; Hawker, C. J.; Pochan, J. M.; Fréchet, J. M. J. *Macromolecules* **1993**, *26*, 1514.
- (71) (a) Cameron, J. H.; Facher, A.; Lattermann, G.; Diele, S. *Adv. Mater.* **1997**, *9*, 398. (b) Precup-Blaga, F. S.; Schenning, A. P. H. J.; Meijer, E. W. *Macromolecules* **2003**, *36*, 56.
- (72) Lakowicz JR. Principles of fluorescence spectroscopy. New York: Kluwer Academic/Plenum Publishers; **1999**.
- (73) (a) Baines, F. L.; Billingham, N. C.; Armes, S. P. *Macromolecules* **1996**, *29*, 3416. (b) Chen, Z. K.; Hoi Sim Lee, N.; Huang, W.; Xu, Y. S.; Cao, Y. *Macromolecules* **2003**, *36*, 1009.
- (74) Stephan, O.; Vial, J. C. *Synth. Met.* **1999**, *106*, 115.
- (75) (a) Li, Y.; Ding, J.; Day, M.; Tao, Y.; Lu, J.; D'iorio, M. *Chem. Mater.* **2004**, *16*, 2165. (b) Du, J.; Fang, Q.; Bu, D.; Ren, S.; Cao, A.; Chen, X. *Macromol. Rapid Commun.* **2005**, *26*, 1651.
- (76) (a) Liu, X. M.; Xu, J.; Lu, X.; He, C. *Macromolecules* **2006**, *39*, 1397. (b) Liu, X. M.; He, C.; Hao, X. T.; Tan, L. W.; Li, Y.; Ong, K. S. *Macromolecules* **2004**, *37*, 5965. (c) Liu, X. M.; He, C.; Huang, J.; Xu, J. *Chem. Mater.* **2005**, *17*, 434.
- (77) (a) Koene, B. E.; Loy, D. E.; Thompson, M. E. *Chem. Mater.* **1998**, *10*, 2235. (b) Gauthier, S.; Fréchet, J. M. J. *Synthesis* **1987**, 383.
- (78) Grell, M.; Bradley, D. D. C.; Inbasekaran, M.; Woo, E. P. *Adv. Mater.* **1997**, *9*, 798.
- (79) Liu, B.; Yu, W.; Lai, Y.; Huang, W. *Chem. Mater.* **2001**, *13*, 1984.
- (80) Xia, C.; Advincula, R. C. *Macromolecules* **2001**, *34*, 5854.

- (81) Klaerner, G.; Miller, R. D. *Macromolecules* **1998**, *31*, 2007.
- (82) Cimrova, V.; Remmers, M.; Neher, D.; Wegner, G. *Adv. Mater.* **1996**, *8*, 146.
- (83) Blondin, P.; Bouchard, J.; Beaupré, S.; Belletête, M.; Durocher, G.; Leclerc, M. *Macromolecules* **2000**, *33*, 5874.
- (84) (a) Lu, J. P.; Tao, Y.; D'iorio, M.; Li, Y. N.; Ding, J. F.; Day, M. *Macromolecules* **2004**, *37*, 2442. (b) Wong, W. Y.; Liu, L.; Cui, D.; Leung, L. M.; Kwong, C. F.; Lee, T. H.; Ng, H. F. *Macromolecules* **2005**, *38*, 4970.
- (85) Hohle, C.; Hofmann, U.; Schloter, S.; Thelakkat, M.; Strohriegl, P.; Haarer, D.; Zilker, S. J. *J. Mater. Chem.* **1999**, *9*, 2205.



Publication

1. C. W. Wu, C. M. Tsai, and H. C. Lin*, "**Synthesis and Characterization of Poly(fluorene)-Based Copolymers Containing Various 1,3,4-Oxadiazole Dendritic Pendants**", *Macromolecules*, **2006**, 39, 4298.
2. C. W. Wu, H. H. Sung, and H. C. Lin*, "**Synthesis and Characterization of Poly(fluorene-*co-alt*-phenylene) Containing 1,3,4-Oxadiazole Dendritic Pendants**", *J. Polymer Sci. Part A: Polymer Chem.*, in Press.
3. C. W. Wu and H. C. Lin*, "**Synthesis and Characterization of Kinked and Hyperbranched Carbazole/Fluorene-Based Copolymers**", *Macromolecules*, **2006**, 39, 7232.
4. C. W. Wu and H. C. Lin*, "**H-Bonded Effects on Novel Supramolecular Dendrimers Containing Electron-Transporting Donor Dendrons and Single/Double H-Bonded Acceptor Emitters**", *Macromolecules*, in Press.



學經歷資料表

姓 名	吳中文
性別	男
出生日期	1976 年 6 月 26 日
婚姻狀況	未婚
E-mail 信箱	wcw399@ms31.hinet.net
聯絡電話	0922323280
通訊地址	新竹縣竹北市自強北路 168 巷 12 號 9 樓
永久地址	台南縣北門鄉雙春村 51 號
學經歷	1996 年 9 月-2000 年 6 月 私立東海大學化學系 2000 年 9 月-2002 年 6 月 國立高雄師範大學化研所碩士班 2002 年 7 月-2003 年 6 月 國立鳳山高中實習教師 2003 年 9 月-2006 年 9 月 國立交通大學材料所博士班
專 長	液晶與有機發光材料開發、合成與物性鑑定
學術著作	<ol style="list-style-type: none"> 1. C. W. Wu, C. M. Tsai, and H. C. Lin*, "Synthesis and Characterization of Poly(fluorene)-Based Copolymers Containing Various 1,3,4-Oxadiazole Dendritic Pendants", <i>Macromolecules</i>, 2006, 39, 4298. 2. C. W. Wu, H. H. Sung, and H. C. Lin*, "Synthesis and Characterization of Poly(fluorene-co-alt-phenylene) Containing 1,3,4-Oxadiazole Dendritic Pendants", <i>J. Polymer Sci. Part A: Polymer Chem.</i>, in Press. 3. C. W. Wu and H. C. Lin*, "Synthesis and Characterization of Kinked and Hyperbranched Carbazole/Fluorene-Based Copolymers", <i>Macromolecules</i>, 2006, 39, 7232. 4. C. W. Wu and H. C. Lin*, "H-Bonded Effects on Novel Supramolecular Dendrimers Containing Electron-Transporting Donor Dendrons and Single/Double H-Bonded Acceptor Emitters", <i>Macromolecules</i>, in Press.